COLLISIONAL (DE-)EXCITATION of NH & ND by He & H2 : Theory, Comparison with experiments and Astrophysical applications

Ragav Ramachandran

Normandie Université

THESE

Pour obtenir le diplôme de doctorat

Spécialité Physique

Préparée au sein de l'Université du Havre

Excitation Collisionnelle des molécules NH et ND par He et H_2 :

Theorie, comparaison avec les expériences et application astrophysique.

Présentée et soutenue par
Ragav RAMACHANDRAN

Thèse soutenue publiquement le 21/02/2020 devant le jury composé de		
Dr. Lola GONZALEZ-SANCHEZ	Professeur à Universidad de Salamanca	Rapporteur
Dr. Jérôme LOREAU	Professeur à KU Leuven kaart	Rapporteur
Dr. Jacek KLOS	Professeur à University of Maryland	Examinateur
Dr. Luca BIZZOCCHI	Chargé de recherche à Max-Planck-Institut für extraterrestrische Physik	Examinateur
Dr. Majdi HOCHLAF	Professeur à Université Gustave Eiffel	Examinateur
Pr. François LIQUE	Professeur à l'Université Le Havre	Directeur de thèse

Thèse dirigée par François LIQUE, LOMC UMR 6294, CNRS-Université du havre Normandie

UNIVERSITÉ LE HAVRE NORMANDIE

ED PSIME

LABORATOIRE ONDES et MILIEUX COMPLEXES

COLLISIONAL (DE-)EXCITATION *of* NH & ND *by* He & H_2 :

Theory, Comparison with experiments and Astrophysical applications

Author:

RAGAV RAMACHANDRAN

Supervisor:

FRANÇOIS LIQUE

A thesis submitted in fulfillment of the requirements for the degree of

Doctor of Philosophy in Physics

On the 21st of February, 2020

Abstract

Ever since the discovery of Ammonia in the interstellar medium in 1968, the study of nitrogen chemistry has been in the limelight. It is now well established that the NH molecule plays a crucial role in the interstellar nitrogen chemistry as it acts as an intermediate during the formation of the ubiquitous ammonia. Abundance of this species is a crucial probe of the nitrogen chemistry. With the advancements in the observational techniques, highly resolved transitions of these molecules in the ISM have been observed. However, the observed abundance ratios of nitrogen hydrides do not match with astrochemical models. Earlier models also predicted a high D/H ratio in nitrogen hydride radicals. The isotopologues are used to probe chemical pathways. Deuterium fractionation should reflect the different formation paths, as it is expected to be different depending on the origin of the deuteration. For accurate analysis of these spectral and continuum observations, non-LTE modeling methods are employed which requires the NH and ND collisional rate coefficients. In this work, we present fine and hyperfine resolved rate coefficients for the (de-)excitation of NH/ND due to collisions with He and that of NH with H_2 that should allow accurate determination of the NH abundance from the observational spectra.

For calculating collisional rate coefficients, the first step is to define the potential energy surface (PES) of the colliding system. In this thesis we present highly correlated *ab initio* PESs of the NH-He and NH-H_2 van der waals complexes. The accuracy of our new PESs has been assessed by comparing the energies of the bound states supported by the PES to the available spectroscopic studies. The good agreement between theoretical results obtained from the new

PESs and experimental results demonstrates the high accuracy our new PESs.

Using the new PES, calculations of the collisional excitation cross sections of the fine-structure and hyperfine levels of NH by He were performed for energies up to 3500 cm^{-1}, which yield, after thermal average, rate coefficients up to 350 K. The calculated rate coefficients are compared with the previous available theoretical data and the experimental measurements at room temperature. From the comparison, we can observe that there is a significant difference between the present and the previous rate coefficients, which is attributed essentially to the inclusion of vibrational effect in the new calculations. We also observe a good agreement with the experiments confirming that inclusion of NH vibration is needed to accurately model the energy transfer in the NH-He collisional system. The collisional excitation cross sections of the fine-structure and hyperfine levels of ND by He were also calculated, using the modified NH-He PES, for energies up to 2000 cm^{-1}, which yield, after thermal average, rate coefficients up to 200 K. These results are compared with the NH-He results to explain the importance of calculating ND-He rate coefficients explicitly rather than scaling the NH-He rate coefficients. We also present the first cross section calculations for NH-H_2. These results would be of particular interest because H_2 is the dominant collisional partner in molecular clouds. As the He and H_2 rate coefficients differ significantly, both the NH-He and NH-H_2 sets of collisional data should be used to revise the NH abundance in space.

To the force that created the Universe

"Remember to look up at the stars and not down at your feet. Try to make sense of what you see and wonder about what makes the universe exist. Be curious. And however difficult life may seem, there is always something you can do and succeed at. It matters that you don't just give up."

— Stephen Hawking

"Primary causes are unknown to us; but are subject to simple and constant laws, which may be discovered by observation, the study of them being the object of natural philosophy."

— Jean Baptiste Joseph Fourier, *The Analytical Theory of Heat (1878)*

"Là où finit le télescope, le microscope commence.
Lequel des deux a la vue la plus grande ?"

— Victor Hugo, *Les Misérables (1862)*

"Then even nothingness was not, nor existence, There was no air then, nor the heavens beyond it.
But, after all, who knows, and who can say whence it all came, and how creation happened?
The gods themselves are later than creation!"

— Nasadiya Sukta, *Rig Veda*

Acknowledgements

My PhD thesis wouldn't have been a success without the guidance and help of the people around me. First and foremost I am extremely indebted to François Lique, for giving me this oppotunity and letting me work under his able supervision and guiding me throughout the course of these 3 years. I would also like to thank Innocent Mutabazi, director of the lab for being a friendly and helpful mentor. I would also like to thank Fabien Doumouchel, kyle Walker, Fidel Alejandro, Cheikh Tidiane Bop, Nezha Bouhafs, Benjamin and all others who are/were a part of our group, for their kind support and enlightening scientific discussions. All the scientists and the research scholars of the Laboratory (Jonathan(bébé), Hrishi, Marc, JBs, Bubaka, Valentine, Abdillah(harami), Emeranciel(Bob Marley), Elynn, Nihad, Camille, Abdessamad, Safa, and other names i missed..) have also been extremely helpful towards me. A big thanks to all. I also express my gratitude towards Sivaprakasam and Bhalamurugan Sivaraman for their valuable advises from time to time and for being my wing men in the field of research. I would especially like to thank Carole, Séverine, Christine, Mano and other admisitrative building staffs for making my administrative life so easy (which wasn't easy at all!!) and for being kind, patient and caring in spite of me not speaking french and even if i did, with lot of mistakes.

I thank my parents (Raji & Ramachandran), sister (Ramya), family and all my friends for their entire support and for bearing with me all these years (ofcourse with fights and disappointments now and then!). I couldn't have even started or completed this thesis without their help and motivation. My BFFs (who are already angry that I haven't been in touch) Ashwin, Deviprasath, Ramiya, SathishK, Balaji, et. al. just for being my bffs this long (it is the toughest job in the Universe!)!! Last but not the least, a special thanks to my bar buddies (Léo, Mathieu(s), Cyprien, Guewen, Nath, Alexis,

Julien, Pierre, etc....), without whom i would have gone crazy long time ago.....

I thank all the doctors and medical professionals who laid hands on me (ofcourse to treat me.. nothing else) for keeping me fit and alive. I should also thank Governments of India and France for not causing any trouble. I would be at debt if i don't thank the team sci-hub (@Sci_Hub) for making my research life a lot easier.

Contents

List of Figures

List of Tables

PART I

INTRODUCTION

Introduction

"My own suspicion is that universe is not only queerer than we suppose, its queerer than we can suppose"

— J.B.S Haldane, *Possible world*

Wondering what makes universe exist does excite us and the more we unravel the mysteries of the universe, the more exciting it gets. From time immemorial homo sapiens sapiens have been questioning what it is and how it came into existence! Of course there is no one answer to it and not all answers are correct, but still the thirst has not quenched and it never will. What started as a philosophical brainchild, with time, took a deep dive into science. Though many eminent people believe that the philosophy is dead and only the scientists are the torch bearers of the knowledge(the grand design - Hawking et al., 2010), I would humbly disagree as I believe that philosophy is the light that lighted the torch and is still a guiding light to many torch bearers. Universe is vast! It is ever evolving both literally and metaphorically. Literal evolution of universe is a fact and the metaphorical evolution of the universe is how the idea of universe has evolved in the minds of the humans over the age. From Aristotle's (4^{th} c. BC) idea of geocentric universe (T. Taylor, 2010) to Aryabhata's (5^{th} c.) heliocentric universe (Sarma et al., 1896); From the idea of Ptolemy (2^{nd} c.) that universe consists of Earth, moon, sun and visible planets (Ptolemaeus, 1515) to the rig veda's

(interpreted in 8th c.) idea that the universe is everlasting and infinite, philosophically the design of universe kept stretching. As far as modern science is concerned, in 1543, Nicolaus Copernicus proposed a heliocentric theory for the universe (Copernicus, 1543), leading to a revolution in the scientific community! Galileo, a champion of Copernican theory, in 1609 made an instrument called "*telescope*" which literally moved the heavens! Bruno proposing solar system not to be the centre of the universe to Herchel (1785) proposing that the Sun is not even the centre of our galaxy (Herschel et al., 1912) and we as a scientific community never stopped and our understanding of universe kept on becoming clearer with the advancements in the theoretical, observational and experimental techniques.

As far as the interstellar medium (ISM) is concerned, until the end of 19th century, the space between the stars were empty or filled with ether! Huggins et al. (1864), based on observations commented on some nebulae that they were not just cluster of stars but "*....objects possessing pecular plan of structures...*". Later, Lockyer (1891) commented that "*that these stars could not be stars in the ordinary sense but swarms of bodies separated from each other*". Hartmann (1904) discovered calcium lines which did not have *oscillations* and concluded that "*... at some point in space in the line of sight between the Sun and δ Orionis there is a cloud which produces that absorption, and which recedes with a velocity of...*" leading to the discovery of first atom in the interstellar medium. Trumpler (1930) found that "*....that there was a general absorbing medium that extinguished starlight....*", demonstrating the presence of a diffuse, absorbing ISM. Payne (1925) found that helium and hydrogen were highly abundant in the stellar atmosphere (though the scientific community rejected her claims at the time). In the 1930s scientists realised the non homogeneity of ISM was suddenly, ISM became dynamic!

Dark clouds are the regions in which most molecules of the ISM are found, and hence are also known as molecular clouds. Alomst 80 years ago, Swings and Rosenfeld (1937) discovered the first interstellar molecules in ISM, CH, based on the observations and hypotheses of Eddington (1926); Russell (1935) & Swings (1937). Subsequently, McKellar (1940) discovered CN and Douglas et al. (1941) discovered CH^+ in the optical spectrum of EM radiation. Jansky (1933) published the detection of radio waves in the space and 30 years later, 26 years after the discovery of first molecule in ISM, the first molecule, OH, was discovered in the radio wavelengths (Weinreb et al., 1963). Subsequently, Cheung et al. (1968) discovered NH_3. In 1972, with the successful launch of the Copernicus satellite (with a UV spectrometer onboard), lead to many observational studies on the interstellar molecules (Herzberg, 1988). Helium was observed in the ISM by Paresce et al. (1973)

and the abundance of He in ISM was first given by Freeman et al. (1977). H_2 being a homonuclear molecule, has zero dipole moment and so it does not emit radio-wavelength lines. Hence it was elusive in ISM for a long time. Molecular hydrogen in interstellar space was first discovered by Carruthers, 1970 in a rocket observation of Lyman band absorption at wavelengths between 100 and 110 nm of starlight from ξ Per. After that there were a series of observations of H_2 in space (Spitzer et al., 1974; Gautier et al., 1976; Treffers et al., 1976;....; Sandford et al., 1993). Heger (1922) and Merrill (1934) noticed several unidentified bands in the spectra, "*diffuse interstellar band*"(DIB), which Allamandola et al. (1989) hypothesized to be due to the polycyclic aromatic hydrocarbond (PAH) and since then several studies have been made to confirm it but still most of these DIBs remain unidentified. The last 5 decades have been a period of wonderful discoveries involving astronomical molecules! Until this day, with the advances in the ground based and space based observational facilities, at least 221 molecules have been detected in space with molecules as complex as ionized buckyballs (C_{60}^+) (Cordiner et al., 2019) have been detected.

Right from the discovery of Ammonia in the interstellar medium (Cheung et al., 1968), the study of nitrogen chemistry has been in the limelight. Nitrogen is an essential component to life on Earth, and studies (for eg, Wollin et al., 1971; Siro Brigiano et al., 2017) suggest direct connections between interstellar ammonia and the formation of biologically important molecules (like amino acids and nucleobases) in space. Recent study also provides new evidences for the formation of complex macro structures when the these molecular building blocks of life are subjected to shocks in the ISM conditions, which answers the missing link between simple amino acids and complex nucleotides and hence the basis for origin of life in the space (and in other planetary conditions).

As far as this thesis is concerned, the molecule of our interest is NH. It is now well established that the NH molecule plays a crucial role in the nitrogen interstellar chemistry (Scott et al., 1997; Hily-Blant, Walmsley et al., 2010; Le Gal et al., 2014), as it acts as an intermediate during the formation of the ubiquitous ammonia both in gas phase and surface of dust grains. In the gas phase, the ion-molecule reaction and the subsequent dissociative

recombination takes place as follows (Herbst et al., 1973):

$$\begin{aligned} N_2 + He^+ &\rightarrow N^+ + N + He \\ N^+ + H_2 &\rightarrow NH^+ + H \\ NH^+ + H_2 &\rightarrow NH_2^+ + H \\ NH_2^+ + H_2 &\rightarrow NH_3^+ + H \\ NH_3^+ + H_2 &\rightarrow NH_4^+ + H \\ NH_4^+ + e^- &\rightarrow NH_3 + H \end{aligned}$$

NH_2^+ & NH_3^+ upon dissociative recombination gives

$$\begin{aligned} NH_2^+ + e^- &\rightarrow \mathbf{NH} + H \\ NH_3^+ + e^- &\rightarrow \mathbf{NH} + H_2 \end{aligned}$$

Also,

$$\begin{aligned} N_2 + H_3^+ &\rightarrow N_2H^+ + H_2 \\ N_2H^+ + e^- &\rightarrow \mathbf{NH} + N \end{aligned}$$

On the surface of dust grain, the neutral-neutral reaction takes place as follows (Hiraoka et al., 1995):

$$\begin{aligned} N + H &\rightarrow \mathbf{NH} \\ NH + H &\rightarrow NH_2 \\ NH_2 + H &\rightarrow NH_3 \end{aligned}$$

Even though the presence of NH was predicted since the discovery of the first molecule (Swings and Rosenfeld, 1937), it was first confirmed by Meyer et al. (1991) (in HD 27778 and HD 24398) and later by Crawford et al. (1997) (in HD 149757) and Weselak et al. (2009) (in HD 149757, HD 163800 & HD 169454) by absorption-line spectroscopy. Using the Long-Wavelength Fabry-Perot spectrometer on board Infrared Space Observatory, the fine-structure rotational lines of NH were detected by Cernicharo et al. (2000) and J. R. Goicoechea et al. (2004). The ground-state hyperfine rotational transition lines of NH were detected using the Heterodyne Instrument for

the Far-Infrared onboard Herschel Space Observatory by C. M. Persson et al. (2010).

The ISM also consists of isotopes like D, ^{13}C, ^{15}N, ^{17}O, etc and so several isotopologues have been discovered over the years. Motivation behind the observational studies of interstellar deuterated molecules was the constraints provided by the deuterium abundance in the stellar atmosphere. It was soon realized that isotopologues of molecules with a H atom had abundances far in excess than the cosmological D/H ratio and that, deuterated molecules rather act as an important probe for the interstellar chemistry. Hence, accurate measurements of interstellar D/H ratio (which means accurate calculation of abundances of deuterated molecules) would give an insight into the chemical evolution in ISM (A. G. G. M. Tielens, 2013). Roueff, Lis et al. (2005) model predicted a high D/H ratio in the nitrogen hydride radicals. Bacmann, Caux et al. (2010) also derived a very high ND/NH ratio for the protostar 16293-2422. Deuterium fractionation should reflect the different formation paths, as it is expected to be different depending on the origin of the deuteration. Bacmann, Daniel et al. (2016) presented the Herschel/HIFI observations of NH and ND in the 16293E prestellar core, a source which is in the vicinity of the Class 0 protostar IRAS16293-2422. The source is known to harbour high abundances of deuterated molecules, and to have cold temperatures for a starless core, making it easier to detect species in absorption against the dust continuum emission.

Hence, accurate measurements of the mass and column density of molecular clouds, which influences their chemistry and evolution, are essential for our understanding of these regions. Column density relationships between simple molecules also plays an important role in identifying the unidentified DIBs. For this, the analysis of observational spectral lines at the radio, sub-millimeter and infrared region of the electromagnetic spectrum are an important device to understand the physical and chemical conditions in the ISM (Tak et al., 2007). These observed spectra are due to the collisional and radiative transition processes of the constituents (atoms and molecules) of the observed region. As we know, ISM is non-homogeneous with regions of various densities. Different processes dominate under different conditions and in order to know which approach to use for the measurements (or we can call it *modeling*), depends on the density and temperature in the region under consideration. In the regions of high densities, where collisions are very frequent, the basic assumption is that the kinetic temperature is equal to excitation temperature i.e., it is in a thermal equilibrium *"Local Thermodynamic Equilibrium (LTE)"*. Under such circumstances, the energy levels (of the constituent atom/molecule) are populated according to

Maxwell-Boltzmann statistics. In such cases, only the *detailed balancing* of the radiative transitions is required. But most regions in ISM is far from thermodynamic equilibrium! Especially, in less dense regions such as the low temperature, molecular clouds of the ISM, the LTE approximation is not valid. Under Non-LTE conditions, there is not only detailed balancing for radiative processes, but also a statistical combination of both radiative and collisional processes (A detailed explanation on theory and need for NLTE is given in Böhm-Vitense, 1992; A. Tielens, 2005 & Roueff and Lique, 2013). Solving this statistical equilibrium requires the knowledge of energy levels, the state-to-state rates for radiative processes and the state-to-state rate for collisional processes. The radiative processes are subject to the quantum mechanical selection rules and comprise spontaneous emission, stimulated emission and absorption (through Einstein coefficients A and B). Therefore for the astrophysics, to obtain the rate coefficients for all energies, all quantum levels, and all interstellar species is of utmost importance. Though the Einstein coefficients for molecules are well studied and values are available for many molecules of astrophysical interest, the collisional rate coefficients are sparsely available in comparison. Elementary collisions involving atoms and molecules play an important role in many gaseous environments, where they provide both the heating and cooling mechanisms (Fléchard et al., 2015) due to the thermal energy transfer between internal degrees of freedom. Especially, In cold molecular clouds, the most abundant species are He and H_2 which account for 20% and 80% of the numerical density, hence collision of the atoms and molecules with these abundant species are of prime importance for the astrophysical modeling (Dulieu et al., 2017)(e^- and atomic H are also important collision partners but out of purview of this thesis).

Along with the observational developments, the experimental, theoretical and technological developments have also took place in the six decades.The development of cold, supersonic and controlled atomic or molecular beams paved way to the extensive experiments in the collision domain. Most of the experiments are based on crossed molecular beam experiments. Toennies et al. (1979) carried out the first high energy scattering experiments of H & H_2 with rare gases. In few year, CRESU (Cinétique de Réaction en Ecoulment Supersonique Uniforme) was designed for studying reactive kinetics of collisions at low temperature. In this, a uniform buffer gas flow was created using a laval nozzle. The shape of the nozzle and the buffer gas controlled the temperature (Dupeyrat et al., 1985; Sims et al., 1994; Mertens et al., 2017; etc..). Using a stark decelerator slowed down the molecular beams to controlled low velocities. It also helped to achieve high state

purity (Gilijamse et al., 2006; Kirste et al., 2012; and others). VMI allowed measurement of differential cross section (Eppink et al., 1997; Vogels et al., 2015; etc...). Particle trapping helped accumulating collision signals over a long time (Willitsch et al., 2008; Sawyer et al., 2011). The cryo-cooled valves used at low crossing angles aided the system to reach low collision energies and using this technique systems like CO-H_2 (Chefdeville, Stoecklin et al., 2012), O_2-H_2 (Chefdeville, Kalugina et al., 2013) were studied. Using the same technique scattering of He was also studied (Lavert et al., 2014; Klein et al., 2017). With merged beam experiments, the symmetric top molecules were studied (Jankunas, Bertsche et al., 2014; Jankunas, Jachymski et al., 2015; Jankunas, Jachymski et al., 2016). In spite of all these developments in the experiments, yet the complete understanding of processes in collisions still remains a challenge due to the experimental difficulties in performing complete experiments in which all relevant quantities are accessible. Hence, extracting the collisional (de-)excitation rate coefficients heavily depend on the theoretical calculations! Even the experimentalists depend on the theoretical outcomes for a number of reasons. The following excerpt from "Atom-Molecule Collision Theory" (R. Bernstein, 2013) would throw some lights on it. *"....the experimentalists considering the construction of ever-more sophisticated apparatus may ask if the additional detail about to be uncovered from the new experiments has enough theoretical "value" to justify the effort. What new scientifically significant information can be expected from the results of the proposed experiments? What are the very meanings of the terms information content, value, significance? if accurate ab initio atom-molecule potential surfaces were available and if accurate quantal scattering calculations could be carried out economically and conveniently, will the need for most of the collision experiments on simple atom-molecule systems would be obviated by the theory? The goal of the experiments is to make detailes, quantitative observations which only test the qualitative predications of the theory, but also serve to evaluate the parameter in the theory which are least well known....."*.

The theoretical formalism for the collision of diatomic molecule with an atom was first given by Arthurs and Dalgarno (1960) and following this Green (1975) generalised the theory for collision between 2 diatoms. These were for closed-shell diatoms. For open-shell molecules, the rotational levels are split by spin-rotation coupling (fine structure). The theory for $^2\Sigma$ and $^2\Pi$ open-shell molecules with structureless atom was given by Dixon et al. (1979), Alexander (1982), Corey and Alexander (1988), etc. Several approximate methods like centrifugal sudden (CS) approximation (McGuire, 1973; McGuire and Kouri, 1974; Kouri et al., 1976; Parker et al., 1977,

Green, 1976, etc.), infinite order sudden (IOS) approximation (Curtiss, 1968a; Curtiss, 1968b; Curtiss and R. B. Bernstein, 1969; Pack, 1974; Parker et al., 1977; Goldflam et al., 1979; Green, 1979) and recoupling methods (Corey and McCourt, 1983; Alexander and Dagdigian, 1985; etc..) were used for open-shell molecules over the time. The full close coupled(cc) theory for $^3\Sigma$ molecules with structureless atom was given by Lique, Spielfiedel, Dubernet et al. (2005). Several studies, including the calculations in this thesis involving He, are based on this theory. The further developments in the theoretical methods for the calculation of collisional rate coefficients are well documented in Roueff and Lique (2013) and Bouhafs (2017) and the interested readers are directed to the references therein. Recently several alternatives to the full quantum time independent CC methods have also been developed, especially for those rotationally inelastic collisions for which the full quantal calculations would otherwise be computationally very costly or impossible. One such alternative is the mixed quantum/classical theory(MQCT) for inelastic scattering (Semenov et al., 2013a; Semenov et al., 2013b; Semenov et al., 2015). Ndengué, Dawes et al. (2017) used the multiconfiguration time dependent Hartree (MCTDH) method to study the atom-triatom collisions (which was extended to diatom-triatom collision system by Ndengué, Scribano et al. (2019)). Loreau, Lique et al. (2018) proposed a statistical method based on the statistical adiabatic channel model (SACM) and showed to obtain accurate rate coefficients for systems like CO-H_2O, C^+-HF (Loreau, Faure et al., 2018; Dagdigian and Kłos, 2018). With the multiplication of the data, it becomes very important to compile all these atomic and molecular data (the energy levels, statistical weights, Einstein A and B coefficients, collision excitatation and de-excitation rate coefficients). There are databases such as the LAMDA, CDMS, NIST, JPL, CHIANTI, BASECOL, HITRAN, GEISA, etc... which compiles these data.

As far as NH, which is central to our thesis, is concerned, it has been extensively studied (especially with He) earlier experimentally and theoretically (Rinnenthal et al., 2000; Rinnenthal et al., 2002; Dagdigian, 1989; Alexander, Dagdigian and Lemoine, 1991; Krems et al., 2003; Stoecklin, 2009; Toboła et al., 2011; Dumouchel et al., 2012). Previously, The relative column densities of nitrogen hydrides ($NH:NH_2:NH_3$) in the protostellar object IRAS 16293-2422 was shown to be 3:1:19 (Hily-Blant, Maret et al., 2010). In the massive cluster-forming region G 10.6-0.4 it was 5.4:2.2:1, and in W49N it was shown to be 3.2:1.9:1 (C. Persson et al., 2012). Le Gal et al., 2014 estimated the ratios in dense clouds to be 3:1:3. Bacmann, Caux et al. (2010) derived a very high deuterium fractionation with an [ND]/[NH] ratio of between 30 and 100%. Roueff, Loison et al. (2015) predicted [ND]/[NH]

between 10% and 6% and Bacmann, Daniel et al. (2016) derived a value of more than 2% at the core and over 20% at the outer regions of 16293E prestellar core using a complete non-LTE model with NH and ND collisional data (collisions with He) published by Dumouchel et al., 2012. There are no studies yet for collision of NH and ND by H_2. This thesis deals with the study of the rotational excitation of NH and ND due to collisions with He and H_2. The main goal of the thesis is to obtain collisional rate coefficients for these collisional systems for different temperatures one can find in the cold ISM.
The thesis is divided into 4 parts.

Part II consists of 4 chapters. In these 4 chapters, we introduce a general background of the collision and theory behind the scattering of a rigid diatom by a structureless atom in the space fixed frame. We also give a brief account of the close coupling bound state method which we use to calculate the bound states energies of the Van der Waals complexes.

Part III consists of 5 chapters. Chapter 5 gives the pure, fine and hyperfine rotational energy levels of NH and ND. Chapter 6 introduces a general theory for the collision dynamics of an open shell $^3\Sigma^-$ diatom with a structureless ^1S atom.

In Chapter 6 and 7, we present new 3 Dimensional potential energy surfaces (PESs) for the NH-He and ND-He complexes, fine-structure resolved state-to-state collisional rate coefficients for the collsion of NH and ND by He, and hyperfine resolved state-to-state collisional rate coefficients for the same.

Chapter 8 introduces a general theory for the collision dynamics of an open shell $^3\Sigma^-$ diatom with a $^1\Sigma$ diatom. We present first ever four dimensional analytical model of the PES for the NH-H_2 system. A first use of this PES to compute the pure rotational level resolved state-to-state scattering calculation for collison of NH by *para*-H_2 and *ortho*-H_2 is reported. We also present the fine structure resolved state-to-state rate coefficients of NH-H_2 calculated using a 2D PES.

In Chapter 9 we present the bound states of the NH-He and NH-Ar complexes excluding and including the fine structures of NH.

PART II

THEORY

CHAPTER 1

Formalism for Collision induced Energy tranfer

"Nothing happens until something moves."

— Albert Einstein

To study collisions in space theoretically, it is first necessary to model the collision in such a way that it would be viable to form a theory! The collision between two species (In the case of this thesis, it is diatom-atom or diatom-diatom) leads to scattering of one species by another. More specifically, in our cases we study only the *inelastic non-reactive scattering*, that is, the 2 species remain unchanged post collision and only the total kinetic energy changes and this energy excites or de-excites the internal modes of the target (the diatom in our case).

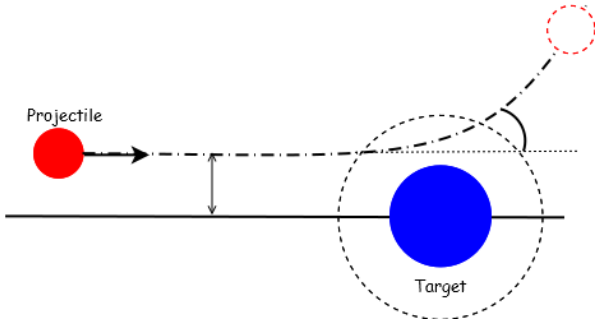

Figure 1.1: A general idea of scattering

Since what we are trying to understand are the collisions between atoms and molecule, we HAVE to delve in the quantum space. (All is not well with classical mechanics! - Shankar, 1994). So what we essentially formalize here is to appropriate the Quantum scattering Theory to study the van der waals

complexes formed by the colliding partners and the molecule of interest and find the scattering cross-section, from which we can get the rate co-efficients. The explanations given in this chapter are based on my understanding of the selected chapters of following textbooks: Griffiths (2017), Child (1996), J. Taylor (1972) and Atkins et al. (2011).

In Quantum mechanics, a system is described by a wavefunction Ψ and the wavefunction $\Psi(x,t)$ evolves in time as

$$i\hbar\frac{\partial\Psi}{\partial t} = H\Psi \tag{1.1}$$

where, $\hbar$ is the reduced planck's constant, and H is an operator called the the Hamiltonion, which actually characterises system that is being studied. This equation can be separated into equations based on the time and space components of the wavefunction, i.e,

$$\Psi(x,t) = \psi(x).\phi(t) \tag{1.2}$$

Substituting 1.2 in 1.1 (and skipping the intermediate steps where we actually separate the variables) we get

$$\boxed{H\psi = E\psi} \tag{1.3a}$$

$$i\hbar\frac{d\phi}{dt} = E\phi \tag{1.3b}$$

where, E is the constant in the dimensions of energy and equates to both left hand side (LHS) and right hand side (RHS) of the equation 1.1. Since time-independent wavefunction satisfies equation 1.3a, this equation is called the time-independent Schrödinger equation and E represents the state of Energy the system is in. For the purpose of computation, we always use the time-independent Schrödinger equation and so, any further mention of "Schrödinger equation" should be, by default, read as **time-independent Schrödinger equation**.

1.1 Quantum scattering

Scattering theory is a very extensive subject and there are several ways to define the scattering and the scattering cross section. I would like to present here, one of the explanations of quantum scattering (QS) and the derivation of scattering cross-section. In this section, I introduce the basics of QST

and in the next chapters move on the theory specific to a computationally feasible, system specific case(s).

The Figure 1.2 gives us a rough idea of how scattering occurs. The colliding

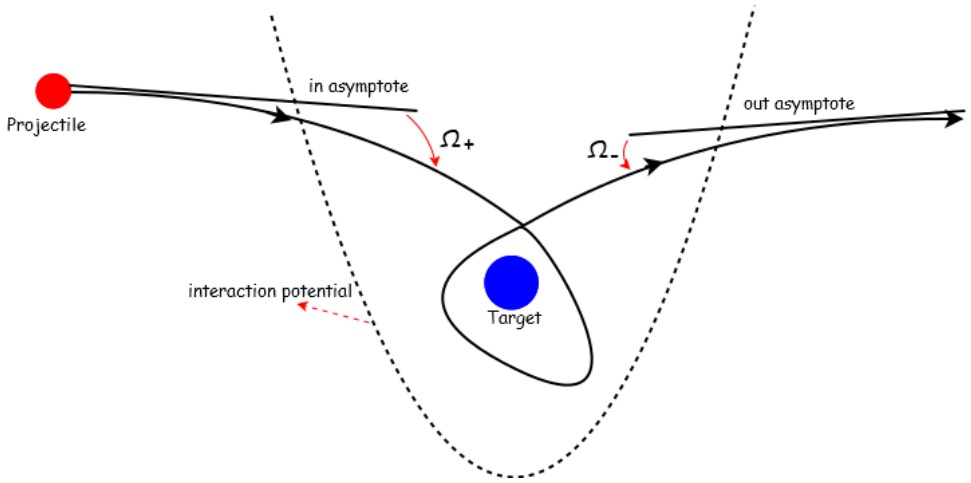

Figure 1.2: A general representation of scattering for an attractive potential

projectile approaches the target; takes an orbit in the interacting region (which will be later defined by the potential (V); the colliding partner departs and moves away from the target. Even though the actual computation is in the time-independent scattering theory domain, we start with the description in the time-dependent scattering to describe the salient features of QS and as the discussion progresses, we will move to the time-independent domain. As we can see that the orbit in the interacting region is very complicated, we ignore the precise details of the orbits while mathematically describing the scattering. Instead, we try to express these orbits in terms of asymptotes close to the approaching (incoming) and departing (outgoing) regions. In summary, we can define the terms as follows:

in asymptote	$\xrightarrow{\Omega_+}$	*actual orbit*	$\xleftarrow{\Omega_-}$	*out asymptote*
$\lvert\psi_{\text{in}}\rangle$	$\rightarrow$	$\lvert\psi\rangle$	$\leftarrow$	$\lvert\psi_{\text{out}}\rangle$

The $\Omega_\pm$ is the moller wave operator which evolves the wavefunction from

in/out asymptote to the actual orbit. That gives,

$$\begin{aligned} |\psi\rangle &= \Omega_{-} |\psi_{\text{out}}\rangle \\ \Rightarrow |\psi_{\text{out}}\rangle &= \Omega^{\dagger}_{-} |\psi\rangle \\ &= \Omega^{\dagger}_{-}\Omega_{+} |\psi_{\text{in}}\rangle \end{aligned} \tag{1.4}$$

If we define an operator, S such that

$$\boxed{S = \Omega^{\dagger}_{-}\Omega_{+}}$$

this gives,

$$|\psi_{\text{out}}\rangle = S |\psi_{\text{in}}\rangle \tag{1.5}$$

Since this operator S relates $|\psi_{\text{out}}\rangle$ directly to the $|\psi_{\text{in}}\rangle$, this is called the *scattering operator*.
We can represent the wavefuntion in terms of an improper momentum eigenvector of the Hamiltonion (In the proceeding chapters you will notice how this will be replaced by the quantum number for the molecular cases).

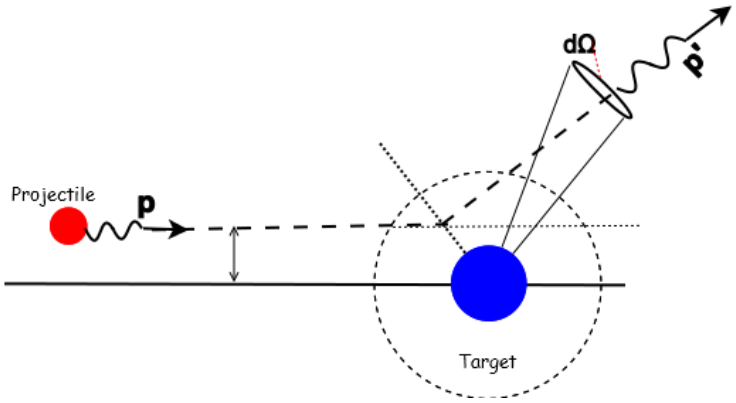

Figure 1.3: Incoming projectile with momentum $|\boldsymbol{p}\rangle$ scattering to an outcoming momentum $|\boldsymbol{p'}\rangle$ through a solid angle dΩ

If Figure 1.3 represnts the scattering, then

$$\begin{aligned} \psi_{\text{in}}(\mathbf{p}) &= \langle \mathbf{p} | \psi_{\text{in}} \rangle \\ \psi_{\text{out}}(\mathbf{p\prime}) &= \langle \mathbf{p\prime} | \psi_{\text{out}} \rangle \end{aligned} \tag{1.6}$$

with the above definition, we write the scattering operator S in the momentum representation as $\langle \boldsymbol{p'} | S | \boldsymbol{p} \rangle$ and this is the *"S-matrix"*. We can

hence think of S-matrix as the probability amplitude that an in state with momentum $\mathbf{p}$ gives an out state with momentum $\mathbf{p\prime}$.
Let us now define an operator $\mathbf{R}$ as $\mathbf{S = 1+R}$.

Since $\mathbf{S}$ commutes with the hamiltonion operator $\mathbf{H}$, $\mathbf{R}$ also commutes with $\mathbf{H}$. That implies,

$$\langle \mathbf{p}' | \, R \, | \mathbf{p} \rangle = -2\pi i . \delta(E_{\mathbf{p}'} - E_{\mathbf{p}}) t(\mathbf{p}' \leftarrow \mathbf{p}) \tag{1.7}$$

Substituting eq. 1.5 in $\mathbf{S = 1+R}$, we get

$$\langle \mathbf{p}' | \, S \, | \mathbf{p} \rangle = \delta(\mathbf{p}' - \mathbf{p}) - 2\pi i . \delta(E_{\mathbf{p}'} - E_{\mathbf{p}}) t(\mathbf{p}' \leftarrow \mathbf{p}) \tag{1.8}$$

The term t($\mathbf{p}' \leftarrow$$\mathbf{p}$) is defined as the *"on-shell"* T- matrix. The scattering amplitude is given by,

$$f(\mathbf{p}' \leftarrow \mathbf{p}) = -(2\pi)^2 m \; t(\mathbf{p}' \leftarrow \mathbf{p}) \tag{1.9}$$

This is gives us,

$$\boxed{\langle \mathbf{p}' | \, S \, | \mathbf{p} \rangle = \delta(\mathbf{p}' - \mathbf{p}) + \frac{i}{2\pi m} . \delta(E_{\mathbf{p}'} - E_{\mathbf{p}}) f(\mathbf{p}' \leftarrow \mathbf{p})} \tag{1.10}$$

For the figure 1.3, the probabibility, w of the particle emerging with momentum, $\mathbf{p\prime}$ anywhere in the element of the solid angle, $d\Omega$ is given by

$$w(d\Omega \leftarrow \psi_{\text{in}}) = d\Omega \int_0^\infty p'^2 \, dp' \, |\psi_{\text{out}}(p')|^2 \tag{1.11}$$

The total number of particles scattering into dΩ is given by $\mathrm{N_{out}}$;

$$\begin{aligned} N_{\text{out}}(d\Omega) &= \int d^2p \, n_{\text{in}} \, w(d\Omega \leftarrow \psi_{\text{in}}) \\ \Rightarrow \frac{N_{\text{out}}(d\Omega)}{n_{\text{in}}} &= \int d^2p \, w(d\Omega \leftarrow \psi_{\text{in}}) \\ \Rightarrow \sigma(d\Omega \leftarrow \psi_{\text{in}}) &= \int d^2p \, w(d\Omega \leftarrow \psi_{\text{in}}) \end{aligned} \tag{1.12}$$

$\sigma(d\Omega \leftarrow \psi_{\text{in}})$ is the cross section for the scattering of the particles and coming out through the solid angle dΩ. Using eqs. 1.5 in 1.6 and writing it in integral form gives,

$$\psi_{\text{out}}(\mathbf{p}') = \int d^3p \; \langle \mathbf{p}' | \, S \, | \mathbf{p} \rangle \; \psi_{\text{in}}(\mathbf{p}) \tag{1.13}$$

Substituting eq. 1.10 in 1.13 we get,

$$\psi_{\text{out}}(\mathbf{p}') = \int d^3p \left[\delta(\mathbf{p}' - \mathbf{p}) + \frac{i}{2\pi m}.\delta(E_{\mathbf{p}'} - E_{\mathbf{p}}) f(\mathbf{p}' \leftarrow \mathbf{p})\right] \psi_{\text{in}}(\mathbf{p})$$
$$\Rightarrow \psi_{\text{out}}(\mathbf{p}') = \psi_{\text{in}}(\mathbf{p}) + \frac{i}{2\pi m} \int d^3p\ \delta(E_{\mathbf{p}'} - E_{\mathbf{p}}) f(\mathbf{p}' \leftarrow \mathbf{p}) \psi_{\text{in}}(\mathbf{p}) \quad (1.14)$$

Substituting eq. 1.14 in 1.11 and hence in eq. 1.12, we get

$$\begin{aligned} & \sigma(d\Omega \leftarrow \psi_{\text{in}}) = d\Omega |f(\mathbf{p}' \leftarrow \mathbf{p})|^2 \\ \Rightarrow \quad & \frac{d\sigma}{d\Omega}(\mathbf{p}' \leftarrow \mathbf{p}) = |f(\mathbf{p}' \leftarrow \mathbf{p})|^2 \quad \left\{ \because \sigma(d\Omega \leftarrow \mathbf{p}) = \frac{d\sigma}{d\Omega}(\mathbf{p}' \leftarrow \mathbf{p})\ d\Omega \right\} \\ & \sigma(\mathbf{p}' \leftarrow \mathbf{p}) = \oint \frac{d\sigma}{d\Omega}(\mathbf{p}' \leftarrow \mathbf{p})\, d\Omega \\ & \sigma(\mathbf{p}' \leftarrow \mathbf{p}) = \oint |f(\mathbf{p}' \leftarrow \mathbf{p})|^2 d\Omega \end{aligned} \quad (1.15)$$

Looking back at eq 1.9,

$$f(\mathbf{p}' \leftarrow \mathbf{p}) = \underbrace{-(2\pi)^2 m}_{\text{A}}\ \underbrace{t(\mathbf{p}' \leftarrow \mathbf{p})}_{\langle \mathbf{p}' | T | \mathbf{p} \rangle}$$

and from eq 1.15 we get,

$$\boxed{\sigma(\mathbf{p}' \leftarrow \mathbf{p}) = A^2 \oint |\langle \mathbf{p}' | T | \mathbf{p} \rangle|^2 d\Omega} \quad (1.16)$$

Hence we have described the Total scattering *cross section* in terms of the on-shell T *matrix*. So, with this idea of cross-section (which is the what we want to calculate), we move to the case specific to our interest, that is, scattering phenomenon in a molecular system. For doing that, first we need to theoretically describe a molecular system.

1.2 Describing a molecular system

In quantum mechanics, the molecular system is described by the Hamiltonian opertor which is defined by the total energy of the constituent electrons and nuclei. If we ignore the spin (we will introduce the effect of spin later!), the system can be described by a coulomb Hamiltonian i.e., the Hamiltonian is a sum of the kinetic energies of electrons, nuclei and the coulomb interactions

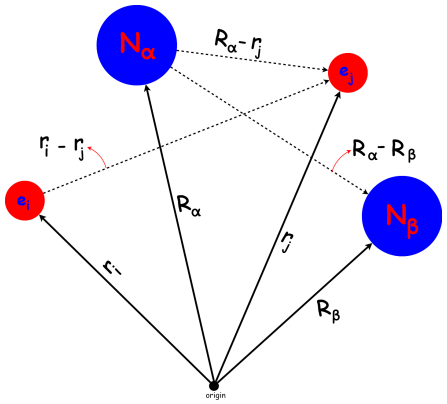

Figure 1.4: A representation of co-ordinates for a system of electrons and nuclei

between them. For a molecular system of n electrons and N nuclei with co-ordinates as represented in fig. 1.4, the Hamiltonian is given by,

$$H = \overbrace{-\frac{\hbar^2}{2}\sum_{\alpha=1}^{N}\frac{1}{M_\alpha}\boldsymbol{\nabla}_\alpha^2}^{\text{Nuclear Kinetic Energy}} \overbrace{-\frac{\hbar^2}{2m_e}\sum_{i=1}^{n}\boldsymbol{\nabla}_i^2}^{\text{Electronic Kinetic Energy}} + \frac{e^2}{4\pi\epsilon_0}\left(\underbrace{\sum_{i,j=1}^{n}\frac{1}{|r_i - r_j|}}_{\text{electron-electron repulsion}} + \underbrace{\sum_{\alpha,\beta=1}^{N}\frac{Z_\alpha Z_\beta}{|R_\alpha - R_\beta|}}_{\text{Nuclear-Nuclear repulsion}} - \underbrace{\sum_{i=1}^{n}\sum_{\alpha=1}^{N}\frac{Z_\alpha}{|r_i - R_\alpha|}}_{\text{electron-nuclear attraction}}\right) \tag{1.17}$$

where, M_α is the mass of α^{th} nuclei, m_e is the mass of the electron, R_α is the distance between origin and the α^{th} nuclei, r_i is the distance between origin and the i^{th}, $\boldsymbol{\nabla}^2$ is the Laplace operator, e is the charge of the electron, ϵ_0 is

the permittivity in vacuum and Z is the atomic number. If,

$$-\frac{\hbar^2}{2}\sum_{\alpha=1}^{N}\frac{1}{M_\alpha}\boldsymbol{\nabla}_\alpha^2 = T_N(\mathbf{R}) \tag{1.18}$$

$$-\frac{\hbar^2}{2m_e}\sum_{i=1}^{n}\boldsymbol{\nabla}_i^2 = T_e(\mathbf{r}) \tag{1.19}$$

$$\frac{e^2}{4\pi\epsilon_0}\sum_{i,j=1}^{n}\frac{1}{|r_i - r_j|} = V_{ee}(\mathbf{r}) \tag{1.20}$$

$$\frac{e^2}{4\pi\epsilon_0}\sum_{\alpha,\beta=1}^{N}\frac{Z_\alpha Z_\beta}{|R_\alpha - R_\beta|} = V_{NN}(\mathbf{R}) \tag{1.21}$$

$$-\frac{e^2}{4\pi\epsilon_0}\sum_{i=1}^{n}\sum_{\alpha=1}^{N}\frac{Z_\alpha}{|r_i - R_\alpha|} = V_{eN}(\mathbf{r},\,\mathbf{R}) \tag{1.22}$$

In short, the Hamiltonian can be written as,

$$\boxed{H = T_N(\mathbf{R}) + T_e(\mathbf{r}) + V_{ee}(\mathbf{r}) + V_{NN}(\mathbf{R}) + V_{eN}(\mathbf{r},\,\mathbf{R})} \tag{1.23}$$

CHAPTER 2

Born-oppenheimer approximation and Potential Energy Surface

"I can make it clearer; I can't make it simpler."

— J. R. Oppenheimer

As we saw in the previous chapter (eq 1.3a), the schrödinger equation is given by

$$H\Psi(\mathbf{r},\mathbf{R}) = E\Psi(\mathbf{r},\mathbf{R}) \tag{2.1}$$

If the Hamiltonian consisted of only pure functions of $\mathbf{r}$ and $\mathbf{R}$, we could have decoupled the equation as we could have written the wavefunction as a product of nuclear and electronic terms,

$$\Psi(\mathbf{r},\mathbf{R}) = \psi(\mathbf{r})\chi(\mathbf{R}) \tag{2.2}$$

But unfortunately, because of the term $V_{eN}(\mathbf{r},\mathbf{R})$, it is not possible. To overcome this hurdle, we use the Born-Oppenheimer approximation.

2.1 The Born-Oppenheimer approximation

In simple words, the Born-Oppenheimer (BO) approximation allows us to separate the nuclear and electronic parts. In this section I will just briefly introduce the BO approximation. For a detailed explanation i would direct the "interested" readers to the Born et al., 1927, its translation by S.M.Blinder, 1998, and Pauling et al., 1935. The physical basis for the BO approximation is the difference in the masses of the atomic nuclei and the electrons. The nuclear constituents are more than 1000 times greater than the mass of

the electrons and with this the Hamiltonian can be approximated in two ways:

(i). Since the acceleration of a particle is inversely proportional to its mass, the electrons are moves (or accelerates) very fast, with respect to the nucleus. So the nucleus is "almost" fixed with respect to the electronic motion. Or, in other words the nuclear distance ($\mathbf{R}$) is parameterized and hence its no more an operator. that is from eq 1.22,

$$V_{\text{eN}}(\mathbf{r},\mathbf{R}) \Rightarrow V_{\text{eN}}(\mathbf{r};\mathbf{R}) \tag{2.3}$$

(ii). The next approximation directly stems from the mass difference. Let us define some γ such that

$$\gamma = \frac{m_e}{M} \qquad \{\text{M is total nuclear mass}\}$$
$$M_\alpha = \frac{m_e}{\gamma \mu_\alpha} \qquad \{\mu_\alpha \text{ is the reduced mass}\}$$

Using this in eq 1.18,

$$\begin{aligned} T_N(\mathbf{R}) &= -\gamma \frac{\hbar^2}{2m_e} \sum_{\alpha=1}^{N} \mu_\alpha \boldsymbol{\nabla}_\alpha^2 \\ T_N(\mathbf{R}) &= -\gamma T'_N(\mathbf{R}) \end{aligned}$$

If,

$$H_{\text{el}} = T_e(\mathbf{r}) + V_{ee}(\mathbf{r}) + V_{NN}(\mathbf{R}) + V_{eN}(\mathbf{r};\, \mathbf{R})$$

then, eq 1.23 becomes,

$$H = H_{\text{el}} - \gamma T'_N(\mathbf{R})$$

And so, the eq 2.1 becomes,

$$\left\{ H_{\text{el}} - \gamma T'_N(\mathbf{R}) \right\} \Psi(\mathbf{r},\mathbf{R}) = E\, \Psi(\mathbf{r},\mathbf{R}) \tag{2.4}$$

Since mass of the nucleus is huge when compared to mass of the electron, the ratio $\frac{m_e}{M}$ is infinitesimally small. Hence γ **is approximately equal to zero** and eq 2.4 becomes,

$$H_{\text{el}}\, \psi(\mathbf{r},\mathbf{R}) = E_{\text{el}}\, \psi(\mathbf{r},\mathbf{R}) \tag{2.5}$$

From eq 2.3, since R is parameterized, the Hamiltonian (H_{el}) and the corresponding Energy (E_{el}) is also parameterized. That is, eq 2.5 becomes,

$$\boxed{H_{\mathrm{el}}(\mathbf{R})\,\psi(\mathbf{r};\mathbf{R}) = E_{\mathrm{el}}(\mathbf{R})\,\psi(\mathbf{r};\mathbf{R})} \tag{2.6}$$

Substituting eq 2.6 back in eq 2.4 and considering the fact the resulting Hamiltonian is purely dependent on $\mathbf{R}$, we get,

$$\boxed{\left\{T_{\mathrm{N}}(\mathbf{R}) + E_{\mathrm{el}}(\mathbf{R})\right\}\psi_{\mathrm{N}}(\mathbf{R}) = E(\mathbf{R})\,\psi_{\mathrm{N}}(\mathbf{R})} \tag{2.7}$$

With eq 2.6 and 2.7, the total hamiltonian has been approximately separated into electronic and nuclear parts using Born-Oppenheimer approximation. How?

- Eq 2.6 is solely the Hamiltonion containing terms that affect the electron. Hence it is the **electronic Schrödinger equation**. We can fix a particular $\mathbf{R}$ (clamped-nuclei) and solve for the wavefunction $\psi(\mathbf{r};\mathbf{R})$ and repeat the same for a range of $\mathbf{R}$. This gives a set of eigenvalues (E_{el}) which forms the *Potential Energy Surface (PES)*. Infact this the key feature of BO approximation. It depicts the electronic structure of the system without bringing the nucleus into the picture.

- Once we solve the eq 2.6, we can write the Total Hamiltonian (H) in terms of nuclear kinetic energy and the PES as in eq 2.7. We can interpret this equation as the movement of the nuclei along the PES of the system. Hence we can call the eq 2.7 as the **"Nuclear Schrödinger equation"** and solving this will give us the scattering cross section for the system.

2.2 Electronic Schrödinger equation and Potential Energy Surface

In this section, a short account of solving the Electronic Schrödinger equation (eq 2.6) to arrive at the PES is presented. We keep this section short, just touching the salient features of the solving technique, because it is not the main focus of this thesis. Yet it is a significant step towards finding the cross-section (as explained in the chapter 1, is the main goal).

From the previous section, we know that the Hamiltonian for the electronic part is given by

$$H_{\mathrm{el}} = -\frac{\hbar^2}{2m_e}\sum_{i=1}^{n}\boldsymbol{\nabla}_i^2 + \frac{e^2}{4\pi\epsilon_0}\sum_{i,j=1}^{n}\frac{1}{|r_i - r_j|} - \frac{e^2}{4\pi\epsilon_0}\sum_{i=1}^{n}\sum_{\alpha=1}^{N}\frac{Z_\alpha}{|r_i - R_\alpha|} + constant \tag{2.8}$$

We can solve this in two ways: one is the *ab intio* method and the other is the semi-empirical method. The choice is made based on the level of accuracy needed and the affordability of computational cost. In this thesis, all the PES are calculated *ab initio*, so we discuss only the *ab intitio* calculation technique. In this method, the electronic wavefunction ($\psi(\mathbf{r;R})$) is defined using a model and the eq 2.6 is solved with just the knowledge of the fundamental values of the atoms in the system. To determine this (electronic) wavefunction, a self-consistent field method called the Hartree-Fock method is first used.

2.2.1 Hartree-Fock (self-consistent field) method

The main difficulty in solving the eq 2.6 is the presence of the electron-electron repulsion term $V_{ee}(\boldsymbol{r})$ in the Hamiltonian because it depends on the electron-electron separation $(r_i - r_j)$. Let us assume that the total electronic wavefunction, ψ is almost similar to a wavefunction, ψ_{e}, which is defined by the schrödinger equation

$$H_{\mathrm{e}}\psi_{\mathrm{e}} = E_{\mathrm{e}}\psi_{\mathrm{e}} \tag{2.9}$$

where, H_e is given by T_e (eq 1.19) + V_{eN} (eq 1.21), and the summation in the eq 1.19 denotes that the many-electron system can be written in terms of unperturbed n-single-electrons, if we ignore the interactions between the electrons. That is,

$$H_{\mathrm{e}} = \sum_{i=1}^{n} h_{\mathrm{i}} \qquad \left\{ \because h_{\mathrm{i}} = -\frac{\hbar^2}{2m_e}\boldsymbol{\nabla}_i^2 - \frac{Ze^2}{4\pi\epsilon_0}\frac{1}{|r_i - R|} \right\} \tag{2.10}$$

(P.S: This is only an exceptional case in this thesis where the Hamiltonian is denoted by a *lowercase* (h) character.)
Now, this eq 2.10 can be separated into n single-electron wave equations with the wavefunction $\psi_a(\boldsymbol{r_i;R})$, where a represents the orbital occupied by the electron and $\mathbf{r_i}$ is the co-ordinate of the i^{th} electron. In short, this can be denoted as $\psi_a(i)$.

$$h_{\mathrm{i}}\psi_{\mathrm{a}}(i) = E_{\mathrm{a}}\psi_{\mathrm{a}}(i) \tag{2.11}$$

The wavefunction ψ_e is product of all the one-electron wavefunctions:

$$\psi_{\mathrm{e}} = \psi_{\mathrm{a}}(1)\psi_{\mathrm{b}}(2)\psi_{\mathrm{c}}(3).....\psi_{\mathrm{z}}(n) \tag{2.12}$$

If we consider the spin of the electrons, then these wavefunctions must obey the Pauli's exclusion principle. That means if one electron in the orbital a has a spin up ($\uparrow$), then the other electron in the same orbital cannot have the same spin. This can be represented by one of the pauli matrices σ_3 and the wavefunction for a particular orbital would be

$$\psi_{\mathrm{a}} = \frac{1}{\sqrt{2}}\psi_{\mathrm{a}}(1)\psi_{\mathrm{a}}(2)(\uparrow(1)\downarrow(2) - \downarrow(1)\uparrow(2)) \tag{2.13}$$

This introduces the concept of spinorbitals which is defined as

$$\psi_a^{\uparrow}(1) = \psi_a(1)\uparrow(1) \qquad \psi_a^{\downarrow}(1) = \psi_a(1)\downarrow(1)$$
$$\psi_a^{\uparrow}(2) = \psi_a(2)\uparrow(2) \qquad \psi_a^{\downarrow}(2) = \psi_a(2)\downarrow(2)$$

Each term in the previous equation is a unique spinorbital and can be represented as $\phi_u(i)$ where u represents the combination of orbital and spin. This single orbital in eq 2.13 can be represented in the form of a determinant.

$$\psi_{\mathrm{a}} = \frac{1}{\sqrt{2}}\begin{vmatrix}\phi_i(1) & \phi_j(1)\\ \phi_i(2) & \phi_j(2)\end{vmatrix} \tag{2.14}$$

The determinant in the eq 2.14 is a Slater determinant. If we extend this single orbital wavefunction to all the orbitals consisting of n-electrons, eq 2.12 can be written in terms of Slater determinant consisting of $n \times n$ elements:

$$\psi_e = \frac{1}{\sqrt{n!}}\begin{vmatrix}\phi_x(1) & \phi_y(1) & \dots & \phi_z(1)\\ \phi_x(2) & \phi_y(2) & \dots & \phi_z(2)\\ \vdots & \vdots & \vdots & \vdots\\ \phi_x(n) & \phi_y(n) & \dots & \phi_z(n)\end{vmatrix} \tag{2.15}$$

In order to find the wavefunction,ψ_e, of the system of n-electrons, we can solve for individual spinorbitals $\phi_u(i)$ using the wave equation called the **Hartree-Fock (HF) equation**:

$$f_i\phi_x(i) = \varepsilon_x\phi_x(i) \tag{2.16}$$

ε_x is the spinorbital energy and f_i is the **fock operator** which incorporates the (previously ignored) electron-electron repulsion term, $\mathrm{V_{ee}}(\mathbf{r})$ as a coulomb operator (J_u) and exchange operator (K_u). The fock operator is defined as:

$$f_i = h_i + \sum_u (J_u(i) - K_u(i)) \tag{2.17}$$

Both the operators $J_u(i)$ and $K_u(i)$ are defined in terms of all spinorbitals ϕ_u. That is, to solve for one spinorbital using eq 2.16, we need the information

about all the other spinorbitals which is like a paradoxial situal! This is overcome by a method of successive approximations until a convergence is achieved. In this method, first a trial set of spinorbitals assumed and the fock operator is formed and using that the HF equations are solved to get a new set of spinorbitals. This new set of spinorbitals are once again used to form a new fock operator and the same procedures are repeated until a self-consistent solution is reached. The choice of the intial trial set depends on the number of electrons (n) in the system and the accuracy of the calculation because for a system of n electrons, the system can have a finite n occupied spinorbitals and also an infinite number of unoccupied spinorbitals which are eigenfunctions of the spinorbital energy. Further details of the trial set are given in the section 2.2.3.

2.2.2 Electronic correlation

Though the fock operator (eq 2.17) incorporates the electron-electron interactions, they are just averages. They are neither instantaneous nor do they account for the electronic distribution. Hence the HF equation does not acknowledge the electron correlations. There are several methods to introduce this correlation in the calculations. In this thesis we have used the coupled cluster method for all our PES calculations, hence we will discuss only this electronic correlation method in this section. For other methods, one can refer to Atkins et al. (2011), Lewars (2010) and R. Bernstein (2013).

2.2.2.1 Coupled Cluster (CC) method

This method introduces a cluster operator C which relates the exact electronic wavefunction, ψ to the wavefunction ψ_e as:

$$\psi = e^C \psi_e$$

and e^C can be series expanded as

$$e^C = 1 + C + \frac{1}{2!}C^2 + \frac{1}{3!}C^3 + \frac{1}{4!}C^4 + ...$$

and the Cluster operator is defined as

$$C = C_1 + C_2 + \ldots + C_n$$

where $\mathbb{C}_n$ is the n-electron excitation operator (i.e, C_1 is 1-electron operator and so on). If the HF wavefuction,ψ_e (eq 2.15) can be written in short as:

$$\psi_e = \|\phi_1 \phi_2 \ldots \phi_l \phi_m \ldots \phi_n\|$$

ϕ_l, ϕ_m are some random occupied spinorbital among the n occupied spinorbitals. Now, a singly excited wavefunction is a single electron is excited from a occupied spinorbital to an unoccupied spinorbital. i.e,

$$\psi'_e = \Phi_l^p = \|\phi_1\phi_2 \ldots \phi_{\mathbf{p}}\phi_m \ldots \phi_n\|$$

Similarly the doubly excited wavefunction can be written as

$$\psi''_e = \Phi_{lm}^{pq} = \|\phi_1\phi_2 \ldots \phi_{\mathbf{p}}\phi_{\mathbf{q}} \ldots \phi_n\|$$

etc.. So, the electron excition operator is given by

$$\begin{aligned} C_1\psi_e &= \sum_{l,p} c_l^p \Phi_l^p \\ C_2\psi_e &= \sum_{l,m,p,q} c_{lm}^{pq} \Phi_{lm}^{pq} \end{aligned}$$

and similarly for C_3 and so on up to C_n. c is the excitation amplitude. So finally the electronic schrödinger equation that is to be solved looks something like

$$\boxed{H_{el}e^C\psi_e = E_{el}e^C\psi_e}$$

While CC method is applied in computations, a few approximations are made. First, the taylor series expansion is finite (since terms beyond C_1^n and so on cannot exist). Second, the C operator includes only specific excitiation. For example, If C is truncated at C_1+C_2, then the approach is called **c**oupled **c**luster **s**ingle **d**ouble excitation (**CCSD**). If C = C_1+C_2+C_3 it is called **CCSDT**. The CC approach is an iterative (variational) technique. As accurate as it is, once we consider higher order excitation for a system with large number of electrons, the computation cost increases beyond practical limits. To overcome, the CC aproach is combined with a non-iterative approach for higher order terms (Raghavachari et al., 1989) . For example, if CC theory is followed for singles and doubles and for the triples, the non-iterative (perturbation) approach is used, it is referred to as **CCSD(T)**.

2.2.3 Basis sets

At the end of section 2.2.1, the trial sets for the HF approach was discussed. Since these are a set of spinorbitals, these are set of basis functions that represent the spinorbitals exactly. Ideally the set must contain infinite number of basis functions because the trial set must consist of infinite number of unoccupied spinorbitals too. But in the computational point of view, this is impossible. Hence a finite basis set has to be chosen taking

into account the computational cost and accuracy. Several basis sets are used in ab initio calculations and new (and better) basis sets keep getting added every now and then. So the posssibilities are infinite! In this thesis, the basis set developed by T.H.Dunning and coworkers (Dunning, 1989) has been used. These are especially designed for post-HF calculations (electronic correlation) and hence the name "*correlation-consistent (cc)*". The usual designation of the cc-set is like "*cc*-pVXZ" where p is for the polarization function, V for valence, X for the number of shells the valence function contains (X could be Double, Triple, quadruple,etc...) and Z stands for zeta. For example, cc-pVDZ denotes *correlation consistent-polarized valence-only Doubly-split zeta* basis set. This basis set can be further augmented to include diffuse functions for lang-range interactions. In that case the basis set is designated as *aug-cc*-pVXZ (X=D,T,Q,5,.....). These basis set can also converge systematically to the complete-basis-set (CBS) limit using empirical extrapolation techniques.

2.3 Analytic representation

The objective of this thesis is to use these *ab initio* electronic potential values to calculate the total wavefunction of the system using eq 2.7 and hence the cross sections. In the next chapter, we will see that solution to eq 2.7 involves solving second-order differential equations by "close coupling" approach in which the equations are expanded in spherical coordinates. So it is necessary to expand our *ab initio* electronic potentials analytically in such a way that it is easily accessible for furthur calculations. Also, it is important to correctly incorporate all the symmetries and angular variations of the system in these analytic form. To represent this, we choose a set of coordinates which can be easily translated while using the PES for dynamic calculations. Fig 2.1 represents the jacobi coordinates for a AB+CD system.

r_{AB} and r_{CD} are the bond lengths of the diatoms AB and CD, R is the distance between the centre-of-masses of AB and CD, Θ is the angle between R and r_{AB}, Θ' the angle between R and r_{CD} and ϕ is the rotation of CD about R. For a AB+C system, R would become the distance between c.o.m of AB and C, Θ' and ϕ will vanish.
For now, let us assume that AB and CD are rigid rotors, which implies r_{AB} and r_{CD} are constants. Therefore, if V represents the analytic form of the PES in the above mentioned coordinates, then $V \equiv V(R,\Theta,\Theta',\phi)$ (and for AB+C system read $V \equiv V(R,\Theta)$). There are several possible analytic forms

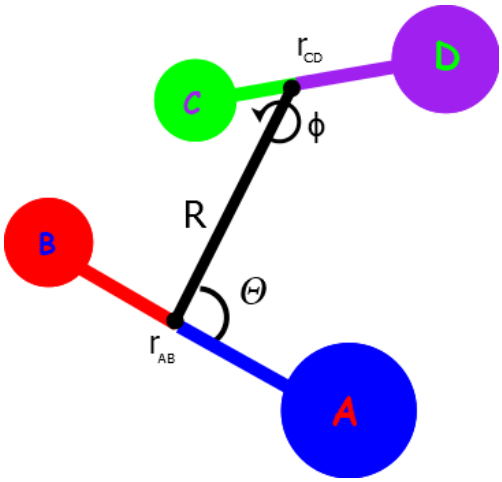

Figure 2.1: A representation of jacobi coordinate.

of a system, but in general, the analytic representation takes the form:

$$V(R, \Theta, \Theta', \phi) = \sum_{\lambda} E_{el}^{\lambda}(R) X_{\lambda}(0, \Theta, \Theta', \phi)$$

where λ is the λ^{th} point on the grid of *ab initio* electronic potential values and X is the angular function.
For the AB+C system the same would be

$$V(R, \Theta) = \sum_{\lambda} E_{el}^{\lambda}(R) X_{\lambda}(0, \Theta)$$

CHAPTER 3

Nuclear Schrödinger equation and Cross Section

"I insist upon the view that 'all is waves'. "

— Erwin Schrödinger

After solving the electronic Schrödinger equation for E_{el} and constructing the PES, next step is to solve the eq 2.7 type equation using the PES. In the chapter 1, we described a very general molecular system consisting of electrons and nucleus. In this chapter, we will further sophisticate the description of our system. We are interested in the collision between atom and diatom/diatom and diatom. Since our focus is only on the nuclear part, if we are to assume that the diatom does not have any vibrational degree of freedom, the diatom becomes a linear rigid rotor.

If we consider the spherical coordinates representing the system to be fixed in space as in fig 3.1, and translate the AB molecule such that its centre of mass coincides with the origin, then the coordinates of AB and CD would be $\mathbf{r} \equiv \mathbf{r}(\theta, \phi)$ and $\mathbf{r}' \equiv \mathbf{r}'(R, \theta', \phi')$ respectively. The total Hamiltonian (the LHS of eq 2.7) in this coordinate system becomes

$$H = H_{\mathrm{AB}}(\mathbf{r}) + H_{\mathrm{CD}}(\mathbf{r}') + T_{\mathrm{N}}(R) + V(R, \Theta)$$

In this chapter we only focus on the collision between a diatom and an atom, say AB + C. Therefore, the $H_{CD} = 0$ and hence

$$H = H_{\mathrm{AB}}(\mathbf{r}) + T_{\mathrm{N}}(R) + V(R, \Theta)$$

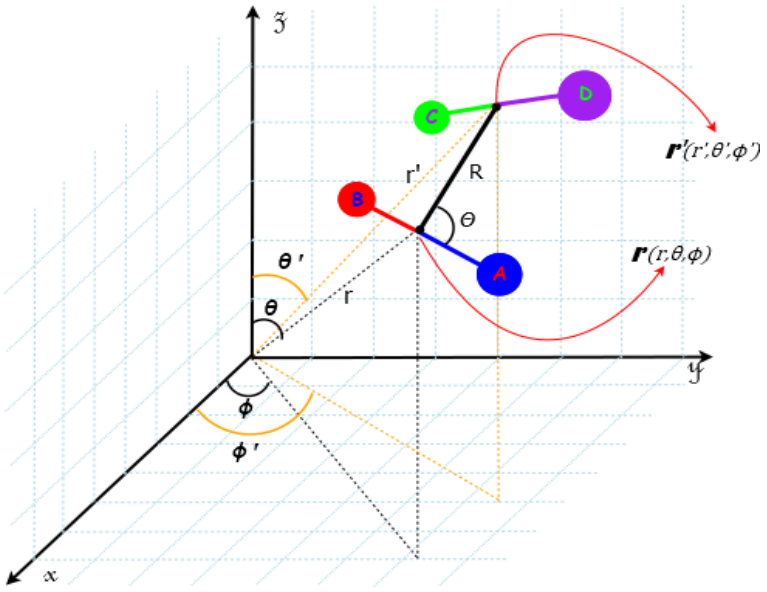

Figure 3.1: Space Fixed co-ordinates for a AB+CD system.

where,

$$H_{\mathrm{AB}} = \frac{\hbar^2}{2I}\mathbf{j}^2 \tag{3.1}$$

$$\begin{aligned} T_{\mathrm{N}}(R) &= -\frac{\hbar^2}{2\mu}\boldsymbol{\nabla}_R^2 \\ &= -\frac{\hbar^2}{2\mu}\left(\frac{\partial^2}{\partial R^2} - \frac{\mathbf{l}^2}{R^2}\right) \end{aligned} \tag{3.2}$$

I is the moment of inertia of the rigid rotor AB; $\boldsymbol{j}$ and $\boldsymbol{l}$ are rotational momentum operator of molecule AB and orbital angular momentum operator of the atom C respectively. The total angular momentum operator is then defined as $\boldsymbol{J} = \boldsymbol{j} + \boldsymbol{l}$ with J as its eigenvalue and M as the projection of J in the z-axis.

Note: The eigenvalues of angular momentum operator L_i is given as follows

$$\mathbf{L}^2 |n, m_n\rangle = n(n+1) |n, m_n\rangle$$
$$\mathbf{L}_z |n, m_n\rangle = m_n |n, m_n\rangle$$

If n is the angular momentum eigenstate, m_n is its projection in z-axis and its value (m_n= -n, -n+1,...,0,..., n-1, n).
In a spherically symmetric system, the eigenstates are given by the wavefunctions which are of the form

$$\psi(r, \theta, \phi) = u(r) Y_n^{m_n}(\theta, \phi) \tag{3.3}$$

where u(r) is the radial part of the wavefunction and $Y_n^{m_n}(\theta, \phi)$ is the spherical harmonics which is defined as

$$Y_n^{m_n}(\theta, \phi) = \langle \theta, \phi | n, m_n \rangle$$

Then the wave equation for the molecule AB is given by

$$H_{\mathrm{AB}} Y_j^{m_j}(\mathbf{r}) = \frac{\hbar^2}{2I} j(j+1) Y_j^{m_j}(\mathbf{r}) \tag{3.4}$$

If the atom C is approaching AB with a kinetic energy E, the total energy of the system for a particular rotational momentum j is

$$E_j = E + \frac{\hbar^2}{2I} j(j+1) \tag{3.5}$$

The total wavefunction of the system $\Psi_{jl}^J(R, \mathbf{r}, \mathbf{r}')$, for a particular *in state* $|j, l\rangle$(or input channel) satisfies the schrödinger equation for the total system

$$H \Psi_{jl}^J(R, \mathbf{r}, \mathbf{r}') = E_j \Psi_{jl}^J(R, \mathbf{r}, \mathbf{r}') \tag{3.6}$$

Since E_j is a sum of incident energy and the energy of the state of target particle, The wavefunction Ψ_{jl}^J is a superposition of initial and final states. The total wavefunction can be expanded in the form of eq 3.3 as

$$\Psi_{jl}^J(R, \mathbf{r}, \mathbf{r}') = \frac{1}{R} \sum_{j'l'} \mathscr{U}_{j'l'}^{Jjl}(R) \mathscr{Y}_{j'l'}^J(\mathbf{r}, \mathbf{r}') \tag{3.7}$$

where

$$\mathscr{Y}_{j'l'}^J(\mathbf{r}, \mathbf{r}') = \sum_{m_j, m_l} \langle j' l' m_j m_l | j' l' J M \rangle \, Y_{j'}^{m_j}(\mathbf{r}) Y_{l'}^{m_l}(\mathbf{r}') \tag{3.8}$$

and $\mathscr{U}^{Jjl}_{j'l'}(R)$, the radial part of the wavefunction, is a superposition of initial state (j,l) and a final (scattered) state (j',l'). For simplicity purpose, we write $\mathscr{U}^{Jjl}_{j'l'}(R)$ as $\mathscr{U}^{J}_{j'l'}(R)$.
Theoretically, j' and l' could have infinite values. But for computation, the terms are truncated at finite numbers until the result are converged to desired significant figures. Substituting eqs 3.1 3.2 3.7 in 3.6, we get

$$-\frac{\hbar^2}{2\mu R}\sum_{j'l'}\left(\frac{\mu}{I}\hat{\mathbf{j}}^2+\frac{\partial^2}{\partial R^2}-\frac{\mathbf{l}^2}{R^2}-\frac{2\mu}{\hbar^2}V(R,\Theta)-\frac{2\mu}{\hbar^2}E_j\right)\mathscr{U}^{J}_{j'l'}(R)\mathscr{Y}^{J}_{j'l'}(\mathbf{r},\mathbf{r}')=0 \tag{3.9}$$

$$\Rightarrow \frac{\hbar^2}{2\mu}\sum_{j'l'}\mathscr{Y}^{J}_{j'l'}(\mathbf{r},\mathbf{r}')\left(\frac{\mu}{I}j'(j'+1)+\frac{\partial^2}{\partial R^2}-\frac{l'(l'+1)}{R^2}-\frac{2\mu}{\hbar^2}E_j\right)\mathscr{U}^{J}_{j'l'}(R)$$
$$=\sum_{j'l'}\mathscr{U}^{J}_{j'l'}(R)V(R,\Theta)\mathscr{Y}^{J}_{j'l'}(\mathbf{r},\mathbf{r}')$$

$$\frac{\hbar^2}{2\mu}\sum_{j'l'}\mathscr{Y}^{J}_{j'l'}(\mathbf{r},\mathbf{r}')\left(\frac{\partial^2}{\partial R^2}-\frac{l'(l'+1)}{R^2}+k^2_{j'j}\right)\mathscr{U}^{J}_{j'l'}(R)=\sum_{j'l'}\mathscr{U}^{J}_{j'l'}(R)V(R,\Theta)\mathscr{Y}^{J}_{j'l'}(\mathbf{r},\mathbf{r}') \tag{3.10}$$

where

$$k^2_{j'j}=\frac{2\mu}{\hbar^2}\left(E_j-\frac{\hbar^2}{2I}j'(j'+1)\right) \tag{3.11}$$

If we orthonormalize the above equation by gram-schmidt process using $\mathscr{Y}^{J}_{j''l''}(\mathbf{r},\mathbf{r}')$, a wavefunction orthogonal to $\mathscr{Y}^{J}_{j'l'}(\mathbf{r},\mathbf{r}')$, we get

$$\boxed{\frac{\hbar^2}{2\mu}\left(\frac{\partial^2}{\partial R^2}-\frac{l'(l'+1)}{R^2}+k^2_{j'j}\right)\mathscr{U}^{J}_{j'l'}(R)=\sum_{j''l''}\mathscr{U}^{J}_{j''l''}(R)\left\langle j''l''JM\right|V(R,\Theta)\left|j'l'JM\right\rangle} \tag{3.12}$$

Hence we arrive at the coupled second order differential equation.These are called the **close-coupling equation**.

3.1 Close-coupling apprach

There are several approaches to solve the eq 3.12 type equations. In this section we discuss one of the most exact methods to mathematically solve

these equations. This approach is used to find the cross-sections throughout this thesis.
In the above equation we observe that we have two orthogonal sets of wavefunction, one that is defined by j, l and the other by j', l'. If we compare this with equations of chapter 1 , these are the in and out wavefunctions. that is, if $|j,l\rangle$ is the initial channel(momentum), $|j',l'\rangle$ is the final channel (momentum).
From the previous chapter, we know that the analytic representation of the electronic potential is, in general, of the form

$$V(R,\Theta) = \sum_{\lambda} E_{el}^{\lambda}(R) P_{\lambda}(\cos(\Theta)) \tag{3.13}$$

$\langle j''l''JM|\, V(R,\Theta)\, |j'l'JM\rangle$ in the eq 3.12 decomposes into

$$\begin{aligned}
\langle j''l''JM|\, V(R,\Theta)\, |j'l'JM\rangle &= \int\int \left(\mathscr{Y}^{J}_{j''l''}(\mathbf{r},\mathbf{r}')\right)^{*} V(R,\Theta)\mathscr{Y}^{J}_{j'l'}(\mathbf{r},\mathbf{r}')\,\mathrm{d}\mathbf{r}\,\mathrm{d}\mathbf{r}' \\
&= \int\int \left(\mathscr{Y}^{J}_{j''l''}(\mathbf{r},\mathbf{r}')\right)^{*} \sum_{\lambda} E_{el}^{\lambda}(R) P_{\lambda}(\cos(\Theta))\mathscr{Y}^{J}_{j'l'}(\mathbf{r},\mathbf{r}')\,\mathrm{d}\mathbf{r}\,\mathrm{d}\mathbf{r}' \\
&= \sum_{\lambda} E_{el}^{\lambda}(R) \underbrace{\int\int \left(\mathscr{Y}^{J}_{j''l''}(\mathbf{r},\mathbf{r}')\right)^{*} P_{\lambda}(\cos(\Theta))\mathscr{Y}^{J}_{j'l'}(\mathbf{r},\mathbf{r}')\,\mathrm{d}\mathbf{r}\,\mathrm{d}\mathbf{r}'}_{f_{\lambda}}
\end{aligned} \tag{3.14}$$

As we know from the Fig.3.1 that $\Theta = \theta - \theta'$, the legendre polynomial P(cos(Θ)) can be written as a function of $\mathbf{r}$ and $\mathbf{r}'$ as

$$P_{\lambda}(\cos(\Theta)) = \frac{4\pi}{2\lambda+1} \sum_{m_{\lambda}} Y_{\lambda}^{m_{\lambda}}(\mathbf{r})(Y_{\lambda}^{m_{\lambda}}(\mathbf{r}'))^{*} \tag{3.15}$$

Substituting eq 3.15 and eq 3.8 in RHS of eq 3.14,

$$\begin{aligned}
f_{\lambda} = \frac{4\pi}{2\lambda+1} \sum_{m_{\lambda},m_j,m_l} \int\int \langle j''l''JM|j''l''m_j m_l\rangle \langle j'l'm_j m_l|j'l'JM\rangle \\
\left(Y_{j''}^{m_j}(\mathbf{r})\right)^{*} (Y_{l''}^{m_l}(\mathbf{r}'))^{*} Y_{\lambda}^{m_{\lambda}}(\mathbf{r})(Y_{\lambda}^{m_{\lambda}}(\mathbf{r}'))^{*} Y_{j'}^{m_j}(\mathbf{r}) Y_{l'}^{m_l}(\mathbf{r}')\,\mathrm{d}\mathbf{r}\,\mathrm{d}\mathbf{r}'
\end{aligned} \tag{3.16}$$

It is an integral of multiple spherical harmonics. The solution to the integral summed over all the projections is

$$\boxed{f_{\lambda} = (-1)^{j'+j''-J}\sqrt{([j'][j''][l'][l''])}\begin{pmatrix} j'' & j' & \lambda \\ 0 & 0 & 0 \end{pmatrix}\begin{pmatrix} l'' & l' & \lambda \\ 0 & 0 & 0 \end{pmatrix}\begin{Bmatrix} j' & l' & J \\ l'' & j'' & \lambda \end{Bmatrix}} \tag{3.17}$$

where $[n]=2n+1$, $\begin{pmatrix}\cdots\\ \cdots\end{pmatrix}$ and $\begin{Bmatrix}\cdots\\ \cdots\end{Bmatrix}$ are wigner 3j and 6j symbols (for the definition refer to Edmonds, 1957 and Rose, 1957).
Therefore, $f_\lambda \equiv f_\lambda^J(j''l'' \leftarrow j'l')$. Substiting this in eq 3.14 gives

$$\langle j''l''JM|\, V(R,\Theta)\, |j'l'JM\rangle = \sum_\lambda E_{el}^\lambda(R) f_\lambda^J(j''l'' \leftarrow j'l') \tag{3.18}$$

And eq 3.12 becomes

$$\frac{\hbar^2}{2\mu}\left(\frac{\partial^2}{\partial R^2} - \frac{l'(l'+1)}{R^2} + k_{j'j}^2\right)\mathscr{U}_{j'l'}^J(R) = \sum_{j''l''\lambda} e_\lambda(R) f_\lambda^J(j''l'' \leftarrow j'l')\mathscr{U}_{j''l''}^J(R) \tag{3.19}$$

To solve the above equation, the collision is subjected to the condition that as R approaches 0, the wavefunction vanishes. So the solution lies in the asymptotic behaviour of the radial wavefunction as R tends to ∞.
From chapter 1, the superposition of incoming and outgoing waves in terms of the scattering matrix is given by

$$\boxed{\mathscr{U}_{j'l'}^J(R) = \delta_{jj'}\delta_{ll'} e^{-i(k_{jj}R - \frac{l\pi}{2})} - \sqrt{\frac{k_{jj}}{k_{j'j}}}\langle j'l'|\, S^J\, |jl\rangle\, e^{i(k_{j'j}R - \frac{l\pi}{2})}} \tag{3.20}$$

This gives us the scattering S-matrix.

3.2 Cross section and Rate coefficient

As we saw in the chapter 1, to define the cross section, we first define the T-matrix as in eq 1.8 is given as

$$\langle j'l'|\, T^J\, |jl\rangle = \delta_{jj'}\delta_{ll'} - \langle j'l'|\, S^J\, |jl\rangle \tag{3.21}$$

So the total **cross section** over all J, l for transition between rotational levels j and j' would be

$$\boxed{\sigma(j' \leftarrow j) = \frac{\pi}{k_{jj}^2[j]}\sum_{J,l,l'}[J]\left|\langle j'l'|\, T^J\, |jl\rangle\right|^2} \tag{3.22}$$

The collisional (de-excitation) **rate coefficient** $(k_{j\leftarrow j'}(T))$ is the Maxwellian average of the collisional cross section $(\sigma_{j\leftarrow j'}(E))$. It is defined as

$$\boxed{k_{j\leftarrow j'}(T) = \sqrt{\frac{8k_BT}{\pi\mu}}\left(\frac{1}{k_BT}\right)^2\int_0^\infty \sigma_{j\leftarrow j'}(E) E\, e^{-\left(\frac{E}{k_BT}\right)}\, \mathrm{d}E} \tag{3.23}$$

where k_B is the boltzmann constant, T is the Temperature and E is the collision Energy.
The excitation rate coefficient is then obtained through detailed balance

$$k_{j' \leftarrow j}(T) = k_{j \leftarrow j'}(T) \, \frac{g_{j'}}{g_j} e^{\left(\frac{E_j - E_{j'}}{k_B T}\right)}$$

CHAPTER 4

Bound States

"Let us call such a state quasi-bound state because it would be an honest bound state if the barrier were infinitely high."

— J.J. Sakurai, *Modern Quantum Mechanics*

In the previous chapter, we saw that for the scattering wavefunctions, the boundary condition is such that the wavefunction vanishes at R=0 and as R tends to infinity, the wavefunction approaches an asymptotic form. For a bound state, the wavefunction vanishes at both the ends of the R. For a potential well, we seek states between the well depth and 0 energy. That is,

$$-V_0 < E < 0$$

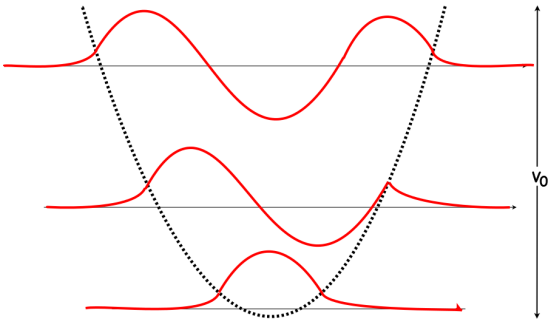

Figure 4.1: Bound states

For our system, as mentioned in the previous chapter, the schrödinger equation is of the form

$$-\left[-\frac{\boldsymbol{\nabla}^2}{2\mu} + E_{el} + H\right]\psi = E\psi \tag{4.1}$$

As we can see, it doesn't contain a first-order derivative term. Hence, the equation can be solved by a technique called log-derivative method (the same technique is used for dynamic calculations too).
Eq 4.1 is of the form

$$-\left[\boldsymbol{\nabla}^2 \; + \; A(R)\right] \psi(R) = 0 \tag{4.2}$$

The bound state wavefunction, $\psi(R)$ is defined such that

$$\psi_b(R) \;\; \rightarrow \;\; 0 \qquad \text{at} \qquad R = 0 \;\&\; R \rightarrow +\infty$$

According to Johnson (1978) and Hutson (1994a), wavefunctions that satify the above conditions can be calculated by a procedure that combines gordan's iterative procedure and the node count method.

4.1 Gordan's iterative procedure

According to Gordon (1969), the eq.4.2 can be integrated outward from the inner boundary and inward from the outward boundary to a common matching point. In this way, M linearly independant solutions with arbitrary derivatives can be calculated. These solutions are grouped as an M×M square matrix wavefunction $\Psi(R)$. Hence this $\Psi(R)$ would also satisfy the eq 4.2. Since $\Psi(R)$ is linearly independent, the correct wavefunction $\psi(R)$ must be possible to be expressed as

$$\psi_b(R) = \Psi(R) \cdot \mathbf{C}$$

where $\boldsymbol{C}$ is a column vector of unknown coefficients.
The procedure is assuming a trial value for the energy (E) and integrate eq 4.2 outward and inward to a common matching point R_m. Let us assume

$$\Psi_l(R) \rightarrow \text{ approaches } R_m \text{ from left}$$

and

$$\Psi_r(R) \rightarrow \text{ approaches } R_m \text{ from right}$$

If the trial value is the eigenvalue then,

$$\psi_b(R) = \Psi_l(R) \cdot \mathbf{l} \qquad R \leq R_m \tag{4.3}$$

and

$$\psi_b(R) = \Psi_r(R) \cdot \mathbf{r} \qquad R \geq R_m \tag{4.4}$$

where $\boldsymbol{l}$ and $\boldsymbol{r}$ are unknown vectors.
Since the eigenfunction is continous, at the matching point R_m,

$$\Psi_l(R_m) \cdot \mathbf{l} = \Psi_r(R_m) \cdot \mathbf{r} = \psi_b(R_m) \tag{4.5}$$

and

$$\Psi_l'(R_m) \cdot \mathbf{l} = \Psi_r'(R_m) \cdot \mathbf{r} = \psi_b'(R_m) \tag{4.6}$$

Combining eqs 4.5 and 4.6 and writing in a matrix form gives

$$\begin{pmatrix} \Psi_l(R_m) & \Psi_r(R_m) \\ \Psi_l'(R_m) & \Psi_r'(R_m) \end{pmatrix} \begin{pmatrix} \mathbf{l} \\ -\mathbf{r} \end{pmatrix} = 0$$

$$\Rightarrow \quad \begin{vmatrix} \Psi_l(R_m) & \Psi_r(R_m) \\ \Psi_l'(R_m) & \Psi_r'(R_m) \end{vmatrix} = 0 \tag{4.7}$$

That implies that the determinant in eq 4.7 becomes 0 at each eigenvalue. Once we know the eigenvalue, the vectors $\boldsymbol{l}$ and $\boldsymbol{r}$ can be found. Hence we find the wavefunction $\Psi(R)$. If we define a log-derivative matrix to be

$$Y(R) = \Psi'(R)\ \Psi^{-1}(R) \tag{4.8}$$

At matching point, eq 4.6 becomes

$$Y_l(R_m)\ \Psi_l(R_m) \cdot \mathbf{l} = Y_r(R)\ \Psi_r(R_m) \cdot \mathbf{r} \tag{4.9}$$

$$\Rightarrow \qquad (Y_r(R_m) - Y_l(R_m))\psi_B(R_m) = 0$$

$$\Rightarrow \qquad \boxed{|Y_r(R_m) - Y_l(R_m)| = 0} \tag{4.10}$$

Eq 4.10 is the matching condition. Hence rather than propagating the wavefunction and its derivative, it is sufficient if we propagate just the long derivative matrix. And, as the log-derivative matrices depend on the energy at which it is solved, the values of energy where the determinant $Y_r(R_m) - Y_l(R_m)$ goes to zero gives the eigenvalues.

4.2 Node count method

Though the previous method to find the eigenvalue is very effective, it requires the trial energy (which is already a guess!) to be close to the

eigenvalue. Also, we cannot know the exact number of eigenvalues between 2 energies. So we cannot be certain if we have found all the eigenvalues or not. This difficulty is overcome by the node count method.
A **node** is defined as the zero of the determinant function $|\Psi(R)|$. Each zero is assigned an integer n and the corresponding eigenvalue E_n. If the node count is greater than n, the trial energy E $\geq E_n$ and if the node count is $\leq n$ the E $< E_n$.

4.3 An Algorithm of implementation

A small algorithm below explains how the procedure works:

1. Initialise the parameters (setting the input parameters)

   a) Potential parameters: E_{min} = well depth, $E_{max} = 0$, the length R (R_{min}, R_{max}) and the mid point (R_{mid}) which is set as the position of the minimum of the potential.

   b) Type of log-derivative propagator to use.

   c) Specify the specific state, J_{TOT} (ground state ($J_{TOT} = 0$) or higher ($J_{TOT} = 1, 2, ...$)).

   d) Set a value (ϵ) for convergence of the energy (the minimum energy difference between $\mathrm{E_{min}}$ and E_{max}) for the iteration to stop.

2. Begin the node count method

   a) Set the trial energy as $E = \frac{1}{2}(E_{min} + E_{max})$. (Hence the name **bisection method**)

   b) Solve eq 4.2 for det$|\Psi(R)|$ to find the number of nodes. If the node count $> n$,

   c) Change $E_{max} = E$ If the node count $\leq n$,

   d) Change $E_{max} = E$

   e) With the new value of E_{max} or E_{min} repeat from step (a).

   f) Stop the above loop once $E_{max} - E_{min} \leq \epsilon$.

3. Begin the Gordon's Procedure
   (Once the above iteration ends, we would be close to the eigenvalue. Hence this energy would be a good guess for the initial trial energy for Gordan's procedure.)

   a) With the new trial energy E, integrate the eq 4.2 inward and outward to a common matching point R_m (R_{mid} would be the best guess.)

   b) Solve for eq 4.10 to find the exact eigenvalue.

4. If the node was more than 1, then go back to 2. and repeat the steps.

5. Once all the eigenvalues are calculated go back to 1., change the J_{TOT} and repeat the steps.

PART III

Results

CHAPTER 5

Spectroscopy of NH/ND

Before getting into the collision of the molecule, it is important to first understand the structure of the molecule. As NH and ND are isotopologue, we can discuss their spectroscopy together (Since H and D differ only by neutron number, there is no difference in the electronic configuration). The electronic orbital structure for the ground electronic state of NH/ND is given in Fig 5.1 The spectroscopic notation for electronic state of a linear

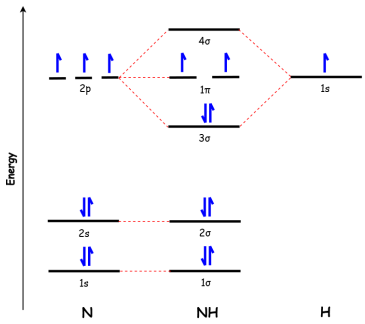

Figure 5.1: The molecular orbital structure for the ground-state of NH/ND

molecule is ${}^{2S+1}\Lambda^s$, where $\Lambda \equiv |M|$; M is the eigenvalue of the L_z=0,±1,±2,... with respective Λ denoted by symbols Σ, Π, Δ,...; S is the total spin of the molecule; s is the symmetry which could be + or -. For the ground state of NH (ND), M=0, S=1, s=-. Therefore, the electronic ground state symmetry of NH/ND is ${}^3\Sigma^-$.

N	Energy (in cm^{-1})	
	NH	**ND**
0	0.0000	0.000
1	32.6796	17.5806
2	97.9975	52.7301
3	195.8717	105.4250
4	326.1786	175.6298
5	488.7537	263.2978
6	683.3913	368.3695
7	909.8448	490.7749
8	1167.8260	630.4314
9	1457.0060	787.2448

Table 5.1: Energies of first 10 pure rotational levels of NH and ND ($^3\Sigma^-$) molecules

5.1 Rotational Energy Levels

If we consider NH/ND to be a non-rigid diatomic molecule, then

$$\begin{aligned} E(N) &= \underbrace{\frac{\hbar^2}{2I}}_{B} N(N+1) - \underbrace{\frac{\hbar^4}{2I^2r^2k}}_{D} N^2(N+1)^2 \\ &= B\ N(N+1) - D\ N^2(N+1)^2 \end{aligned} \tag{5.1}$$

where B and D are rotational constant and centrifugal distortion constant respectively and N is the nuclear rotational angular momentum of NH/ND. I, r and k are moment of inertia, distance between the 2 atoms and force constant respectively. The B and D values for NH in the ground electronic state ($^3\Sigma^-$) are 16.34320634 cm^{-1} and 0.0017139 cm^{-1} respectively. And, the B and D values for ND in the $^3\Sigma^-$ state are 8.7913 cm^{-1} and 0.0004904 cm^{-1} respectively. Substituting these values, and values for N gives the rotational energy levels of NH and ND. For the purpose of clarity, we will call this as *pure* rotational energy levels. Table 5.1 gives first 10 *pure* rotational levels of the NH and ND molecules.

5.1.1 Fine splitting of Energy levels of NH/ND

In the beginning of this chapter, we showed that the $^3\Sigma^-$ state of NH/ND has 2 unpaired electrons and $\Lambda = 0$. Since $\Lambda = 0$, the spin-orbit coupling is zero. But due to the presence of a non-zero spin-spin coupling, NH/ND molecules are represented by a intermediate coupling scheme (intermediate between Hund's case (a) and (b)). In this case, the total angular momentum of the molecule,j is defined as

$$\boldsymbol{j} = \boldsymbol{N} + \boldsymbol{S} \tag{5.2}$$

Due to the non-zero electron spin, the molecule has a non-zero electron spin dipole moment. Because of this arises the **fine structure** splitting of NH/ND molecules. Fine structure splitting is due to the Spin-rotation coupling and spin-spin coupling. Spin-rotation coupling is the interaction of electron spin magnetic moment and the molecular rotation magnetic moment. Spin-spin coupling is the interaction between the magnetic moments of the 2 unpaired electrons. In the intermediate coupling scheme, the effective Hamiltonian of the molecule is

$$\mathbf{H}_{eff} = \mathbf{H}_{rot} + \mathbf{H}_{sn} + \mathbf{H}_{ss} \tag{5.3}$$

where $\mathbf{H}_{rot}$, $\mathbf{H}_{sn}$ and $\mathbf{H}_{ss}$ are the rotational Hamiltonian, spin-rotation Hamiltonian and spin-spin Hamiltonain of the molecule repectively. They are given by

$$\begin{aligned}
\mathbf{H}_{rot} &= B\boldsymbol{N}^2 - D\boldsymbol{N}^4 \\
\mathbf{H}_{sn} &= \gamma(\boldsymbol{N} \cdot \boldsymbol{S}) \\
\mathbf{H}_{ss} &= \frac{2}{3}\lambda(3\boldsymbol{S}_z^2 - \boldsymbol{S})
\end{aligned}$$

where B and D are rotational constant and centrifugal distortion constant respectively, and γ and λ are spin-rotation and spin-spin coupling constants respectively. (the vibrational dependance of γ and λ is ignored) The γ and λ values (used in this thesis) for NH in the ground electronic state ($^3\Sigma^-$) are -0.0550 cm^{-1} and 0.9200 cm^{-1} repectively and the same for ND are -0.0294 cm^{-1} and 0.9184 cm^{-1} respectively. Since the multiplicity of the NH/ND is 3 (*2S+1*), each N is split into 3 levels (2 levels with (-1)^N parity and 1 level with (-1)$^{N+1}$ parity). Since the H_{ss} is not zero in the case of 2 unpaired electrons, this term mixes the states with same parity which leads to intermediate coupling of states. In this case, the 3 levels are labeled $\boldsymbol{F_1}$, $\boldsymbol{F_2}$ and $\boldsymbol{F_3}$.

In *"pure"* hund's case (b) (that is, if we neglect the Spin-spin coupling),

the 3 levels would correspond to *j=N+1*, *j=N* and *j=N-1*. That is, if the wavefunctions corresponding to the levels of pure hund's case (b) are denoted as $|N = j-1, S, j, m_j\rangle$, $|N = j, S, j, m_j\rangle$ and $|N = j+1, S, j, m_j\rangle$ respectively, the intermediate coupled wavefunctions for $j \geq 1$ is written as

$$|F_1, j, m_j\rangle = \cos\alpha\,|N = j-1, S, j, m_j\rangle + \sin\alpha\,|N = j+1, S, j, m_j\rangle$$
$$|F_2, j, m_j\rangle = |N = j, S, j, m_j\rangle$$
$$|F_3, j, m_j\rangle = -\sin\alpha\,|N = j-1, S, j, m_j\rangle + \cos\alpha\,|N = j+1, S, j, m_j\rangle$$

where α is the mixing angle and can be obtained by diagonalization of the Hamiltonian $\mathbf{H}_{eff}$. The eigenvalue corresponding to these wavefunctions gives the energies of the respective rotational levels. If eigenvalue corresponding to $|N = j-1, S, j, m_j\rangle$, $|N = j, S, j, m_j\rangle$ and $|N = j+1, S, j, m_j\rangle$ are $E_1(j)$, $E_2(j)$ and $E_3(j)$ respectively, the corresponding eigenvalues of the intermediate coupled wavefunctions would be $E_{F_1}(j)$, $E_{F_2}(j)$ and $E_{F_3}(j)$.

$\mathbf{H}_{eff}\,|N, S, j, m_j\rangle$ gives

$$E_1(j) = Bj(j-1) - Dj^2(j-1)^2 + \gamma(j-1) + \left(\frac{2}{3} - \frac{2j}{2j+1}\right)\lambda$$
$$E_2(j) = Bj(j+1) - Dj^2(j+1)^2 - \gamma + \frac{2}{3}\lambda$$
$$E_3(j) = B(j+1)(j+2) - D(j+1)^2(j+2)^2 - \gamma(j+2) + \left(\frac{2}{3} - \frac{2(j+1)}{2j+1}\right)\lambda$$

and $\mathbf{H}_{eff}\,|F_i, j, m_j\rangle$ gives E_{F_i} in terms of E_1, E_2 and E_3 as follows

$$E_{F_1}(j) = \frac{1}{2}\left(E_1(j) + E_3(j) - \sqrt{(E_1(j) - E_3(j))^2 + \frac{16j(j+1)}{(2j+1)^2}\lambda^2}\right) \quad (5.4)$$
$$E_{F_2}(j) = E_2(j) \quad (5.5)$$
$$E_{F_3}(j) = \frac{1}{2}\left(E_1(j) + E_3(j) + \sqrt{(E_1(j) - E_3(j))^2 + \frac{16j(j+1)}{(2j+1)^2}\lambda^2}\right) \quad (5.6)$$

Table 5.2 gives first 15 fine structure resolved rotational levels of the NH and ND molecules.

N	j	Energy (in cm^{-1})		Label (N,F_i)
		NH	ND	
0	1	0.0000	0.0000	0,F_1
1	0	31.5706	16.4292	1,F_3
1	2	32.5046	17.4339	1,F_1
1	1	33.3556	18.2367	1,F_2
2	1	97.5646	52.2348	2,F_3
2	3	97.7164	52.5040	2,F_1
2	2	98.6736	53.3862	2,F_2
3	4	195.5071	105.1418	3,F_1
3	2	195.6137	105.0764	3,F_3
3	3	196.5477	106.0810	3,F_2
4	5	325.7409	175.2996	4,F_1
4	3	326.0268	175.3606	4,F_3
4	4	326.8546	176.2858	4,F_2
5	4	488.6854	263.0855	5,F_3
5	5	489.4297	263.9537	5,F_2

Table 5.2: Energies of first 15 fine structure resolved rotational levels of the NH($^3\Sigma^-$)

5.1.2 Hyperfine structures

Another significant interaction that affects the rotational levels of NH and ND is the presence of a non-zero nuclear spin. For NH and ND molecules, both the N, H(D) nuclei have a non-zero spin ($I_N = 1$, $I_H = \frac{1}{2}$, $I_D = 1$). This introduces additional quantum numbers namely F_1 and F, which are defined as

$$\boldsymbol{F_1} = \boldsymbol{j} + \boldsymbol{I_H}$$

and

$$\boldsymbol{F} = \mathbf{F_1} + \boldsymbol{I_N}$$

The hyperfine splitting is characterised mainly by the presence of nuclear quadrupole moment and interaction between the nuclear spin and total angular momentum of the molecule (other nuclear spin interactions are very negligible).
So, the hamiltonian describing the hyperfine structures is given as

$$\mathbf{H}_{hf} = \mathbf{H}_Q + \mathbf{H}_{ij}$$

where

$$\mathbf{H}_Q = \sum_{k=1}^{2} \frac{(eQq)_k}{2I_k(2I_k-1)j(2j-1)} \left[3(\mathbf{I}_k \cdot \boldsymbol{j})^2 + \frac{3}{2}(\mathbf{I}_k \cdot \boldsymbol{j}) - I_k(I_k+1)j(j+1)\right]$$

$$\mathbf{H}_{ij} = \sum_{k=1}^{2} C_k(\mathbf{I}_k \cdot \boldsymbol{j})$$

where eQq are the quadrupole coupling constants and C is the nuclear spin-rotation interaction. Hence the total Hamiltonian of the molecule, $\mathbf{H}_{mol}$ is equal to $\mathbf{H}_{eff} + \mathbf{H}_{hf}$. The eigenvalue of $\mathbf{H}_{mol}\,|N, j, F_1, F\rangle$ would give the energies of the hyperfine rotational levels. But for NH and ND, the hyperfine splitting of energy levels is very small when compared to the fine structures. Also since the spin of H and D are different, the splitting is different for NH and ND (Notice the difference in the F_1 and F of table 5.3 and table5.4).

N	j	F_1	F	Energy (in cm^{-1})
0	1	1.5	0.5	0.0000
0	1	1.5	1.5	0.0006
0	1	1.5	2.5	0.0017
0	1	0.5	0.5	0.0036
0	1	0.5	1.5	0.0049
1	0	0.5	0.5	31.5728
1	0	0.5	1.5	31.5728
1	1	1.5	2.5	33.3572
1	1	0.5	1.5	33.3574
1	1	1.5	0.5	33.3582
1	1	1.5	1.5	33.3582
1	1	0.5	0.5	33.3586
2	1	0.5	1.5	97.5641
2	1	0.5	0.5	97.5663
2	1	1.5	0.5	97.5699

Table 5.3: Energies of first 15 hyperfine structure resolved rotational levels of the NH($^3\Sigma^-$)

N	j	F_1	F	Energy (in cm^{-1})
0	1	0	1	0.0000
0	1	1	2	0.0006
0	1	1	0	0.0011
0	1	1	1	0.0011
0	1	2	3	0.0018
0	1	2	2	0.0023
0	1	2	1	0.0026
1	0	1	0	16.4292
1	0	1	1	16.4292
1	0	1	2	16.4292
1	1	2	1	18.2187
1	1	1	0	18.2195
1	1	1	1	18.2195
1	1	1	2	18.2195
1	1	0	1	18.2199

Table 5.4: Energies of first 15 hyperfine structure resolved rotational levels of the ND($^3\Sigma^-$)

In the next chapters, we will see how these fine and hyperfine splitting of energy levels will affect the bound states, cross section and the rate co-efficients of the systems involving NH and ND.

CHAPTER 6

NH-He: PES and Scattering Calculations

$NH(^3\Sigma^-)$-$He(^1S)$ (the notation for the ground state of Helium atom is ^1S since it is a noble gas) collisions have been extensively studied earlier (Rinnenthal et al., 2002; Krems et al., 2003; Cybulski et al., 2005; Toboła et al., 2011). The advancement in the computational capabilities opens new avenues for enhancement. In this chapter, we will discuss some these improvements and the effect of these improvements on the rate coefficients.

6.1 Potential Energy Surface

Previously, Cybulski et al., 2005 calculated NH-He PESs. They did the *ab initio* calculations using spin-restricted coupled-cluster method with aug-cc-pvQZ basis set. The depth of their potential well was around 19.86 cm^{-1} at R=6.33a_0 and $\Theta = 62.3°$. Several studies were done using these PES and it proved to be successful. However, these calculations do not take into account the intramolecular vibrational motion of the NH molecule. Several recent studies (Bouhafs and Lique, 2015, Kalugina et al., 2014, Lique, 2015) have shown the importance of inclusion of the vibrational motion of light molecular hydrides and its effect on the dynamic calculations. So, in this chapter **we present and use the PES which includes the vibrational motion of NH molecule**.

For the new *ab initio* calculations, the NH-He geometry is described in Jacobi coordinates as in Fig 6.1.

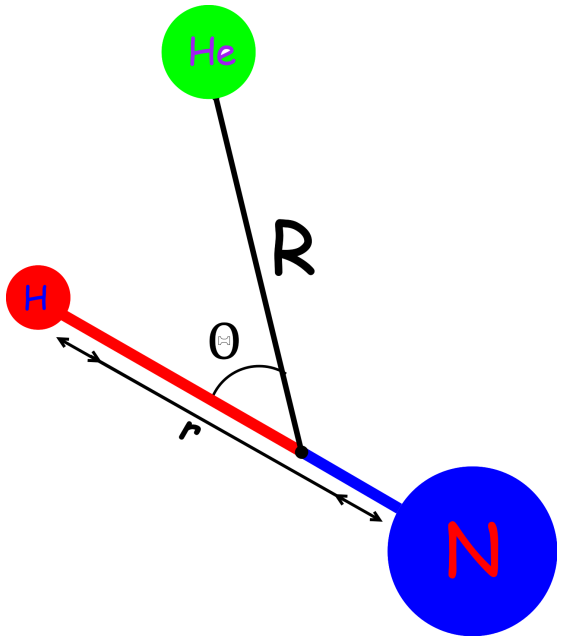

Figure 6.1: Jacobi coordinates for NH-He

The new *an initio* calculations were carried out using partially spin-restricted coupled cluster method with single, double and perturbative triple excitation [$RCCSD(T)$] with the aug-cc-pVXZ(X=T,Q,5) basis sets (section 2.2.2.1 and 2.2.3) using the MOLPRO package (Werner et al., 2010). The energies were extrapolated to the Complete Basis Set(CBS) limit using the following function

$$E_R(X) = E_R(\infty) + Be^{-(X-1)} + Ce^{-(X-1)^2} \tag{6.1}$$

where X is the cardinal number of the basis set(X=3,4,5 in this case). $E_R(\infty)$ is the estimated energy at CBS limit as X$\rightarrow \infty$, and B and C are constant parameters. The energies at all geometries were also corrected for the basis-set superposition error. This was done using the counterpoise method proposed by Boys et al., 1970. In this method, the energies of NH and He are computed separately using the full basis set used for calculating energies of NH-He. These quantities are then differenced so that the errors cancel out.

$$V(R) = E_{NH-He}(R) - (E_{NH}(R) + E_{He}(R)) \tag{6.2}$$

where *V(R)* is the BSSE corrected potential. The *an initio* calculations were carried out for a range of values. R varied from 35.0a_0 to 3.0a_0; Θ varied from 0° to 180° in steps of 10° and r =$[1.6, 1.8, 1.95, 2.2, 2.4]a_0$

The *ab initio* points were analytically represented as a 3-dimensional potential energy surface by intrapolating the points in the form:

$$V_{3D}(r, R, \Theta) = \sum_{n=1}^{N_{max}} \sum_{l=1}^{L_{max}} d_{m0}^{l+m-1}(\Theta) A_{nl}(R)(r - r_e)^{n-1} \tag{6.3}$$

$d_{m0}^{l+m-1}(\Theta)$ is the reduced wigner (Edmonds, 1957) rotation matrix, N_{max} is n(r), L_{max} is n(Θ), r_e is the equilibrium bond length of NH molecule (For our calculations, $r_e = 1.95a_0$) and $A_{nl}(R)$ is the matrix containing the *an initio* points *V(R)*. This 3D-PES takes into account the vibrations of NH up to the vibrational state v=2. So, we can find the expectation value of the 3D potential at any of the vibrational states up to v=2. It gives us a 3D PES averaged over the bond lengths (which will be henceforth referred as ***3D-avg PES***).

$$\begin{aligned} V_{av}(R, \Theta) &= \langle v(r)| V_{3D}(r, R, \Theta) |v(r)\rangle \\ &= \sum_{n=1}^{N_{max}} \sum_{l=1}^{L_{max}} d_{m0}^{l+m-1}(\Theta) A_{nl}(R) \quad \langle v(r)| (r - r_e)^{n-1} |v(r)\rangle \end{aligned} \tag{6.4}$$

The wavefunction $|v(r)\rangle$ was calculated by Bouhafs and Lique, 2015. $\langle v(r)| (r - r_e)^{n-1} |v(r)\rangle$ values are given in table 6.1. The contour plot of the 3D-avg PES over the ground vibrational state ($v = 0$) is presented in fig 6.2. We have also computed a new PES from the *ab initio* points but for a fixed internuclear distance (r = 1.99 bohr)(this will be referred as ***2D PES*** throughout this thesis).

	n=1	**n=2**	**n=3**	**n=4**	**n=5**
***v*=0**	1.0000	0.0346	0.0214	0.0026	0.0026
***v*=1**	1.0000	0.1060	0.0729	0.0185	0.0185
***v*=2**	1.0000	0.1814	0.1385	0.0548	0.0548

Table 6.1: $\langle v(r)| (r - r_e)^{n-1} |v(r)\rangle$ values for given n and vibrational state,v.

The global minima of the interaction potential for the 3D-avg PES is -19.71 cm^{-1} at $R = 6.30a_0$ and $\Theta = 64°$. If we compare the 3D-avg PES with the PES of Cybulski et al., the overall difference (absolute) between the 2 PESs are depicted in the fig 6.3. The colormap gives the energy difference. The white region means the differences are > 0.1 cm^{-1}. As we can see from the figure, there is a very few region where there are no differences (0). Also

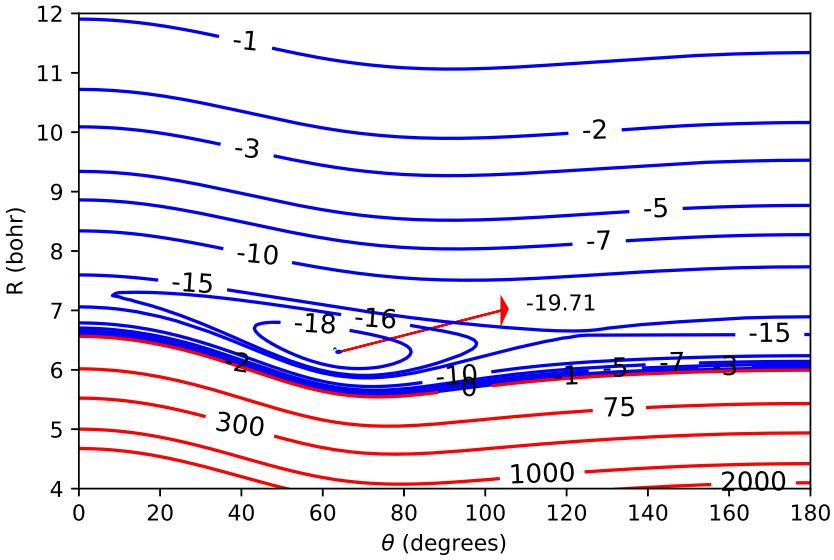

Figure 6.2: Contour plot of 3D-avg NH-He PES as a function of R and Θ.

the differences are very asymmetric. Approximately, we can say that the differences are significant as He approaches close to the center of mass of NH on the side of N. The position of global minima of the 2 PESs are in good agreement.

6.2 Collisonal Dynamics of NH($^3\Sigma^-$) with He(^1S)

In chapter 3, we perceived the theory for dynamics of molecule-diatom system where the molecule does not have any unpaired electrons (i.e., a closed-shell molecule). But, since we know that NH has 2 unpaired electrons in its ground state (i.e., its an open-shell molecule), we saw the importance of considering the spin interactions (fine and hyperfine structures) from the previous chapter. In this section, we rewrite equations of chapter 3 to include the spin in the dynamic equations.

6.2.1 Fine Structure transitions

From eq 5.2,

$$j = N + S$$

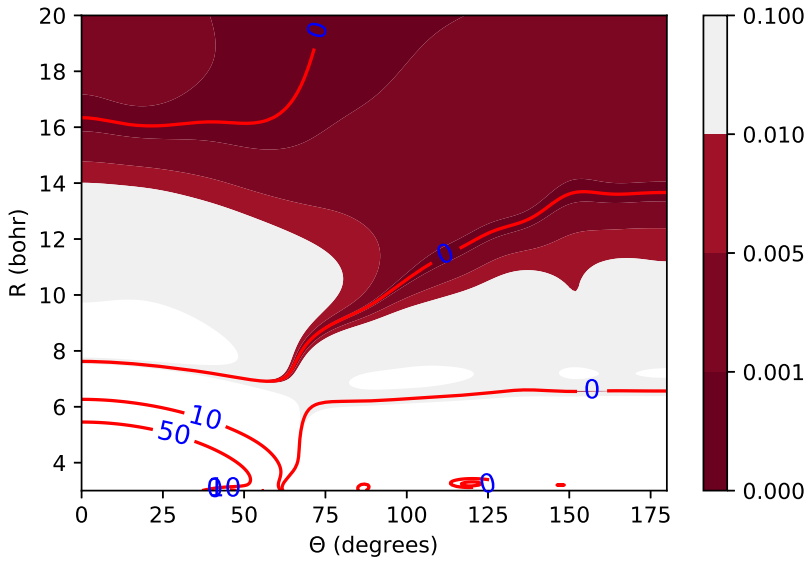

Figure 6.3: Difference between 3D-avg PES and PES of Cybulski et al., 2005. The energies are in cm^{-1}.

Therefore the wavefunction for NH molecule in *pure* hund's case (b) can be defined as

$$\mathscr{Y}^{j'}_{N'S'}(\mathbf{r}) = \sum_{m_N, m_S} \langle N'S'm_N m_S | j'm_j \rangle \, Y^{m_N}_{N'}(\mathbf{r}) Y^{m_S}_{S'}(\mathbf{r}) \tag{6.5}$$

with $E_{N'S'}$ as the energy of the corresponding level. If the total angular momentum of the system is defined as $J_T = j + l$, then the total wavefunction of eq 3.7 becomes,

$$\Psi^{J_T}_{NSjl}(R, \mathbf{r}, \mathbf{r}') = \frac{1}{R} \sum_{N'j'l'} \mathscr{U}^{J_T Njl}_{N'j'l'}(R) \mathscr{Y}^{J_T}_{N'j'l'}(\mathbf{r}, \mathbf{r}') \tag{6.6}$$

with

$$\mathscr{Y}^{J_T}_{N'j'l'}(\mathbf{r}, \mathbf{r}') = \sum_{m_j, m_l} \langle j'l'm_j m_l | j'l'J_T M \rangle \, \mathscr{Y}^{j'}_{N'S'}(\mathbf{r}) Y^{m_l}_{l'}(\mathbf{r}') \tag{6.7}$$

Therefore the close-coupling equations of eq 3.12 would become

$$\frac{\hbar^2}{2\mu}\left(\frac{\partial^2}{\partial R^2} - \frac{l'(l'+1)}{R^2} + k^2_{N'S'}\right) \mathscr{U}^{J_T}_{N'j'l'}(R) = \sum_{N''j''l''} \mathscr{U}^{J_T}_{N''Sj''l''}(R) \, \langle N''Sj''l''J_T M | \, V(R, \Theta) \, | N'Sj'l'J_T M \rangle \tag{6.8}$$

To solve these equations, we exploit the fact that the $\boldsymbol{N}$ and $\boldsymbol{S}$ are weakly coupled in the hund's case(b) molecules. Hence we can rewrite the coupling scheme of the system as follows

$$N + l = J$$

and

$$J + S = J_T$$

That is, total angular momentum of open-shell system (J_T) is a sum of total angular momentum of closed-shell system (J) and spin angular momentum of open-shell system (S). This, along with the fact that the potential V is independant of the spin and the orientation of the sytem in the space-fixed coordinate, felicitates us to write the potential matrix, wavefunction and hence the cross section of an open-shell system in terms of the closed shell system. This simplifies the equations as follows

$$\begin{aligned}\langle N''Sj''l''J_TM|V(R,\Theta)\,|N'Sj'l'J_TM\rangle = \sum_{J''}(-1)^{j'-j''-l'+l''}[J'']\sqrt{[j'][j'']} \\ \times \begin{Bmatrix} S & N' & j' \\ l' & J_T & J \end{Bmatrix}\begin{Bmatrix} S & N'' & j'' \\ l'' & J_T & J \end{Bmatrix}\langle N''l''JM_J|\,V(R,\Theta)\,|N'l'JM_J\rangle\end{aligned} \tag{6.9}$$

where $\langle N''l''JM_J|\,V(R,\Theta)\,|N'l'JM_J\rangle$ is simply the potential matrix of closed-shell system (eq 3.18) given by

$$\langle N''l''JM_J|\,V(R,\Theta)\,|j'l'JM_J\rangle = \sum_{\lambda} E^{\lambda}_{el}(R) f^{J}_{\lambda}(N''l'' \leftarrow N'l') \tag{6.10}$$

Substituting eq 6.10 in eq 6.9 and simplifying the three 6-j matrices gives the **interaction potential matrix** as

$$\begin{aligned}\langle N''Sj''l''J_TM|\,V(R,\Theta)\,|N'Sj'l'J_TM\rangle = \sum_{\lambda}(-1)^{S-\lambda-J_T}\sqrt{[N'][N''][j'][j''][l'][l'']} \\ \times E^{\lambda}_{el}(R)\begin{pmatrix} N'' & N' & \lambda \\ 0 & 0 & 0 \end{pmatrix}\begin{pmatrix} l'' & l' & \lambda \\ 0 & 0 & 0 \end{pmatrix}\begin{Bmatrix} j' & l' & J_T \\ l'' & j'' & \lambda \end{Bmatrix}\begin{Bmatrix} j' & N' & S \\ N'' & j'' & \lambda \end{Bmatrix}\end{aligned} \tag{6.11}$$

Now, if we consider the **intermediate coupling**, the total wavefunction corresponding to the total angular momentum J_T would be,

$$\Psi^{J_T}_{F_ijl}(R,\mathbf{r},\mathbf{r}') = \frac{1}{R}\sum_{F_i'j'l'} \mathscr{U}^{J_TF_ijl}_{F_i'j'l'}(R)\mathscr{Y}^{J_T}_{F_i'j'l'}(\mathbf{r},\mathbf{r}')$$

with

$$\mathscr{Y}^{J_T}_{F_i'j'l'}(\mathbf{r},\mathbf{r}') = \sum_{m_j,m_l} \langle j'l'm_jm_l|j'l'J_TM\rangle\, \mathscr{Y}^{m_j'}_{F_i'j'}(\mathbf{r})Y^{m_l}_{l'}(\mathbf{r}')$$

And the total wavefunction satisfies the Schrödinger equation,

$$H_{eff}\Psi^{J_T}_{F_ijl}(R,\mathbf{r},\mathbf{r}') = E_T^{F_ij}\Psi^{J_T}_{F_ijl}(R,\mathbf{r},\mathbf{r}')$$

Then, the total energy of the NH-He system for a particular level F_ij of NH (eq 3.5) becomes

$$E_T^{F_ij} = E + E_{F_ij}$$

where E is the kinetic energy of the He atom and E_{F_ij} is the energy of the F_ij level of NH.
Hence, the close-coupled equations for the intermediate coupling would be

$$\frac{\hbar^2}{2\mu}\left(\frac{\partial^2}{\partial R^2} - \frac{l'(l'+1)}{R^2} + k^2_{F_i'j'}\right)\mathscr{U}^{J_T}_{F_i'j'l'}(R) = \sum_{F_i''j''l''} \mathscr{U}^{J_T}_{F_i''j''l''}(R)\,\langle F_i''j''l''J_TM|\,V(R,\Theta)\,|F_i'j'l'J_TM\rangle \tag{6.12}$$

And, $\langle F_i''j''l''J_TM|\,V(R,\Theta)\,|F_i'j'l'J_TM\rangle$ and $\langle N''Sj''l''J_TM|\,V(R,\Theta)\,|N'Sj'l'J_TM\rangle$ are related as follows:

$$\langle F_i''j''l''J_TM|\,V(R,\Theta)\,|F_i'j'l'J_TM\rangle = \sum_{N''N'} c^{j'}_{N'F_i'}c^{j''}_{N''F_i''}\,\langle N''Sj''l''J_TM|\,V(R,\Theta)\,|N'Sj'l'J_TM\rangle \tag{6.13}$$

Substituting eq 6.11 in eq 6.13 and hence in in eq 6.12 and subjecting it to the condition that the wavefunction vanishes as R approaches 0, very similar to what we did in chapter 3, gives the solution as follows

$$\mathscr{U}^{J_T}_{F_i'j'l'}(R) = \delta_{NN'}\delta_{jj'}\delta_{ll'}e^{-i(k_{F_ij}R-\frac{l\pi}{2})} - \sqrt{\frac{k_{F_ij}}{k_{F_i'j'}}}\,\langle F_i'j'l'|\,S^{J_T}\,|F_ijl\rangle\, e^{i(k_{F_i'j}R-\frac{l\pi}{2})} \tag{6.14}$$

This gives us the S-matrix. And the T matrix

$$\langle F_i'j'l'|\,T^{J_T}\,|F_ijl\rangle = \delta_{NN'}\delta_{jj'}\delta_{ll'} - \langle F_i'j'l'|\,S^{J_T}\,|F_ijl\rangle \tag{6.15}$$

So the total **cross section** over all J_T for transition between rotational levels N,F_i and N',F_i' would be

$$\boxed{\sigma(F_i'j'l' \leftarrow F_ijl) = \frac{\pi}{k_{F_ij}^2[j]} \sum_{J_T,l,l'} [J_T] \left| \langle F_i'j'l' | \, T^{J_T} \, | F_ijl \rangle \right|^2} \tag{6.16}$$

The collisional de-excitation **rate coefficient** is hence defined as

$$\boxed{k_{F_ij \leftarrow F_i'j'}(T) = \sqrt{\frac{8k_BT}{\pi\mu}} \left(\frac{1}{k_BT}\right)^2 \int_0^\infty \sigma_{F_ijl \leftarrow F_i'j'}(E) E \, e^{-\left(\frac{E}{k_BT}\right)} \, \mathrm{d}E} \tag{6.17}$$

6.2.2 Hyperine Structure transitions

As we can notice from the table 5.3, hyperfine splitting of the NH levels are very small. Hence, the hyperfine levels can be assumed to be degenerate. Then, the integral cross sections corresponding to transitions between hyperfine levels of the NH molecules can be obtained from scattering S-matrix between fine structure levels using a recoupling method. This makes the dynamic calculations for the hyperfine transitions much simpler. For computational convenience, we introduce the opacity tensor $P^K_{F_i'j' \leftarrow F_ij}$ where K is the order of the tensor. The opacity tensor is derived from the S-matrix as follows:
From eq 6.15, T-matrix in terms of S-matrix (for fine-structure) is given by

$$\langle F_i'j'l' | \, T^{J_T} \, | F_ijl \rangle = \delta_{NN'}\delta_{jj'}\delta_{ll'} - \langle F_i'j'l' | \, S^{J_T} \, | F_ijl \rangle$$

From this, a reduced T-matrix is defined in terms of the order of the opacity tensor (K) as

$$\begin{aligned} \langle F_i'j'l' | \, T^K \, | F_ijl \rangle =& (-1)^{-j-l'}[K]\sqrt{[j'][j]} \\ & \times \sum_{J_TN'N} c^j_{NF_i} c^{j'}_{N'F_i'} (-1)^{J_T} [J_T] \begin{Bmatrix} l' & j' & J_T \\ j & l & K \end{Bmatrix} \begin{Bmatrix} K & j & j' \\ S & N' & N \end{Bmatrix} \\ & \times \langle F_i'j'l' | \, T^{J_T} \, | F_ijl \rangle \end{aligned}$$

And hence the opacity tensor is defined as

$$P^K_{F_i'j' \leftarrow F_ij} = \frac{1}{[K]} \sum_{ll'} \left| \langle F_i'j'l' | \, T^K \, | F_ijl \rangle \right|^2$$

We can arrive at cross-section for transition between hyperfine levels $|N, j, F_1, F\rangle$ and $|N', j', F_1', F'\rangle$ with respect to the opacity tensor of fine

structure transitions using a recoupling method derived in detail in Daniel et al., 2004 and the modalities are explained in Faure et al., 2012. The final cross-section is hence given as follows:

$$\sigma(N'j'F_1'F' \leftarrow NjF_1F) = \frac{\pi}{k^2_{NjF_1F}}[F_1][F_1'][F'] \sum_K \begin{Bmatrix} F_1 & F_1' & K \\ F' & F & I_H \end{Bmatrix} \begin{Bmatrix} j & j' & K \\ F_1' & F_1 & I_N \end{Bmatrix} P^K_{F_i'j' \leftarrow F_ij} \tag{6.18}$$

6.3 Results

6.3.1 Fine structure resolved scattering

The scattering calculations were performed for the main ^{14}N and ^{4}He isotopes by solving close-coupled equations using the MOLSCAT code (Hutson, 1994b). The MOLSCAT codes were modified using the equations in sec 7.3, to include Fine structure of the energy levels and the intermediate coupling scheme.

Using this modified MOLSCAT codes, the scattering calculations were performed for a total energy grid of 3500 cm^{-1} with variable steps. For the energies below 1250 cm^{-1},the step was equal to 1 cm^{-1}; between 1250 and 1500 cm^{-1}, it was increased to 5 cm^{-1}; and for the energy interval 1500 – 3500 cm^{-1}, it was increased to 10. The reason for using finer energy grids at lower energies is because the resonances that occur in the cross sections at low energies can be well noticed.

Before doing the actual calculations, it is necessary to set the values of various variable parameters involved in the MOLSCAT codes to ensure convergence of the inelastic cross sections. Firstly, it is necessary to include several energetically inaccessible (closed) levels in the calculations for the cross section to converge. For our calculations, at the largest energies, the NH rotational basis was extended to $N = 20$ to ensure convergence of the rotational cross sections between levels with $N \leq 8$. It is also needed to converge inelastic cross sections with respect to partial waves. The total angular momentum quantum number J needed for the convergence was set up to 81 for the inelastic cross sections.

In MOLSCAT, it is necessary to adjust the propagator's parameters in order to ensure convergence of cross section. For all the energies, the minimum and maximum integration distances were $R_{min} = 3.0$ bohr and R_{max} varied between 50 and 80 bohr. The STEPS parameter was adjusted for each range

of energies in order to obtain a step length of the integrator sufficient to ensure convergence. The values of the STEPS parameter decreases with increasing energy (from 50 to 10 for the given energy ranges). The reduced mass of the NH–He system is $\mu = 3.1600$ amu. (For further information of the parameter and their value of convergence, refer Appendix A)

With these input parameters, the integral state-to-state cross sections are calculated. Even though our main goal is to calculate the rate coefficients, it is still interesting to plot the cross-sections. Figure 6.4 presents the energy variation of the integral cross sections for transitions from the initial rotational level $N = 0$,F_1 of NH.

By averaging over a Maxwellian distribution of the collisional velocities using the equation 3.23, we obtained thermal rate coefficients for excitation and de-excitation transitions between fine-structure levels of NH. We obtained rate coefficients for temperatures up to 350 K. The thermal dependence of the state-to-state rate coefficients is illustrated in Fig.6.5 for transitions out of the $N = 0$, F_1 level.

6.3.2 Hyperfine resolved excitations

Using the S-matrix of the fine structure resolved state-to-state dynamic calculations, we calculated the hyperfine resolved NH–He cross sections using the procedure described in section 6.2. Then, by averaging the cross sections over a Maxwellian distribution of the collisional velocities, we obtained thermal rate coefficients for excitation and de-excitation transitions between hyperfine levels of NH. We obtained rate coefficients for temperatures up to 150 K. Figure 6.6 presents the temperature variation of the hyperfine resolved NH–He rate coefficients for a selected transitions.

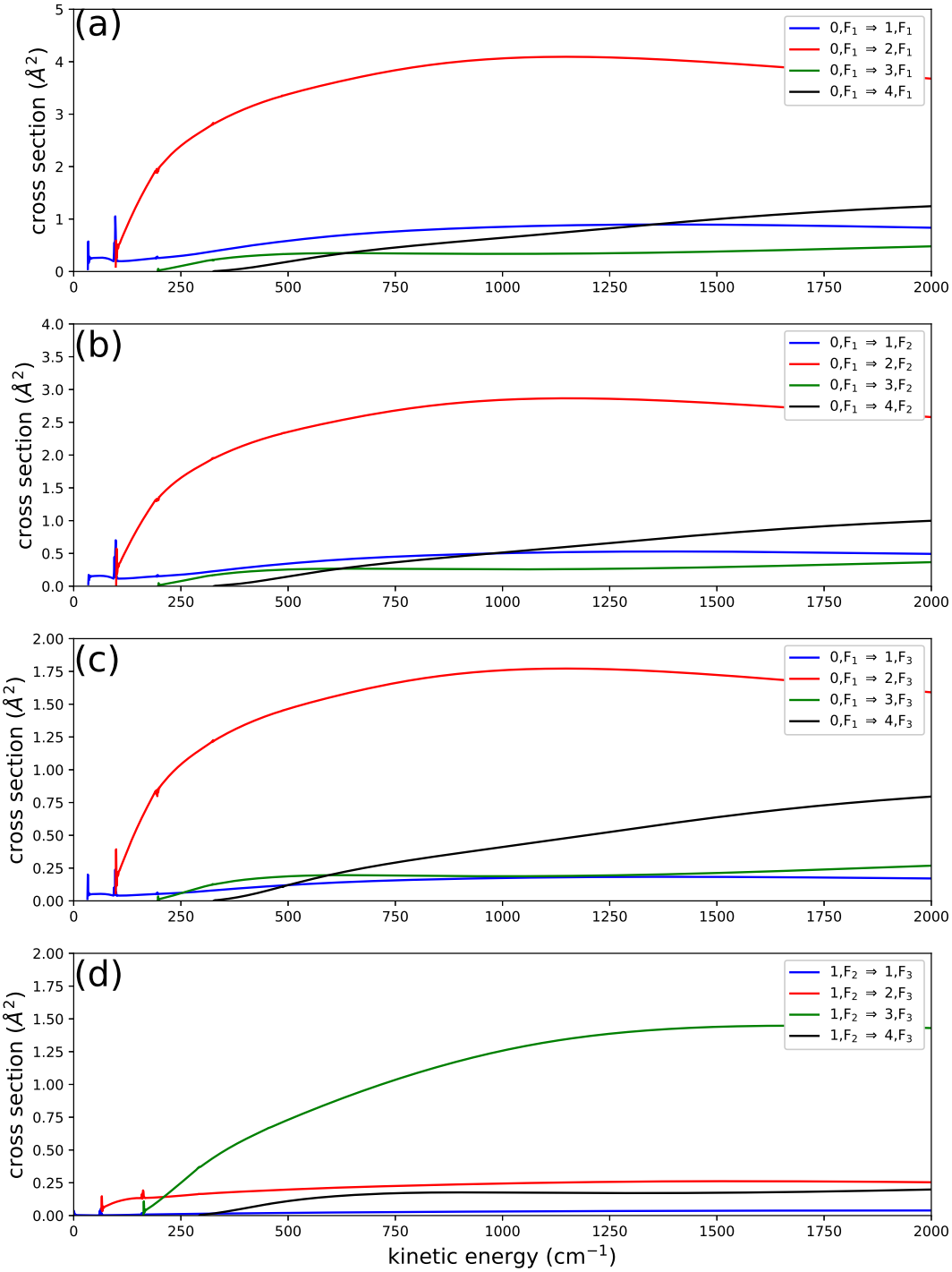

Figure 6.4: Collisional excitation cross sections of NH by He from N=0,F_1.(a) is for F-conserving transitions, while (b-d) are for F-changing transitions.

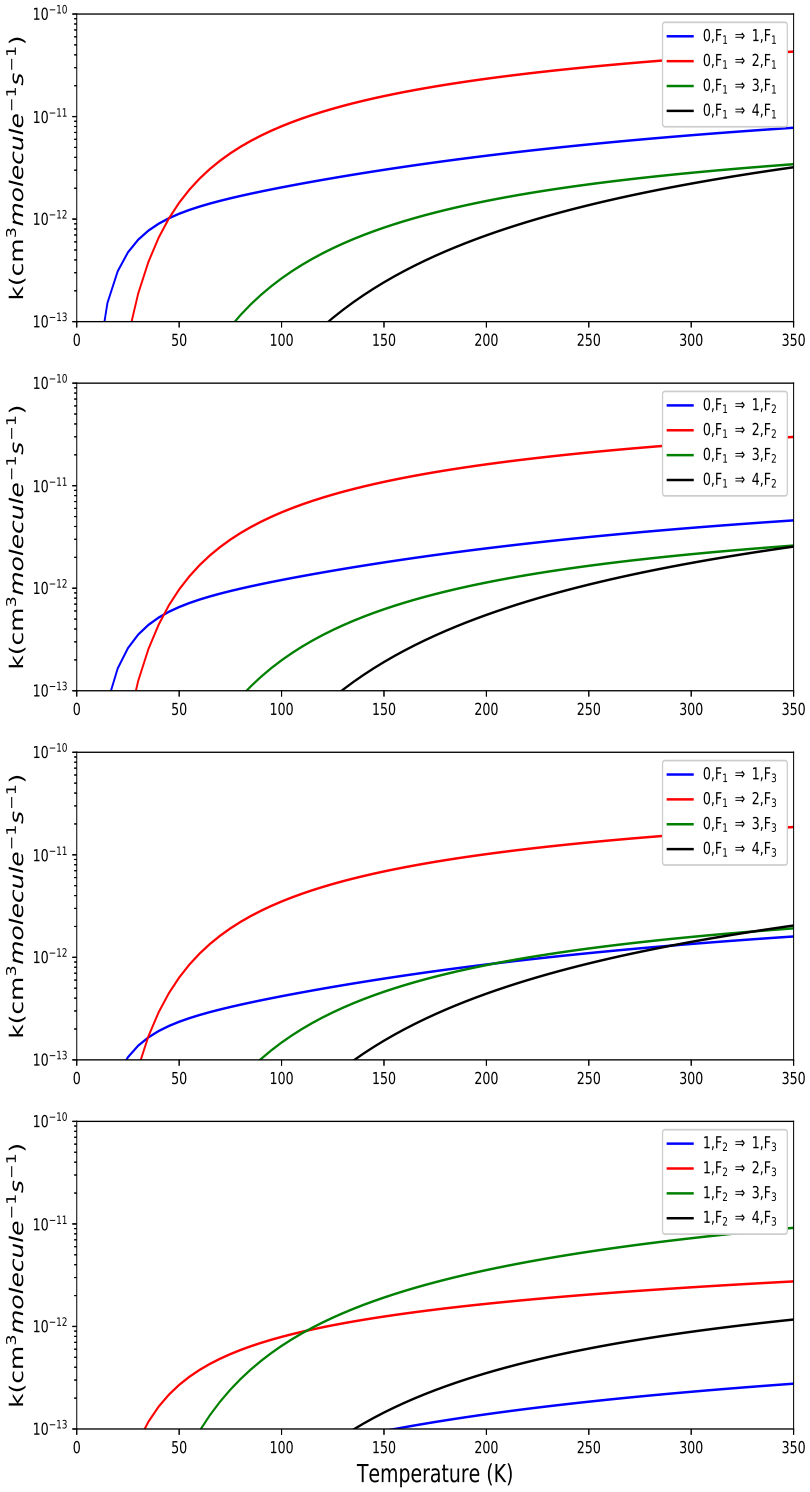

Figure 6.5: Temperature dependent rate-coefficients of collision of NH by He from N=2,F_1 for fine structure resolved levels.(a) is a representation of F-conserving transitions, while (b-d) represents F-changing transitions.

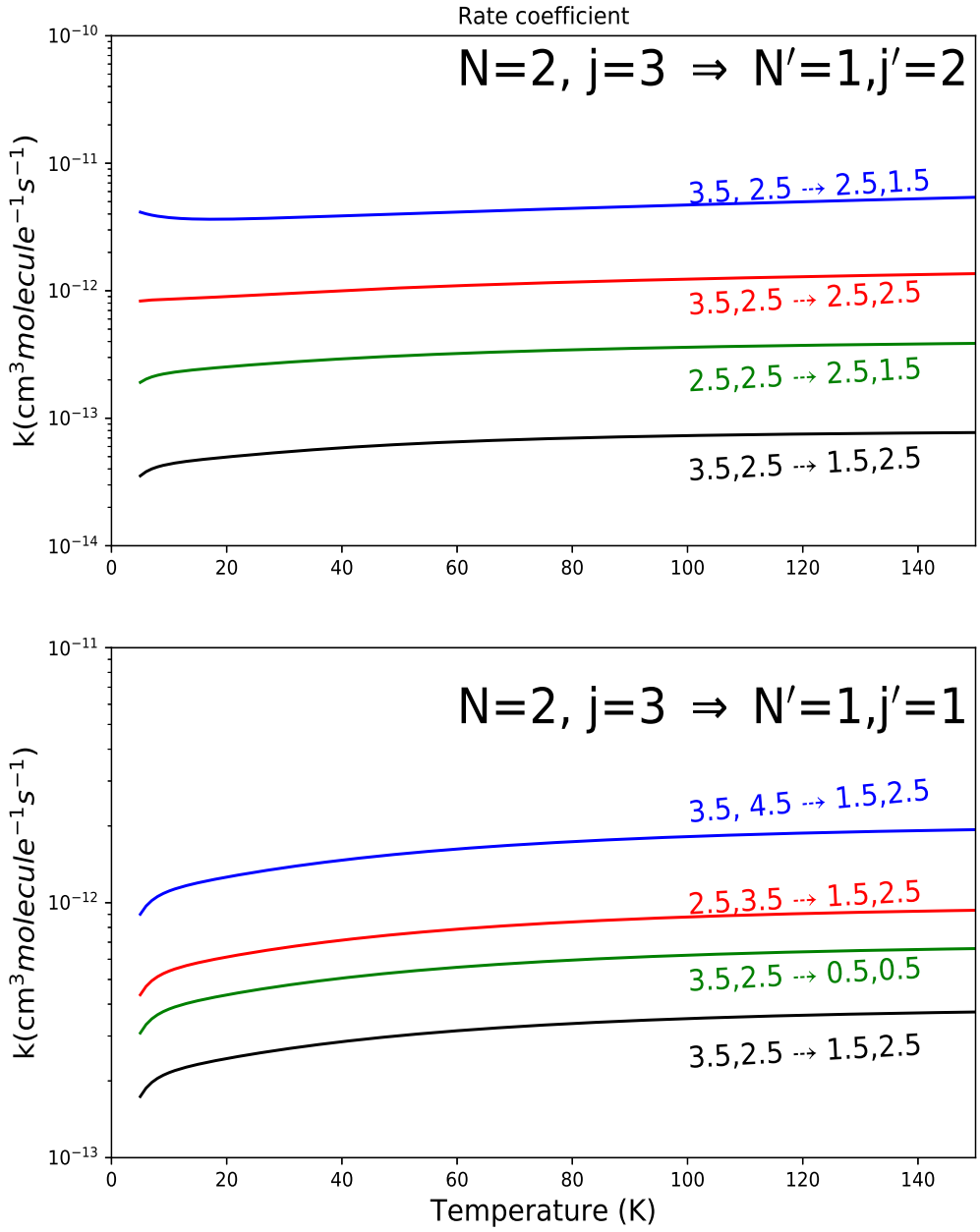

Figure 6.6: Temperature dependent rate-coefficients of collision of NH by He from N=2,F_1 for hyperfine resolved levels.(a) is a representation of F-conserving transitions, while (b) represents F-changing transitions.

6.4 Observations and Discussions

6.4.1 Fine Structure excitations

We can see from fig 6.4 that the resonances appear at low collisional energies. This is related to the presence of an attractive potential well of a depth of ≈20 cm^{-1}, which allows for the He atom to be temporarily trapped there and hence quasi-bound states to be formed before the complex dissociates (Smith et al., 1979; Christoffel et al., 1983). However, few resonances are seen in the excitation cross sections since the energy spacing between two rotational levels is generally large in comparison to the well depth of the NH–He PES.

The magnitude of the cross sections shown in Fig 6.4 seems to be governed by the following propensity rules:

1. The cross sections decrease with increasing ΔN, which is the usual trend for rotational excitation. In addition, even ΔN transitions are favored over odd ΔN transitions. This is a consequence of dominant even anisotropy of the PES over the odd anisotropy (i.e., the radial coefficients $A_{ln}(R)$ of Eq.6.4 with even l dominates over those with odd l).

2. A propensity rule exists for F-conserving transitions ($\Delta j = \Delta N$ in the case of pure Hund's case (b)).

The rate coefficients obviously display the same propensity rules as seen in the integral cross sections. In particular,the rate coefficients for F-conserving transitions are generally larger than those for F-changing transitions. The same propensity rules were previously observed in NH–He (Toboła et al., 2011) collisions. The latter propensity, predicted theoretically (Alexander and Dagdigian, 1983), is general for molecules in the $^3\Sigma^-$ electronic state and was previously observed in $O_2(X^3\Sigma^-)$-He (Orlikowski, 1985, Lique, 2010) and $SO(X^3\Sigma^-)$-He (Lique, Spielfiedel, Dubernet et al., 2005) collisions.

We can compare our results with the previous theoretical and experimental works. First, we compare the results of the present work with that of Toboła et al., 2011. Figure 6.7 presents the comparison of the kinetic energy variation of the collisional cross sections for some selected transitions obtained from the 3D-avg PES, 2D PES and from Toboła et al., 2011 using the PES of Cybulski et al., 2005. We can notice from the figure, some deviations (as large as a factor of 2) exist between the two sets of data,

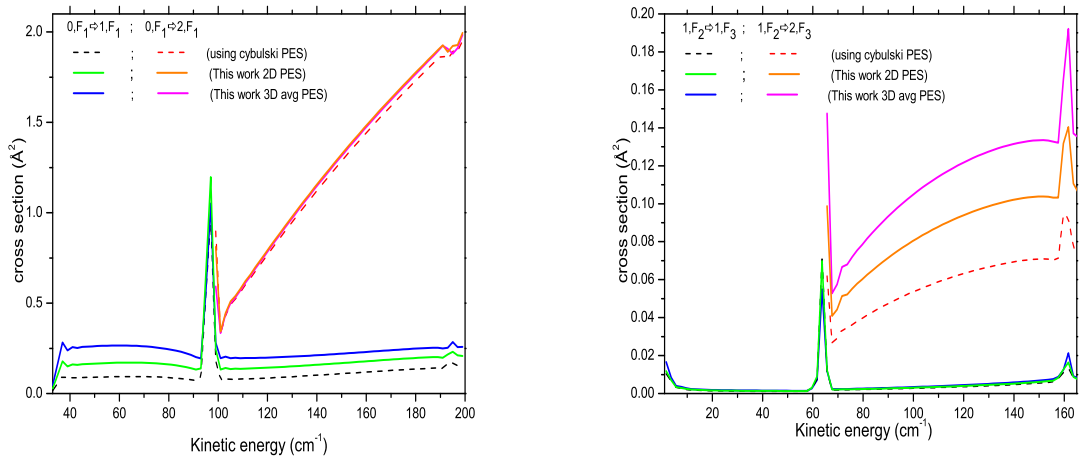

Figure 6.7: Comparison between NH-He fine structure cross sections obtained from the 3D-avg PES, the 2D PES, and the Cybulski PES. The left panel is a representation of F-conserving transitions, while the right panel represents F-changing transitions.

especially for transitions with odd ΔN. These deviations are not only due to the use of different PESs but also due to the inclusion of the vibration of NH in the new PES. This can be illuminated by comparing the 3D-avg PES and the Toboła et al., 2011 results with the cross sections of the 2D PES (orange and green lines of fig.6.7). We notice a significant part of the difference between the cross sections from the new PES and from the PES of Cybulski et al., 2005 comes from the inclusion of the NH vibration, confirming again the importance of inclusion of the intramolecular vibration.

Secondly, to juxtapose the results of the present work with the experiments, we compare the calculated rate coefficients at 300 K with the experimental results of Rinnenthal et al., 2002. The comparison is essentially between the sum of all rate coefficients from a particular state N,F_i. Table 6.2 presents these values. We can notice a good global agreement between the theoretical and experimental results. The total theoretical and experimental rate coefficients decrease with increasing N, as can be seen for the average total rate coefficients from the table 6.2. Such behavior is explained by the energy gap with the closest levels that increase with increasing N.

Thirdly, we can compare the experimental and theoretical state-to-state rate coefficients of NH-He also. Fig 6.8 presents the scatter diagram of the two.

The overall agreement between theoretical and experimental data is

N	F_1		F_2	
	Theory*	**Experiment***	**Theory***	**Experiment***
0	10.23	8.3		
1	10.13	13.01	10.85	12.66
2	10.96	13.39	13.04	20.73
3	10.62	9.62	12.61	13.25
4	9.67	8.44	11.38	12.87
5	8.52	6.13	9.89	11.07
6	7.31	3.44	8.45	7
7	5.99	3.11	6.91	6.01

N	F_3	
	Theory*	**Experiment***
0		
1	12.48	24.48
2	17.69	9.18
3	11.96	10.04
4	10.45	16.28
5	9.02	9.48
6	7.63	6.98
7	6.21	6.26

Table 6.2: Total rate coefficients (in units of 10^{-11}cm^{3}s^{-1}) out of the N,F_i states as a function of the initial nuclear rotation quantum number N at 300 K. (* *"Theory"* refers to the rate coefficients of 3D-avg PES and *"experiment"* refers to the results of Rinnenthal et al., 2002).

reasonably good despite some significant deviations. Most of the experimental collisional data are reproduced within a factor of 2-3. The mean deviation between the experimental and theoretical rate coefficients is a factor of 5 with very few exceptions. These large deviations are for the rate coefficients with the smaller magnitude that are probably more difficult to measure experimentally. Indeed,the error bar mentioned by Rinnenthal et al., 2002 is 0.08×10^{-11} cm^{3}s^{-1} and largely exceeds the value of these low magnitude rate coefficients.
Also, it is worth mentioning that the experimental results do not show the usual F-conserving propensity rules, and the experimental rate coefficients do not fulfill the detailed balance as already noticed in the work of Toboła et al., 2011.

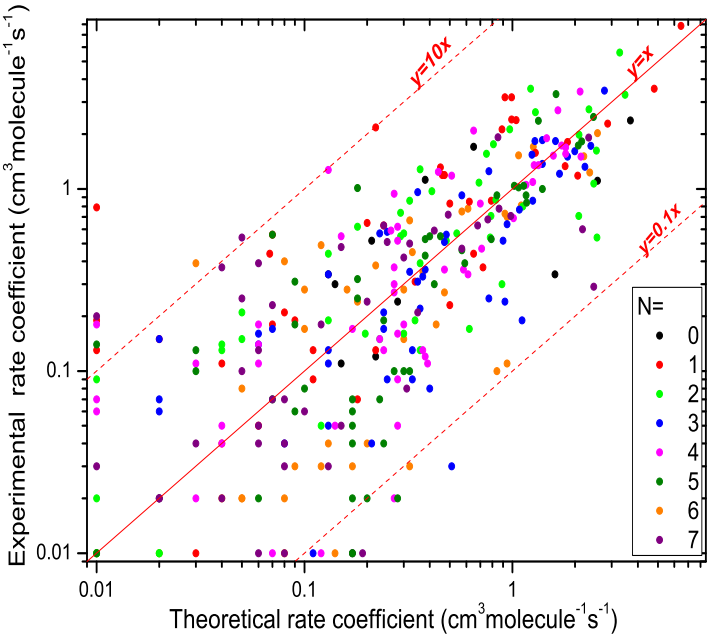

Figure 6.8: Experimental and theoretical state-to-state NH-He rate coefficients.

6.4.2 Hyperfine excitations

For the collision of NH by He, the hyperfine rate coeffients seems to be governed by the following propensity rules: For both $\Delta j = \Delta N$ and $\Delta j \neq \Delta N$ transitions, the largest rate coefficients are

1. if $\Delta F_1 = \Delta j$ then $\Delta F = \Delta\ F_1$,
2. if $\Delta F_1 = \Delta j \pm 1$ then $\Delta F = \Delta F_1 \pm 1$.

These relations must be combined both with the range of allowed values for the quantum number F and with the degeneracy factor $(2F+1)$ and it significantly modifies the propensity rules for transitions. The $\Delta F = \Delta F_1 = \Delta j$ propensity rule is more pronounced for $\Delta j = \Delta N$ transitions than for the $\Delta j \neq \Delta N$ ones and hence the only well defined propensity rule for NH-He hyperfine transitions is $\Delta F = \Delta F_1 = \Delta j$.

CHAPTER 7

ND-He: PES and Scattering Calculations

In the introduction, we saw the significance of isotopic substitutions in the ISM and hence the importance of studying the (de-)excitation of isotopologues. For modeling the abundance, usually the rate coefficients of the main isotopologue are used for the secondary isotopologue. It may work for the heavier atoms, but for light atoms like H, it may not be reliable because the relative mass difference between H and D is significant. Hence each isotopologue needs to be specifically studied. In this chapter, we study the collision of ND by He.

7.1 Potential Energy Surface

For *ab initio* calculations, the ND-He geometry is described in Jacobi coordinates as in Fig 7.1.r_{ND} denotes the centre of mass of the ND molecule while r_{NH} denotes the centre of mass of NH and r_a is the difference between the centre of masses.

Since the ground state electronic potentials of NH-He and ND-He are the same in the Born-Oppenheimer approximation, we use the NH-He interaction potential for ND-He also. The main difference between the NH-He and ND-He is the difference in the position of the centre of mass. This difference is introduced computationally as a displacement in the Jacobi coordiante in the analytic expansion of the PES using the following equations:

$$\Theta = Sin^{-1}\left(\frac{R' Sin\Theta'}{R}\right)$$

$$R = \sqrt{R'^2 + r_a^2 + 2R' r_a cos\Theta'}$$

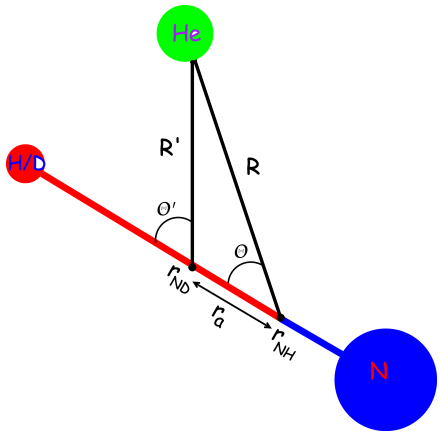

Figure 7.1: Jacobi coordinates for ND-He and NH-He.

where Θ, Θ', R, R', r_a are defined as in fig.7.1.
For averaging the 3D PES over the vibrational state, we evaluate the ND vibrational wavefunction ($|v(r)>$) using the DVR method. $\langle v(r)|\,(r-r_e)^{n-1}\,|v(r)\rangle$ values are given in table 7.1. Fig. 7.2 shows the contour plot of the 3D averaged ND-He PES. The position of the well depth are unchanged. The effect of the shift in the position of centre of mass on the PES can be noticed by looking at the difference between the ND-He PES and the NH-He PES. Fig. 7.3 is the contour plot of the differences between the 3D-avg PESs of NH-He and ND-He.

	n=1	**n=2**	**n=3**	**n=4**	**n=5**
***v*=0**	1.0000	0.0252	0.0153	0.0014	0.0007
***v*=1**	1.0000	0.0767	0.0503	0.0094	0.0046
***v*=2**	1.0000	0.1301	0.0924	0.0272	0.0150

Table 7.1: $\langle v(r)|\,(r-r_e)^{n-1}\,|v(r)\rangle$ values for given n and vibrational state,v.

7.2 Results

7.2.1 Fine structure excitations

For the scattering calculations of ND-He collisions, the cross-sections are calculated using the close coupling (Arthurs, Dalgarno and Bates, 1960) method. To solve the quantum coupled equations, we use the MOLSCAT

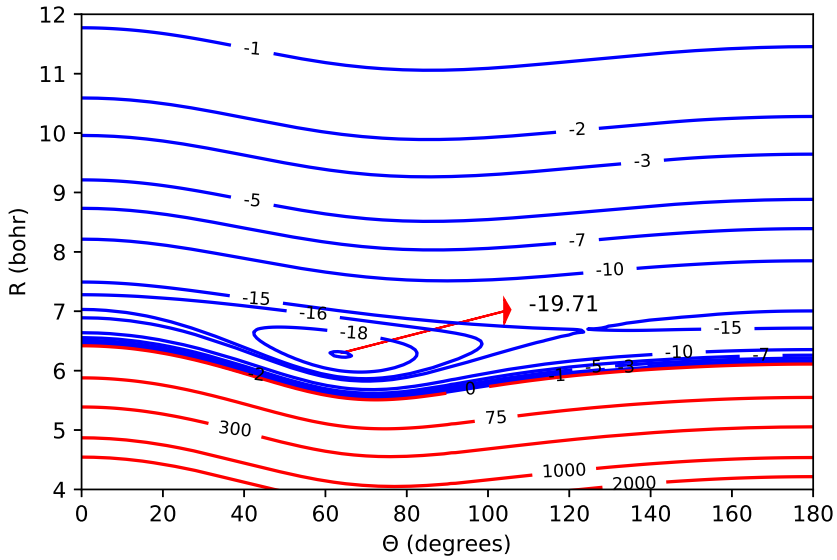

Figure 7.2: Contour plot of 3D-avg ND-He PES as a function of R and Θ.

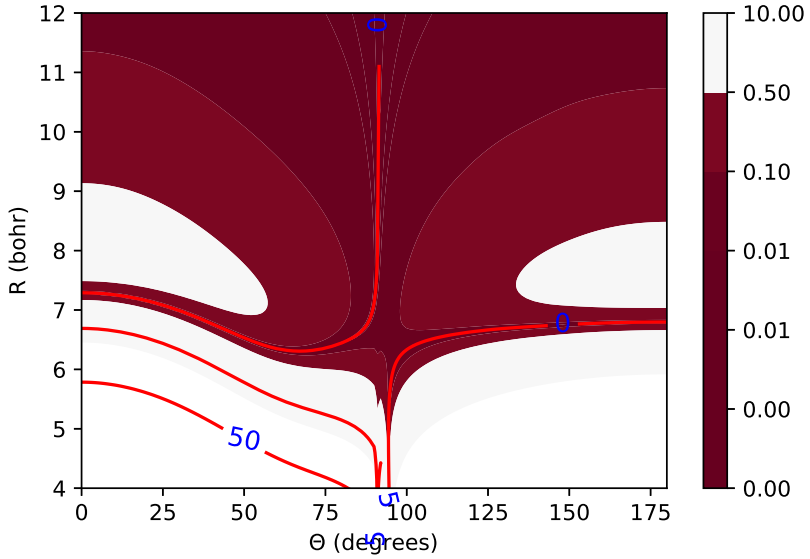

Figure 7.3: Difference between 3D-avg PES of NH-He and ND-He. The energies are in cm^{-1}.

(Hutson, 1994b) code modified (as mentioned in the previous chapter) to take into account the fine structure energy levels of ND. The cross sections are computed for a total energy grid of 2000 cm^{-1}. For the convergence of the inelastic cross section, the ND rotational basis was extended up to N=22 for cross sections between levels with N<8. The rotational basis varied with varying energies. Also, the propagator parameters (integration distance and STEPS) were adjusted to ensure the convergence of the cross section. The convergence values of the paramenters are given in Appendix A. The reduced mass (μ) of the ND-He system is 3.202 amu (compared to μ of NH-He which is 3.1600 amu). Figure 7.4 presents the energy variation of the integral cross sections for transitions from the initial rotational level N = 0,F_1 of ND.

By averaging over a Maxwellian distribution of the collisional velocities using the equation 3.23, we obtain the thermally averaged rate coefficients for excitation and de-excitation transitions between fine-structure levels of ND. We obtained rate coefficients for temperatures up to 200 K. The thermal dependence of the state-to-state rate coefficients is illustrated in Fig. 7.5 for transitions out of the $N = 0$, F_1 level.

7.2.2 Hyperfine structure

Using the S-matrix of the fine structure resolved state-to-state dynamic calculations of ND-He, we calculated the hyperfine resolved ND–He cross sections using a procedure similar to what we did in the previous chapter. Then, by averaging the cross sections over a Maxwellian distribution of the collisional velocities, we obtained thermal rate coefficients for excitation and de-excitation transitions between hyperfine levels of NH. We obtained rate coefficients for temperatures up to 150 K. Figure 7.6 presents the temperature variation of the hyperfine resolved ND–He rate coefficients for a selected transitions.

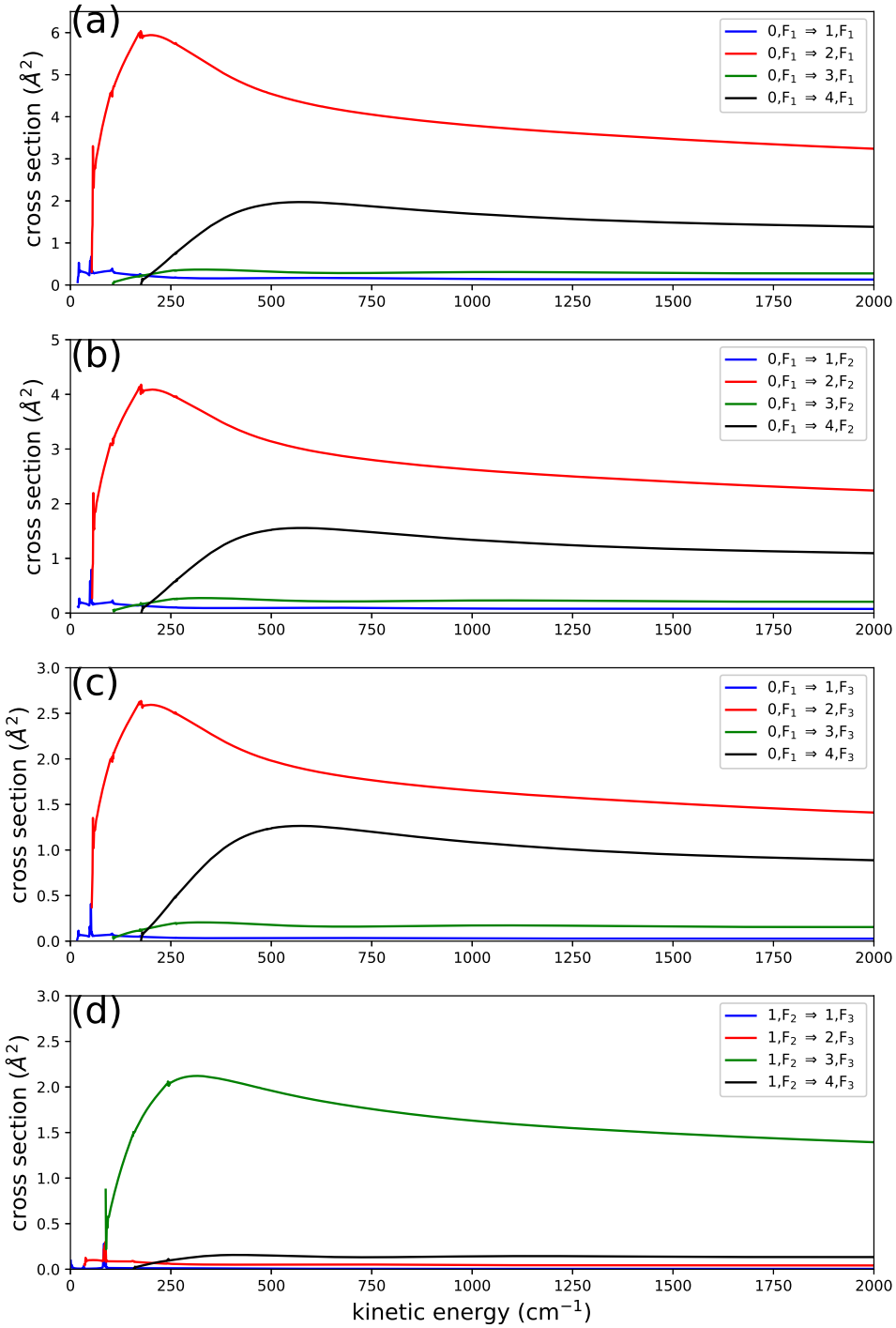

Figure 7.4: Collisional excitation cross sections of ND by He from N $0,F_1$.(a) is for F-conserving transitions, while (b-d) are for F-changing transitions.

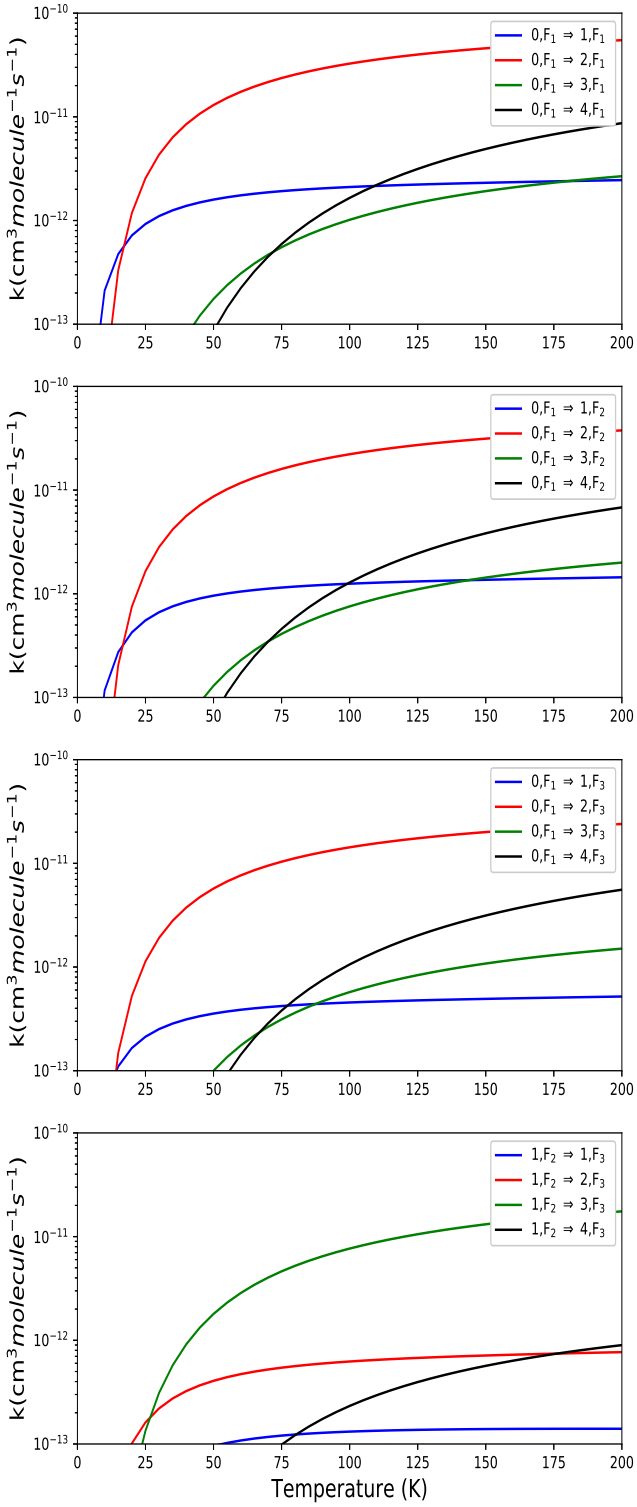

Figure 7.5: Temperature dependent rate-coefficients of collision of ND by He from N=2,F_1 for hyperfine resolved levels.(a) is a representation of F-conserving transitions, while (b-d) represents F-changing transitions.

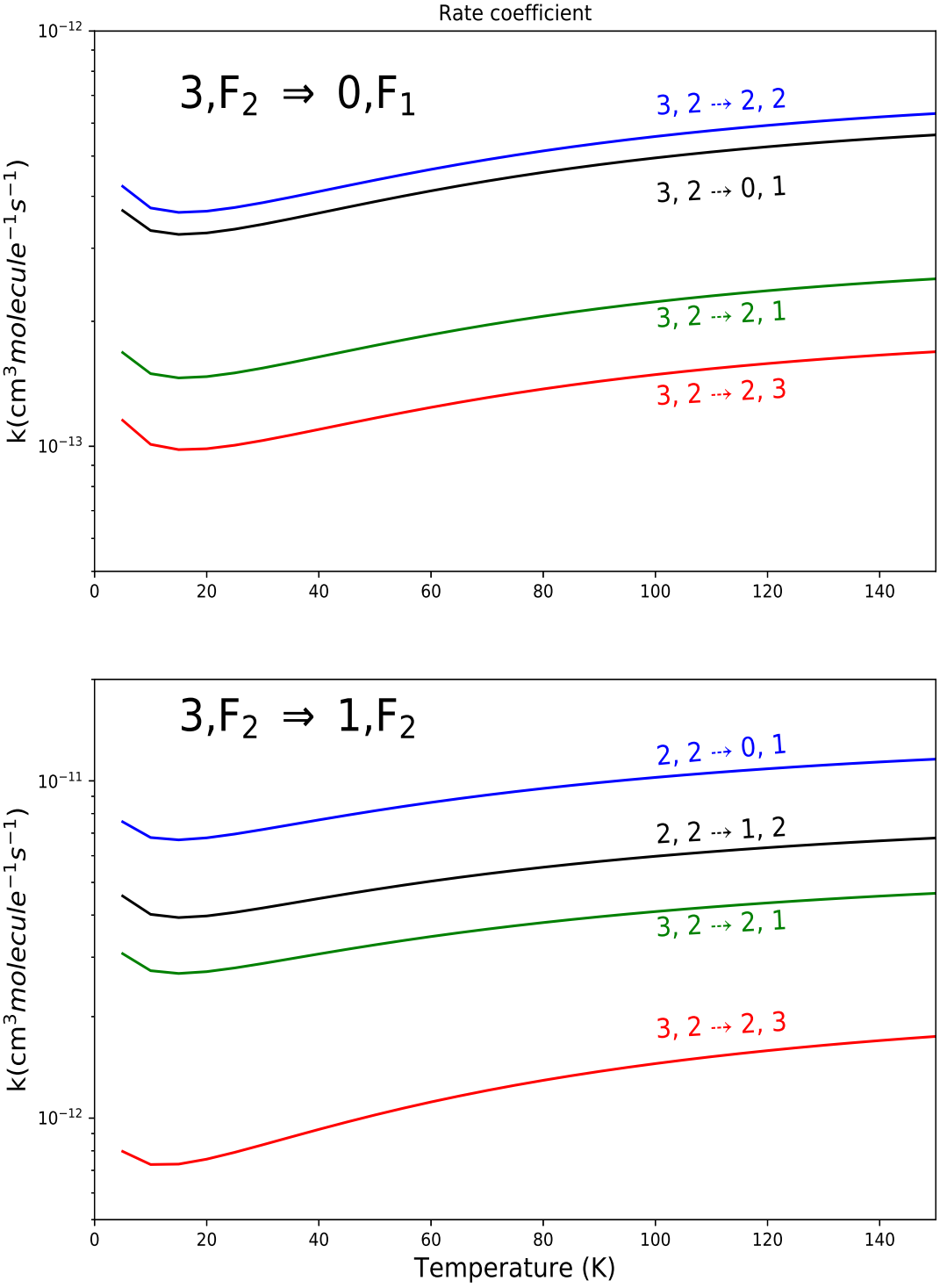

Figure 7.6: Temperature dependent rate-coefficients of collision of ND by He from N=3,F_2 for hyperfine resolved levels.(a) is a representation of F-changing transitions, while (b) represents F-conserving transitions.

7.3 Observations and Discussions

We can see from fig. 7.4, resonances appear at low collisional energies. As observed in NH-He cross section (fig. 6.4), we notice resonances in the cross section at low kinetic energies for the ND-He collisions too. These resonances, related to the feshbach and orbiting resonances, are due to the asymptotically closed channel and quasi-bound states (Chandler, 2010; Naulin et al., 2014).

For the fine structure resolved transitions, the magnitude of the cross sections shown in Fig 7.4 decreases with increasing ΔN and *even*-ΔN transitions are favored over *odd*-ΔN transitions. Similarly, F-conserving transitions are favoured over F-changing transitions. For the hyperfine resolved transitions (fig. 7.6), the rate coeffient is governed by the propensity rules that for both $\Delta j = \Delta N$ and $\Delta j \neq \Delta N$ transitions, the largest rate coefficients are $\Delta F = \Delta\ F_1$ if $\Delta F_1 = \Delta j$ and $\Delta F = \Delta F_1 \pm 1$ if $\Delta F_1 = \Delta j \pm 1$. These are the same propensity rules which were observed for NH-He (de-)excitations.

To show the significance of H/D substitution in NH, we compare the results of NH-He and ND-He scattering calculations. Due to the difference in the nuclear spin of H and D, we cannot directly compare the results of ND-He hyperfine structure resolved rate coefficients with that of the NH-He. But, since we have calculated them directly from the fine structures, the differences will be transmitted to the hyperfine transitions too.[1] Hence we compare the results of NH-He and ND-He fine-structure resolved scattering calculations.

Fig. 7.7 compares the cross sections of the collisions of NH and ND by He for a few fine-structure resolved state-to-state transitions. As we can notice from figs. 7.7, there are significant differences between the values of ND-He and NH-He. The differences are larger at low energies than at high energies. The pattern of differences in cross sections are similar for both excitation and de-excitation. This can be clearly noticed from table 7.2. The main

[1] We could compare these results (fine and hyperfine) with the Dumouchel et al., 2012 results to show the significance of use of the new PES, but since it had some energy level misrepresentations, we cannot directly correlate them. Hence the comparison is ignored.

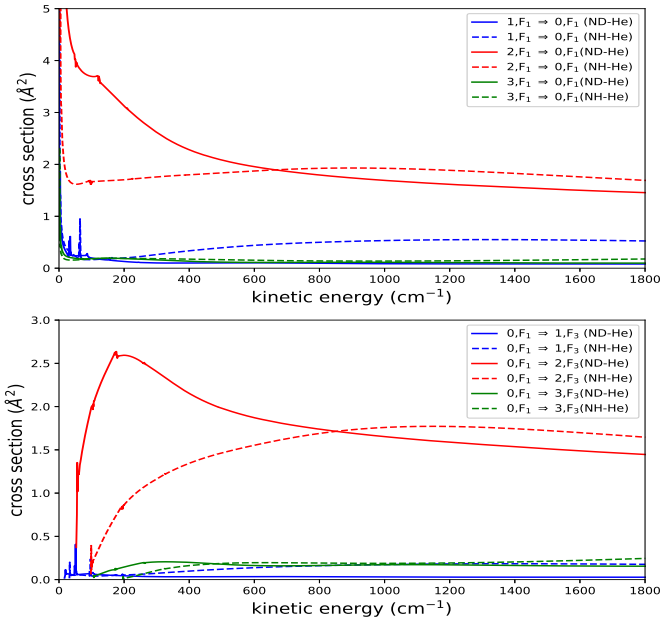

Figure 7.7: comparing the fine-structure resolved cross-section of ND-He (solid line) and NH-He (dashed line).

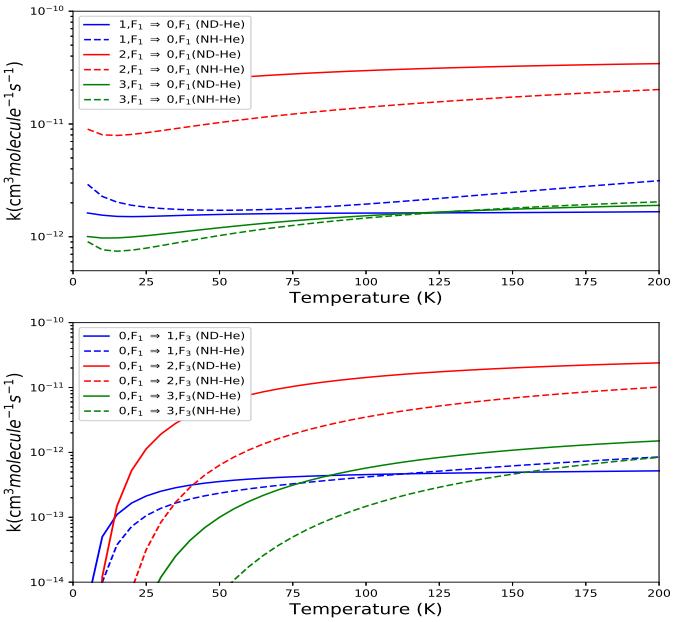

Figure 7.8: comparing the fine-structure resolved rate coefficients of ND-He (solid line) and NH-He (dashed line).

Transition	E =100 cm^{-1}			E =500 cm^{-1}		
	NH	ND	ND	NH	ND	ND
$0,F_1 \rightarrow 1,F_1$	0.243	0.213	0.335	0.586	1.001	0.165
$0,F_1 \rightarrow 2,F_1$	0.252	2.486	4.569	3.380	3.666	4.542
$0,F_1 \rightarrow 1,F_3$	0.044	0.045	0.070	0.121	0.209	0.034
$0,F_1 \rightarrow 2,F_3$	0.113	1.091	2.000	1.464	1.598	1.980
$0,F_1 \rightarrow 2,F_2$	0.573	1.687	3.104	2.353	2.530	3.138
$4,F_1 \rightarrow 1,F_1$	0.207	0.288	0.263	0.293	0.228	0.204
$4,F_1 \rightarrow 2,F_1$	0.562	2.055	3.697	1.282	2.459	3.540
$4,F_1 \rightarrow 3,F_1$	1.587	1.405	0.632	1.460	1.151	0.412
$4,F_1 \rightarrow 2,F_2$	0.157	0.202	0.555	0.335	0.306	0.687
$4,F_1 \rightarrow 2,F_3$	0.088	0.088	0.303	0.216	0.174	0.452

Table 7.2: comparison of cross-sections (in Å^2) of NH-He, ND-He with NH-He PES and ND-He with ND-He PES

reason for the huge differences between ND-He and NH-He cross sections at lower energies is the differences in the energy levels of NH and ND. Since the lower energy levels of ND are closely spaced when compared to NH, the cross sections of ND-He are higher than that of NH-He.

Next, to show the importance/effect of inclusion of the change in the position of the centre of mass, we present in table 7.2, a comparison between the cross sections of: (a) NH-He; (b) ND-He calculated using the NH-He PES, energy levels of ND and the reduced mass of ND-He and (c) the exact ND-He cross sections calculated using the ND-He PES (fig. 7.2), energy levels of ND and reduced mass of ND-He, for 2 different energies. We can notice that all 3 cross sections differ significantly. If we compare the two ND-He cross sections, the differences in the values show the importance of including the shift in the position of centre of mass. Especially for even ΔN, the difference between the two ND-He cross sections are very large.

Fig. 7.8 compares the rate coefficients of the collisions of NH and ND by He for a few fine-structure resolved state-to-state transitions. The figure shows that the rate coefficients also differ significantly. In general, the even ΔN transitions have larger differences than the odd ΔN transitions. Except for the $\Delta N = 1$ transitions, for all the transitions, the ND-He rate coefficients are higher than that of NH-He. Also, for these transitions, the differences are more at lower temperatures and decreases with increasing temperature. But for $\Delta N = 1$ transitions, the case seems to be reversed.

Based on the above observations, the difference between NH-He and ND-He

can be attributed to the following parameters (in the order of significance):

- The shift in the position of centre of masses of NH and ND.
- The difference in the energy levels of NH and ND (rotational constant difference)
- The difference of the reduced masses of NH-He (3.160 amu) and ND-He (3.202 amu).

CHAPTER 8

NH-H_2: PES and Scattering Calculations

As mentioned in the introduction, molecular hydrogen is the most abundant molecule in the ISM and hence an important collisional partner. Astrophysicists often use scaled He collisional rate coefficients to approximate excitation by H_2. The use of this approximation has previously been found to be inaccurate (Dubernet, M.-L. et al., 2006; Lanza et al., 2014; Bouhafs, Lique et al., 2017). In this chapter we present the collision of NH by H_2.

Hydrogen has a nuclear spin of 1/2 and hence for H_2 the nuclear spins of the hyrogen can either be in the same direction (I=1) or the opposite (I=0). This leads to the *ortho-* ($o$$H_2$) and *para-* ($p$$H_2$) forms, also called nuclear-spin isomers of H_2. To satisfy the exclusion principle, the rotational levels of $o$$H_2$ are given by odd values of the rotational quantum number j, while the levels of $p$$H_2$ have even j values. Both $o$$H_2$ and $p$$H_2$ are important collisional partner, so we have to consider the collisional processes for both species separately.

8.1 Potential Energy Surface

For the *ab initio* calculations, the NH-H_2 geometry is described in Jacobi coordinates as in Fig 8.1.

R is the distance between the centre-of-masses of NH and H_2, Θ is the angle between R and the bond length of NH, Θ' the angle between R and the bond length of H_2 and ϕ is the azimuthal angle representing the rotation of H_2 about R. The PES is calculated for a fixed NH and H_2 bond distance of 1.99 bohr and 1.44 bohr respectively. Θ and Θ' varies between 0° and 180° while ϕ varied between 0° and 90°.

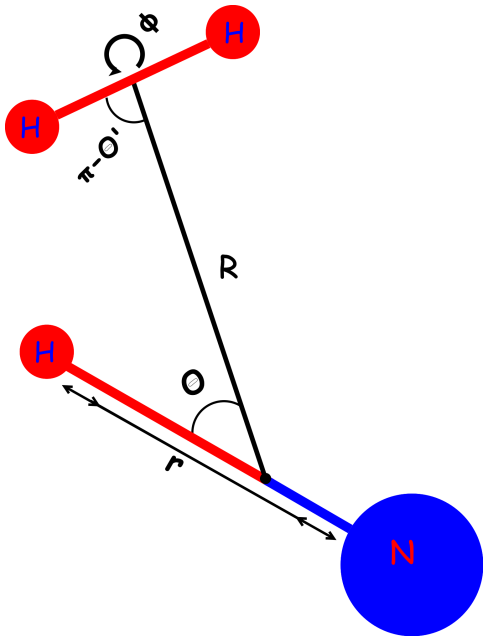

Figure 8.1: Jacobi coordinates for NH-H_2.

The new *an initio* calculations were carried out using partially spin-restricted coupled cluster method with single, double and perturbative triple excitation [$RCCSD(T)$] using F12a method(Adler et al., 2007; Knizia et al., 2009) with the *aug-cc-p*VTZ(AVTZ) basis set (section 2.2.2.1 and 2.2.3) using the MOLPRO package (Werner et al., 2010). To obtain the analytic representation accessible for close coupling solutions, the *ab initio* points are fitted as described in section 2.3 for a radial grid of R with $0 \leq L_1 \leq 10$ and $0 \leq L_2 \leq 4$ giving a total of 86 radial expansion coefficients (L_1 and L_2 are the Legendre polynomial expansion terms in he interaction potential associated with NH and H_2 respectively). Figure 8.2 shows contour plots of the analytical potential. Each contour is a 2-Dimensional cut of the 4D NH-H_2 PES.

The Global minima for this PES is at $R = 6.30$ bohr, $\Theta = 180°$ and $\Theta' = 0°/180°$ with a well depth of 149.10 cm^{-1}. The PES also has another local minima at $R = 6.80$ bohr, $\Theta = 0°$ and $\Theta' = 90°$ with a well depth of 109.54 cm^{-1}.

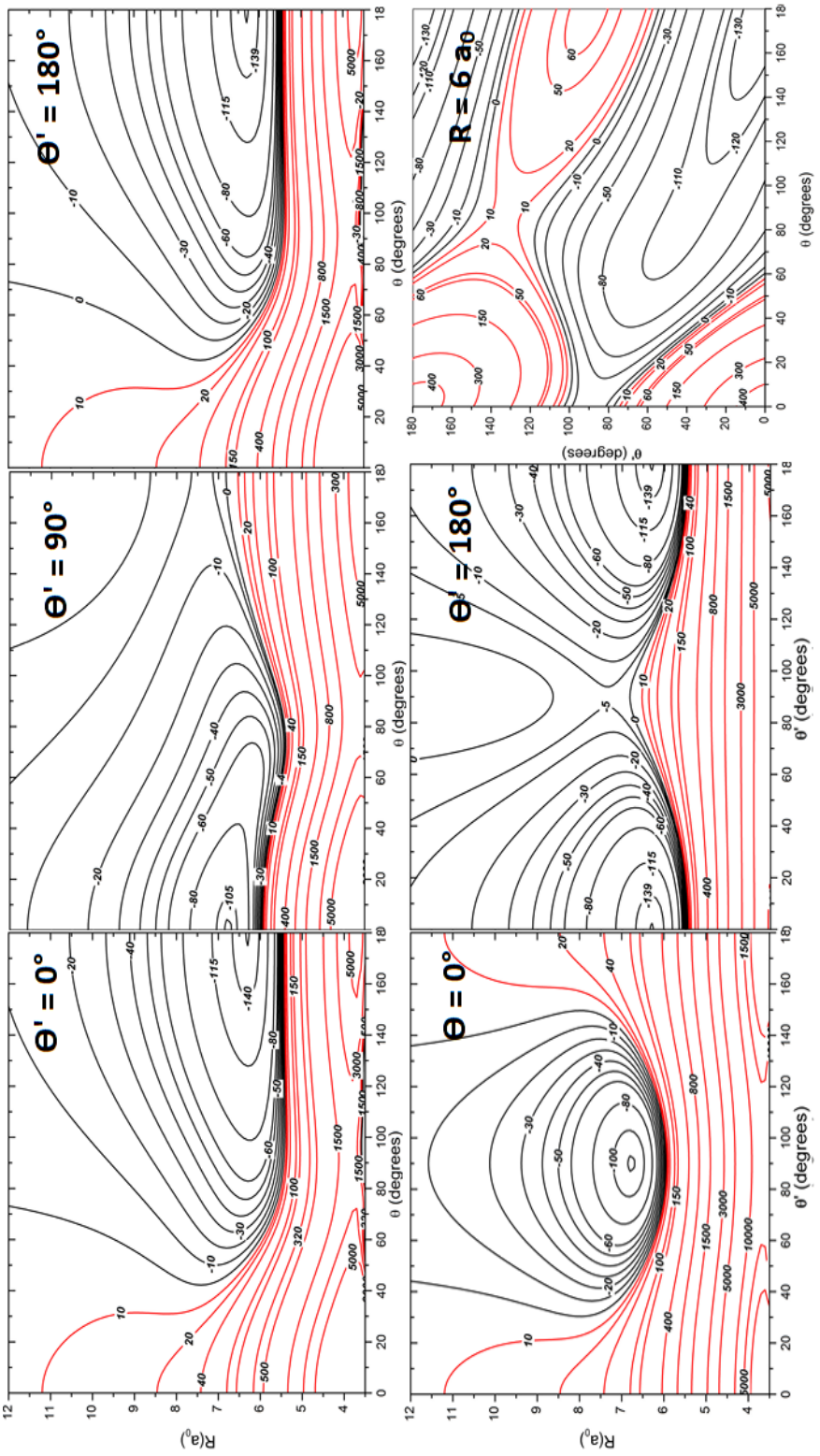

Figure 8.2: Contour plot of 4D NH-H_2 PES for fixed values of co-ordinates mentioned in each contour.

8.2 Collisonal Dynamics of diatom with diatom

The detailed derivation for the case of closed shell diatom-diatom collision was first given by Green (1975). In the beginning of chapter 3, we introduced the total Hamiltonian for a diatom-diatom system. If we don't consider $H_{CD} = 0$, then we can write

$$H_{\mathrm{AB}} = \frac{\hbar^2}{2I}\mathbf{j_1}^2 \tag{8.1}$$

$$H_{\mathrm{CD}} = \frac{\hbar^2}{2I}\mathbf{j_2}^2 \tag{8.2}$$

where the molecule AB and CD are closed-shell molecule. With this, we can get the close-coupling equations for for diatom-diatom system (similar to eq. 3.12) as follows

$$\frac{\hbar^2}{2\mu}\left(\frac{\partial^2}{\partial R^2} - \frac{l'(l'+1)}{R^2} + k^2_{\gamma'\gamma}\right)\mathscr{U}^J_{\gamma'}(R) = \sum_{\gamma''}\mathscr{U}^J_{\gamma''}(R)\,\langle j''_1 j''_2 j''_{12} l'' J|\,V(R,\Theta,\Theta',\Phi)\,|j'_1 j'_2 j'_{12} l' J\rangle \tag{8.3}$$

where, j_1 and j_2 are the rotational momenta quantum numbers of the molecules AB and CD respectively. l is the orbital momentum of the collision, $j_{12} = j_1 + j_2$, $J = j_{12} + l$. $\gamma \equiv j_1 j_2 j_{12} l$.

If the electronic potential $V(R,\Theta,\Theta',\Phi)$ is of the form

$$V(R,\Theta,\Theta',\Phi) = \sum_{\lambda_1\lambda_2\lambda} E_{el}^{\lambda_1\lambda_2\lambda}(R) \sum_{m_1 m_2 m} \langle \lambda_1\lambda_2 m_1 m_l | j'\lambda' JM\rangle\, Y^{m_1}_{\lambda_1}(\mathbf{r}) Y^{m_2}_{\lambda_2}(\mathbf{r}') Y^{m}_{\lambda}(\mathbf{R}) \tag{8.4}$$

the term $\langle j''_1 j''_2 j''_{12} l'' J|\,V(R,\Theta,\Theta',\Phi)\,|j'_1 j'_2 j'_{12} l' J\rangle$ becomes

$$\begin{aligned}\langle j''_1 j''_2 j''_{12} l'' J|V(R,\Theta,\Theta',\Phi)\,|j'_1 j'_2 j'_{12} l' J\rangle = \sum_{\lambda_1\lambda_2\lambda} E_{el}^{\lambda_1\lambda_2\lambda}(R)(-1)^{J+j'_1+j'_2+j'_{12}} \\ \times \sqrt{([j'_1][j''_1][j'_2][j''_2][j'_{12}][j''_{12}][l'][l''][\lambda]^2[\lambda_1][\lambda_2])}\begin{pmatrix}\lambda & l'' & l'\\ 0 & 0 & 0\end{pmatrix} \\ \times \begin{pmatrix}\lambda_1 & j''_1 & j'_1\\ 0 & 0 & 0\end{pmatrix}\begin{pmatrix}\lambda_2 & j''_2 & j'_2\\ 0 & 0 & 0\end{pmatrix}\begin{Bmatrix} l'' & l' & \lambda\\ j'_{12} & j''_{12} & J\end{Bmatrix}\begin{Bmatrix} j''_{12} & j''_2 & j''_1\\ j'_{12} & j'_2 & j'_1\\ \lambda & \lambda_2 & \lambda_1\end{Bmatrix}\end{aligned} \tag{8.5}$$

Then the solution to eq. 8.3, subject to boundary condition that the wavefunction vanishes as R $\rightarrow$ 0 and the S-matrix is expressed as follows

$$\boxed{\mathscr{U}^{J}_{\gamma'}(R) = \delta_{\gamma\gamma'} e^{-i(k_{\gamma\gamma}R - \frac{l\pi}{2})} - \sqrt{\frac{k_{\gamma\gamma}}{k_{\gamma'\gamma}}} \langle\gamma'| S^{J} |\gamma\rangle e^{i(k_{\gamma'\gamma}R - \frac{l'\pi}{2})}} \tag{8.6}$$

where,

$$k^2_{\gamma'\gamma} = \frac{2\mu}{\hbar^2}(E + E_\gamma - E_{\gamma'})$$

From the S-matrix, the cross section is obtained as

$$\boxed{\sigma(j'_1 j'_2 \leftarrow j_1 j_2) = \frac{\pi}{k^2_{\gamma\gamma}[j_1][j_2]} \sum_{J, j_{12}, j'_{12}, l, l'} [J] \left|\delta_{\gamma\gamma'} - \langle\gamma'| S^{J} |\gamma\rangle\right|^2} \tag{8.7}$$

This gives the cross section for pure rotational level resolved (de-)excitation of closed-shell linear rigid rotor - linear rigid rotor collision. These equations are directly implemented in the default MOLSCAT codes ITYPE=3 (Hutson, 1994b). But, we know that NH is an open-shell molecule and we saw the importance of considering the spin interactions (fine structures) for atom-diatom system from chapter 6. In the next section, we rewrite the above equations to include the spin in the dynamic equations similar to what we did in section 6.2.

8.2.1 Collisonal Dynamics of NH($^3\Sigma^-$) with H_2($^1\Sigma$)

Similar to sec. 6.2, we start from the pure hund's (b) case of the NH molecule and later we will consider the intermediate coupling case.

In the *pure* hund's case (b), the total angular momentum quantum number for NH molecule is given by

$$j_1 = N + S$$

where, N is rotational momentum quantum numbers of NH molecule. Hence the wavefunction of the NH molecule would be given by eq. 6.5. Therefore the close-coupling equations becomes

$$\frac{\hbar^2}{2\mu}\left(\frac{\partial^2}{\partial R^2} - \frac{l'(l'+1)}{R^2} + k^2_{\beta'\beta}\right)\mathscr{U}^{J_T}_{\beta'}(R) = \sum_{\beta''} \mathscr{U}^{J_T}_{\beta''}(R) \langle\beta'' J_T| V(R, \Theta, \Theta', \Phi) |\beta' J_T\rangle \tag{8.8}$$

where, $\beta \equiv NSj_1j_2j_{12}l$. N and j_2 are the rotational momenta quantum numbers of the molecules NH and H_2 respectively. l is the orbital momentum of the collision, $j_{12} = N + j_2$, $J = j_{12} + l$ and $J_T = J + S$.

If the interaction potential is in the form of eq. 8.4, then the term $\langle \beta'' J_T | V(R, \Theta, \Theta', \Phi) | \beta' J_T \rangle$ would become

$$\begin{aligned}\langle \beta'' J_T | V(R, \Theta, \Theta', \Phi) | \beta' J_T \rangle = \sum_{J j_{12} j'_{12}} (-1)^{j''_R + j'_R + j''_2 + j'_2 + l'' + l'} \\ \times [J'] \sqrt{[j'_1][j''_1][j'_R][j''_R][j'_{12}][j''_{12}]} \\ \times \begin{Bmatrix} N' & j'_2 & j'_{12} \\ l' & J' & j'_R \end{Bmatrix} \begin{Bmatrix} N'' & j''_2 & j''_{12} \\ l'' & J & j''_R \end{Bmatrix} \begin{Bmatrix} j'_R & N' & J \\ S & J_T & j'_1 \end{Bmatrix} \\ \times \begin{Bmatrix} j''_R & N'' & J \\ S & J_T & j''_1 \end{Bmatrix} \langle j''_1 j''_2 j''_{12} l'' J | V(R, \Theta, \Theta', \Phi) | j'_1 j'_2 j'_{12} l' J \rangle \end{aligned} \tag{8.9}$$

where, $j_R = j_2 + l$ and $\langle j''_1 j''_2 j''_{12} l'' J | V(R, \Theta, \Theta', \Phi) | j'_1 j'_2 j'_{12} l' J \rangle$ is given by eq.8.5.

For **intermediate coupling** case, the close-coupling equation would hence be

$$\frac{\hbar^2}{2\mu} \left(\frac{\partial^2}{\partial R^2} - \frac{l'(l'+1)}{R^2} + k^2_{\alpha'\alpha} \right) \mathscr{U}^{J_T}_{\alpha'}(R) = \sum_{\alpha''} \mathscr{U}^{J_T}_{\alpha''}(R) \langle \alpha'' J_T | V(R, \Theta, \Theta', \Phi) | \alpha' J_T \rangle \tag{8.10}$$

where, $\alpha \equiv F_i \gamma \equiv F_i j_1 j_2 j_{12} l$. $\langle \alpha'' J_T | V(R, \Theta, \Theta', \Phi) | \alpha' J_T \rangle$ can be written in terms of $\langle \beta'' J_T | V(R, \Theta, \Theta', \Phi) | \beta' J_T \rangle$ as follows

$$\langle \alpha'' J_T | V(R, \Theta, \Theta', \Phi) | \alpha' J_T \rangle = \sum_{N'' N'} c^{j'}_{N' F'_i} c^{j''}_{N'' F''_i} \langle \beta'' J_T | V(R, \Theta, \Theta', \Phi) | \beta' J_T \rangle \tag{8.11}$$

Therefore the solution to the close coupled eq.8.10 subject it to boundary condition that the wavefunction vanishes as $R \to 0$ (as we did before) would be

$$\mathscr{U}^{J_T}_{\alpha'}(R) = \delta_{\alpha\alpha'} e^{-i(k_{\alpha\alpha} R - \frac{l\pi}{2})} - \sqrt{\frac{k_{\alpha\alpha}}{k_{\alpha'\alpha}}} \langle \alpha' | S^{J_T} | \alpha \rangle e^{i(k_{\alpha'\alpha} R - \frac{l'\pi}{2})} \tag{8.12}$$

This gives us the S-matrix. So the total **cross section** over all J_T for transitions between fine-structure resolved rotational energy levels of any

$^3\Sigma^- - ^1\Sigma$ system F_i,j_1,j_2 and F_i',j_1',j_2' would be

$$\sigma(F_i', j_1', j_2' \leftarrow F_i, j_1, j_2) = \frac{\pi}{k_{\alpha\alpha}^2[j_1][j_2]} \sum_{J_T, j_{12}, j_{12}', l, l'} [J_T] \left| \delta_{\alpha\alpha'} - \langle \alpha' | \, S^{J_T} \, | \alpha \rangle \right|^2 \tag{8.13}$$

$$k_{\alpha\alpha}^2 = \frac{2\mu E}{\hbar^2}$$

where, E is the relative kinetic energy.
The collisional de-excitation **rate coefficient** is hence defined as

$$k_{F_i j_1 j_2 \leftarrow F_i' j_1' j_2'}(T) = \sqrt{\frac{8 k_B T}{\pi \mu}} \left(\frac{1}{k_B T} \right)^2 \int_0^\infty \sigma_{F_i j_1 j_2 \leftarrow F_i' j_1' j_2'}(E) E \, e^{-\left(\frac{E}{k_B T}\right)} \, \mathrm{d}E \tag{8.14}$$

8.3 Influence of H_2 basis on scattering calculations

Before starting the scattering calculations, it is necessary to select a suitable rotational basis set for H_2 to ensure the convergence of the cross section. In this section we investigate the effect of various possible rotational basis sets on the pure rotational level resolved state-to-state cross sections. The comparison of selected pure rotational level resolved cross sections computed for a selected total energy of NH-H_2 collisions are presented in Table 8.1.

Energy (cm^{-1})	***para*-H_2**			***ortho*-H_2**	
	j_2**=0**	j_2 **= 0,2**	j_2 **= 0,2,4**	j_2 **= 1**	j_2 **= 1,3**
50	0.2494	0.3626	0.3624	-	-
100	19.0338	19.4505	19.4383	-	-
200	0.5098	0.7662	0.7631	19.0825	19.3520
300	0.1880	0.1753		2.8846	2.9075
1000	0.0105	0.0084		0.0566	0.0509

Table 8.1: values of cross section (in $Å^2$) for the highest transition of each energy.

For E = 50 and 100 cm^{-1}, there were no transitions for collisions with *ortho*-H_2 because the energies were below the threshold energy for the transition.

For *para*-H_2, there is a considerable difference in the cross sections between $j_2 = 0$ and $j_2 = 0, 2$ basis sets up to 300 cm^{-1} (37% for 50 cm^{-1} & 7% for 300 cm^{-1}) but for the basis sets $j_2 = 0, 2$ and $j_2 = 0, 2, 4$ the differences are very negligible (0.05% for 50 cm^{-1} & 0.4% for 100 cm^{-1}). It is interesting to note that for E = 300 cm^{-1}, the difference is negative which is different from other energies where the differences are positive. Even for E=1000 cm^{-1}, the difference is negative (-22%). With regards to the *ortho*-H_2 basis sets, $j_2 = 1$ and $j_2 = 1, 3$, the differences in the cross sections for energies 200, 300 and 1000 cm^{-1} are $\approx$ 1.4%, 0.8% & 0.1% respectively.

Up to 300 cm^{-1} there are no new transitions with increase in the basis of j_2. But at and beyond 1000 cm^{-1} there are new transitions. The cross sections of the $j_2 \rightarrow j_2'$ transitions [where, $j_2 = 0$ or 1 and $j_2' = 2$ or 3] are very less for *ortho*-H_2 (of the order of 10^{-3} $Å^2$), while for both *ortho*- and *para*-H_2 the cross sections for $j_2' \rightarrow j_2'$ transitions are higher when compared to $j_2 \rightarrow j_2$. With respect to the computational cost, the time taken for calculations with j_2 = 0,2,4 is too CPU consuming when compared to other 2 basis sets of *para*-H_2 and for *ortho*-H_2, time taken with j_2 = 1,3 is a lot more when compared to $j_2 = 1$.

From the calculations, we can hence say that j_2 = 0,2 would be more suitable for performing the scattering calculations for *para*-H_2 and $j_2 = 1$ for *ortho*-H_2.

8.4 Results and observations

8.4.1 *Pure* rotational level resolved scattering calculation

Using the NH-H_2 4D PES, we performed the first scattering calculations for the transitions between the *pure* rotational levels (N) of NH and H_2 (j_2) using the default MOLSCAT code (Hutson, 1994b) for linear rigid rotor - linear rigid rotor type collision (section 8.2). The value of convergence of various parameters used in the calculations are given in appendix A. The rotational basis set for H_2 is set based on the analysis of section 8.3. Figure 8.3 presents the energy variation of the integral cross sections for transitions between *pure* rotational levels of NH and H_2. In which, figures 8.3.1 presents the cross sections for a selected transtions between NH-$p$$H_2$($j_2$=*0*) levels

and figures 8.3.2 presents the cross sections for a selected transtions between NH-oH$_2$(j_2=*1*) levels.

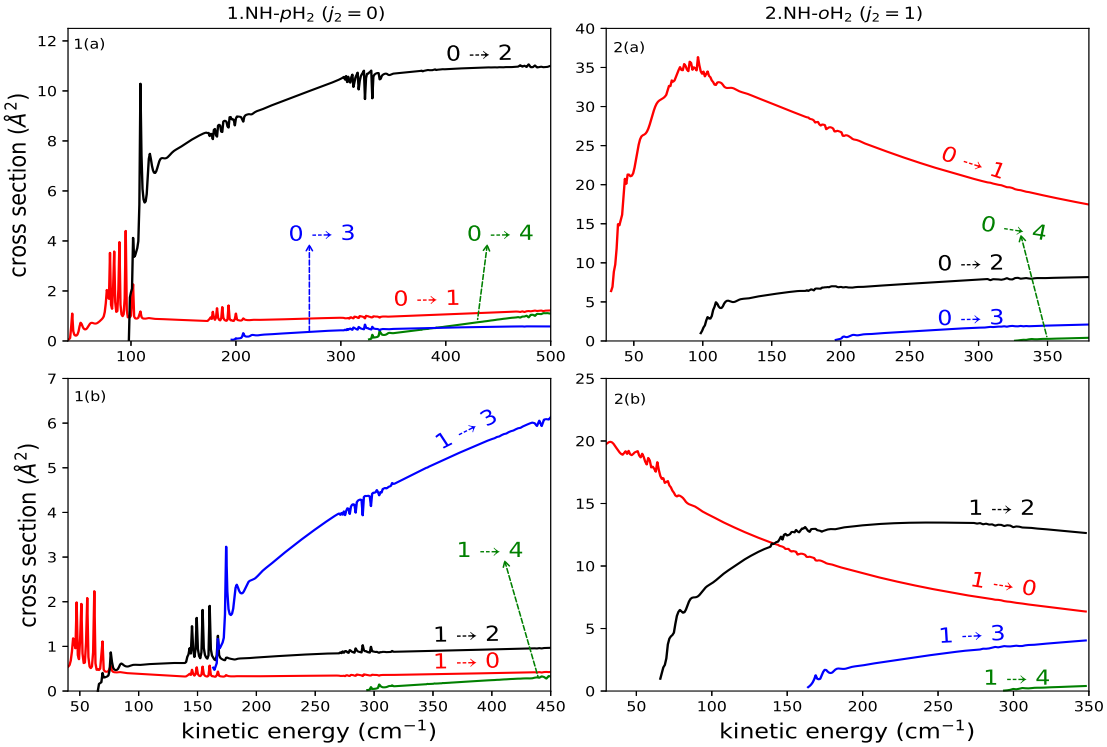

Figure 8.3: Collisional excitation cross sections of NH by H_2 for pure rotational level transitions using 4D NH-H_2 PES. 1(a)&(b) are collision of NH by *para*-H_2; 2(a)&(b) are collision of NH by *ortho*-H_2.

From the fig. 8.3 we can compare the effect of *ortho*-H_2 and *para*-H_2 on the cross section. We observe sevaral rosonance features at multiple regions of the kinetic energy spectrum. These can be associated with the quasi-bound states formed, within the multiple potential wells present in the NH-H_2 PES, due the temporary trapping of the H_2 molecules in these barriers. And the resonances beyond the potential well depth energies can be attributed to the shape of the potential wells (shape resonances). We can also observe that the intensity of the resonance are more for NH-pH$_2$ collsions when compared with NH-oH$_2$ collisions. That is, the NH-oH$_2$ cross sections are comparitively smoother. This difference is because of the fact that, for H$_2$(j_2ge1) has a lot of resonances when compared to H$_2$(j_2=*0*) and hence most of them get overlapped (Lanza et al., 2014). We can cleary notice that the magnitude of cross sections of NH-oH$_2$ collisions are higher than that of

NH-pH$_2$. For NH-pH$_2$, even-ΔN (especially ΔN=2) transitions have larger cross sections compared to other transitions, while the same propensity rule doesn't seem to be the case for NH-oH$_2$.

By averaging over a Maxwellian distribution of the collisional velocities, we obtain thermally averaged rate coefficients for excitation and de-excitation transitions between the *pure* rotational levels of NH and H_2. We obtained rate coefficients for temperatures up to 60 K. Fig.8.4 compares the rate co-efficients of NH-pH$_2$ and NH-oH$_2$ for selected transitions.

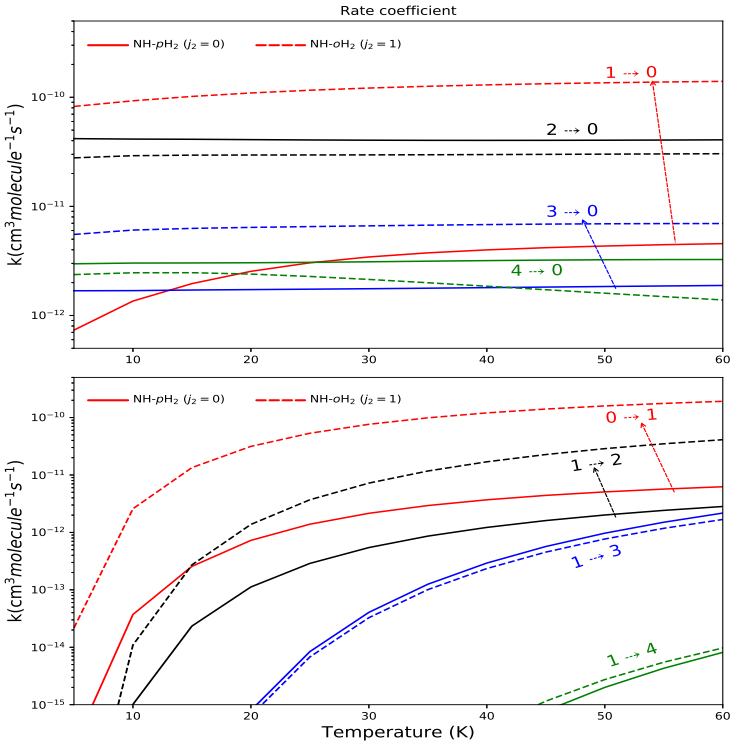

Figure 8.4: Comparing the temperature dependent rate-coefficients of collision of NH by *para*-H_2 (solid) and *ortho*-H_2 (dashed) for a selected pure rotational level transitions.

Obviously, the rate coefficients displays the same propensity rules as observed for the cross sections. From fig.8.4 we can notice that, for odd-ΔN transitions, the NH-oH$_2$ collision (de-)excitations have larger rate-coefficients when compared to that of NH-pH$_2$ while for the even-ΔN transitions it is the reverse. In general, the differences between the NH-pH$_2$ and NH-oH$_2$ rate-coefficients, decreases with increasing ΔN.

These comparisons are worth mentioning because these differences demonstrates the need for dedicated calculations for NH-pH$_2$ and NH-oH$_2$ explicitly rather than using the same rate-coefficients for both or scaling one data to the other.

8.4.2 Fine structure resolved scattering calculation

For performing the fine structure resolves scattering calculations with the 4D NH-H$_2$ PES, we tried to implement the modifications to the linear rigid rotor - linear rigid rotor collision type of MOLSCAT codes as discussed in section 8.2.1. We could reproduce the fine-structure resolved energy levels of the NH-pH$_2$ and NH-oH$_2$ complexes but there are a few nodi in translating these to the interaction potential matrix and so, for now, it is being considered as a future prospect.

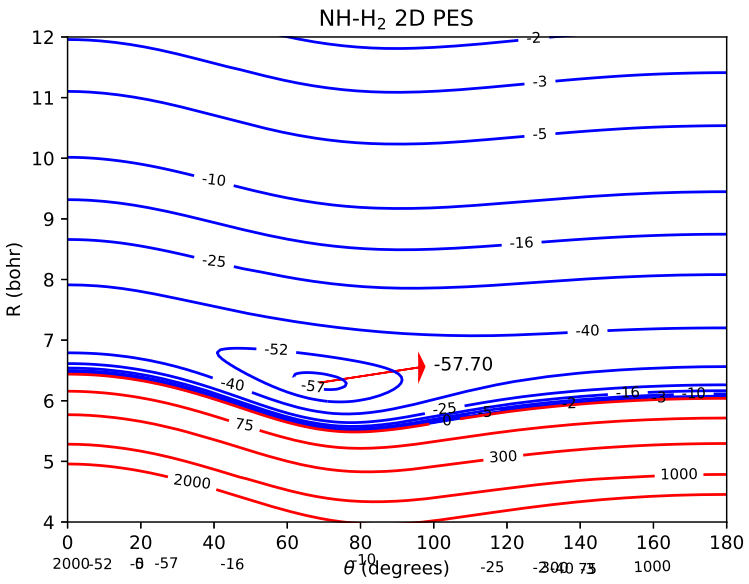

Figure 8.5: Contour plot of averaged 2D NH-H$_2$ PES as a function of R and Θ.

In order to get a preliminary idea of the rate-coefficients of the fine structure resolved transitions of NH colliding with H$_2$ and to compare them with that of the collisions with He, we performed the scattering calculations with the averaged 2D NH-H$_2$ PES. For this, the 4D PES is integrated over all the Θ'

and Φ angles. This reduces the diatom-diatom system to diatom-atom "like" system. Hence we can use the modified MOLSCAT code for linear rigid rotor - atom collsion type (The same that was used for NH-He and ND-He scattering calculations). Fig.8.5 shows the contour plot of the averaged 2D NH-H_2 PES. Using this PES in the MOLSCAT codes that was modified to take into account the fine structures of the NH energy levels, we solve the quantum coulpled equations to get the cross sections. The scattering calculations were performed up to a total energy of 1000 cm^{-1} with a step of 1 cm^{-1}. The value of convergence of various parameters used in the calculations are given in appendix A. The reduced mass of the NH–H_2 system is μ = 1.7600 amu.

Fig.8.6 presents the energy variation of the integral cross sections for transitions from the initial rotational level $N = 0, F_1$ of NH. As observed in the case of pure rotational level resolved cross sections of NH-$p$$H_2$ collisions, the fine structure resolved transitions also have several resonance features at multiple regions. Also, the propensity rules and pattern of cross section variation with respect to kinetic energy is similar to that of the NH-$p$$H_2$($j_2$=0) cross sections. Hence we can say that the averaged 2D PES of NH-H_2 is only equivalent to collision of NH by H_2 in its ground rotational level (j_2=0).

We also obtain the thermally averaged rate coefficients for excitation and de-excitation transitions between fine-structure levels of NH. We obtain rate coefficients for temperatures up to 120 K. This thermal dependence of the state-to-state rate coefficients is illustrated in Fig.8.7. The magnitude of the rate coefficients (and also the cross sections) are governed by the same propensity rules which were observed in NH-He and ND-He fine structure (de-)excitations and the NH-$p$$H_2$.

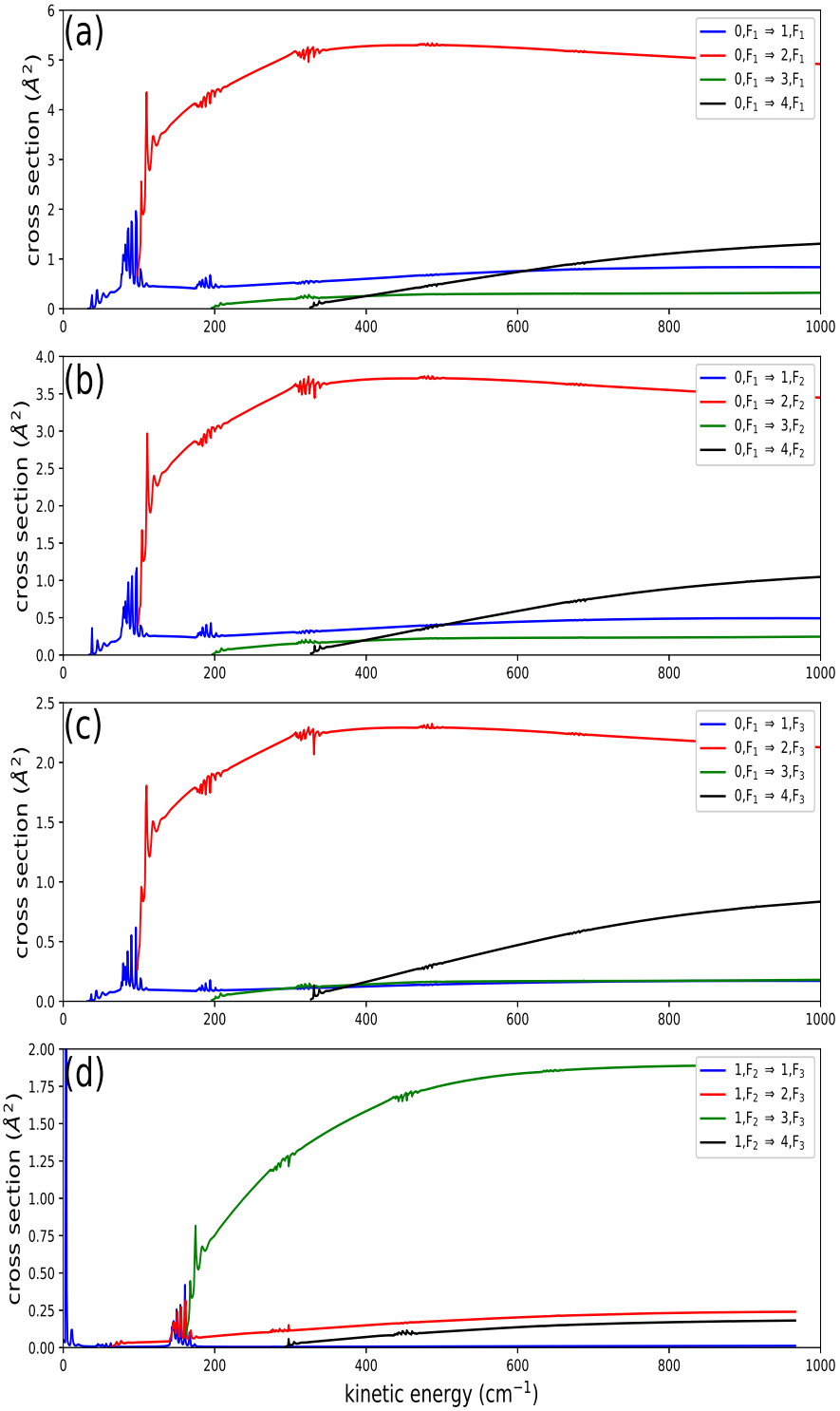

Figure 8.6: Collisional excitation cross sections of NH by H_2 from N=0,F_1. (a) is for F-conserving transitions, while (b-d) are for F-changing transitions.

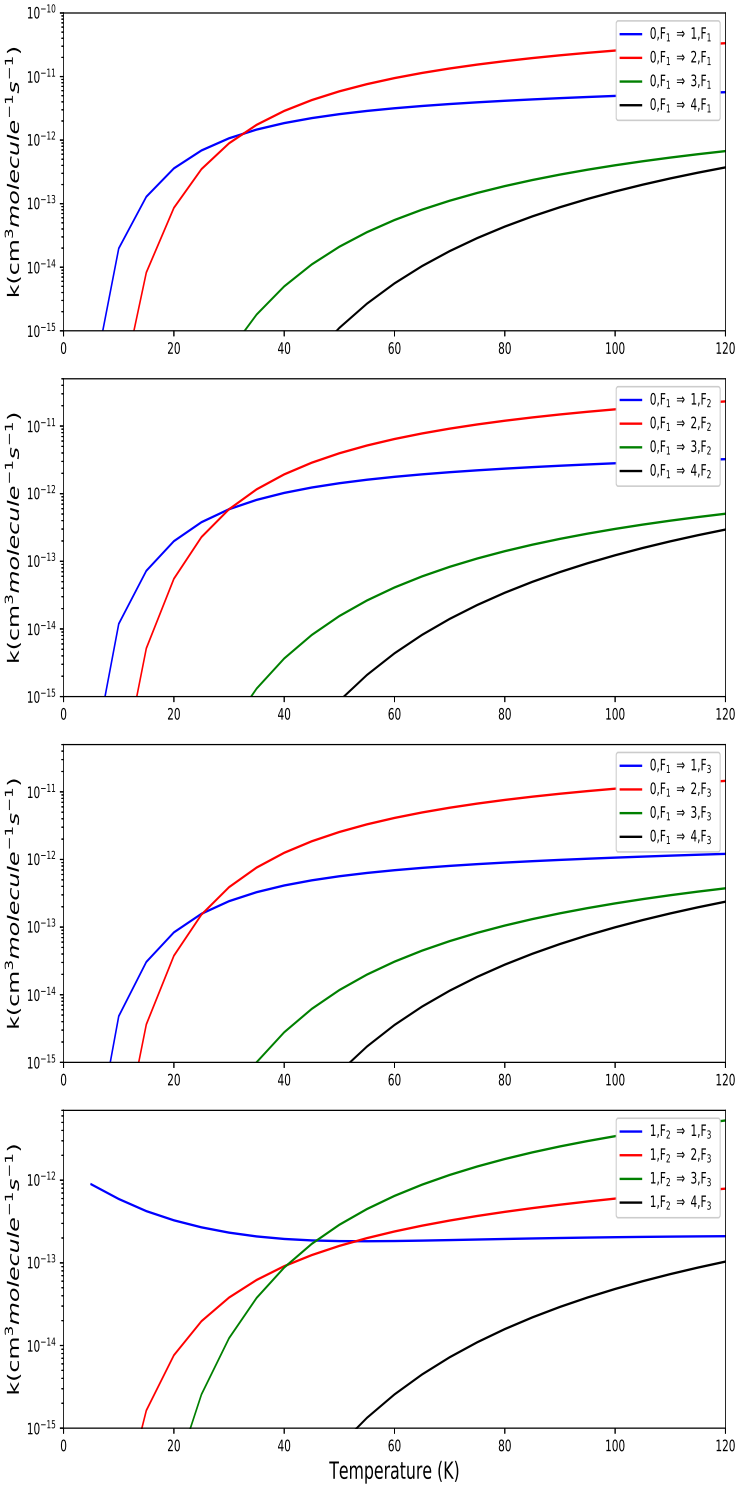

Figure 8.7: Temperature dependent rate-coefficients of collision of NH by H_2. (a) is a representation of F-conserving transitions, while (b-d) represents F-changing transitions.

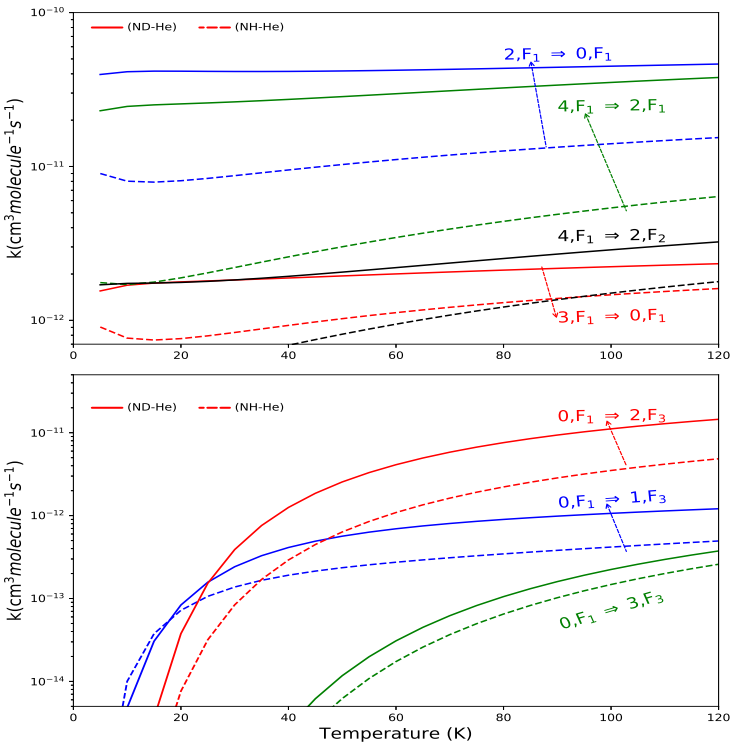

Figure 8.8: comparing the fine-structure resolved rate coefficients of NH-H_2 (solid line) and NH-He (dashed line).

Fig.8.8 compares the fine structure resolved rate coefficients of the collisions of NH by He and H_2 for selected transitions. In general, there are significant differences between the values of NH-He and NH-H_2 rate coefficients. For all the transitions, the NH-H_2 rate coefficients are larger than that of NH-He. From fig.8.8(a) we can notice that the differences are larger for the even-ΔN transitions than the odd-ΔN transitions. Additionally, the F-conserving transition have larger differences than the F-changing transitions. Also, the differences decreases with increasing ΔN (read even-ΔN and odd-ΔN separately).

Based on the above observations, we can safely say that He can neither be used as a model or can be scaled for H_2 in its ground rotational state, let alone the complete H_2 in its ground electronic state. Hence this proves the need for calculating the rate coefficients for collisions with H_2 separately rather than using the data of He.

CHAPTER 9

Bound states of van der Waals systems

In this chapter, I present the calculation of the bound states of the NH-He and NH-Ar van der Waals complexes in its ground electronic state.

9.1 NH–He bound state calculations

As discussed in chapter 4, the bound state energies are the eigenvalues of the close coupled equations below the dissociation energy which satisfies the boundary conditions ($\psi_b(R) = 0$ at R=0 and as $R \rightarrow +\infty$). To find such eigenvalues, the approach described in chapter 4 is used. This is implemented as explained in section 4.3 in the BOUND (Hutson, 1993) codes.

The bound state calculations were performed for the main ^{14}N and ^{4}He isotopes. The coupled equations were solved using the log derivative method. The calculations were performed with a propagator step size of 0.01 bohr, and the other propagation parameters were taken as the default BOUND input. The input parameters E_{min} and R_{MID} were decided based on the PES which has a global minimum with energy = -19.7135 cm^{-1} at R= 6.30 bohr ($RMID$). Based the convergence of the output, the parameters R_{MAX} and J_{MAX} were set at R_{MAX}= 40a$_0$ and J_{MAX}= 14.

The bound energy levels of the NH-He complex computed with the Cybulski et al. (2005) PES and the 3D-avg PES without considering the fine-structures of NH are listed in Table 9.1. Energies are given relative to the ground state energy of NH. Calculations with the Cybulski et al. (2005) PES were

J	l	Energy (in cm^{-1})		
		Cybulski et al. (2005)	3D-avg PES	Cybulski PES
0	0	-4.4174	-4.3236	-4.4176
1	1	-3.7818	-3.6904	-3.7821
2	2	-2.5375	-2.4587	-2.5382
3	3	-0.7538	-0.6886	-0.7550

Table 9.1: NH–He bound energy levels (in cm^{-1}) obtained excluding the NH fine structure. Energies are relative to the ground-state energy of NH. All the levels correspond to the approximate quantum numbers $N = 0$. J and l correspond to the total and orbital angular momentum of the complex, respectively.

performed to validate the codes. The bound energy levels in Cybulski et al. (2005) are also reported for the purpose of comparison.

In the next step, the BOUND code is modified to calculate fine-structure resolved bound states for the NH-He complex. This was done in two main steps. Normally, in the in-built rigid diatom + atom type interactions, pure rotational levels of NH are constructed directly from the input details (B and D values of NH) and these energy levels are identified by a unique set of quantum numbers. To include the fine-structure, we introduce a subroutine which calculates the energies of each level using the equations 5.6. Once the energy levels and the corresponding unique quantum numbers are assigned, the same algorithm described in chapter 4 is introduced in the bound code to find the eigenvalues. The fine-structure resolved bound states of the NH-He complex published in Cybulski et al. (2005) are compared with the bound states calculated with the new 3D-avg PES and the PES of Cybulski et al. (2005) in table 9.2. Energies are given relative to the ground state energy of NH.

9.1.1 Discussions

Firstly, from tables 9.1 and 9.2, we can confirm that NH-He complex supports a bound state and that the energy of these bound states are in very good agreement with that of the Cybulski et al. (2005). The dissociation energy of the complex is slightly smaller ($D_0 = 4.3237$ cm^{-1}) than the one calculated with the previous Cybulski et al. PES ($D_0 = 4.4097$ cm^{-1}). The small difference (0.08 cm^{-1}) is attributed to the differences between well depth of the Cybulski and 3D-avg PES of NH–He.

J	l	Energy (in cm^{-1})		
		Cybulski et al. (2005)	3D-avg PES	Cybulski PES
1	0	-4.4174	-4.3216	-4.4177
0	1	-3.7790	-3.6868	- 3.7792
1	1	-3.7832	-3.6922	-3.7835
2	1	-3.7815	-3.6908	-3.7818
1	2	-2.5365	-2.4579	-2.5368
2	2	-2.5385	-2.4595	-2.5391
3	2	-2.5372	-2.4585	-2.5379
2	3	-0.7536	-0.69038	-0.7561
3	3	-0.7542	-0.68922	-0.7599
4	3	-0.7537	-0.68845	-0.7596

Table 9.2: NH–He bound energy levels (in cm^{-1}) obtained **including** the NH fine structure. Energies are relative to the ground-state energy of NH. All the levels correspond to the approximate quantum numbers $N = 0$,F_1. J and l correspond to the total and orbital angular momentum of the complex, respectively.

J	l	Bound state energy (in cm^{-1}) using 2D PES
0	0	-4.3897
1	1	-3.7555
2	2	-2.5140
3	3	-0.7360

Table 9.3: NH-He bound states (excluding the fine-structures) energies calculated using 2D PES

Also, if we compare the bound states calculated from 2D PES and 3D-avg PES with that of the Cybulski et al. (2005) values, we realise the effect of the larger basis set and the effect of inclusion of the vibrations of NH. As, we can see from table 9.3 and 9.1 , there is a 0.63 - 2.4 % difference between the values of Cybulski et al. (2005) and the energy from 2D PES. And, if we compare the bound state energies calculated using 2D PES and 3D-avg PES, we notice a 1.5 - 6.6 % difference between the values which demonstrates the significance of inclusion of the NH vibrations.

To compare the results of the present work with the experimental results of Kerenskaya et al. (2004), the values in table 9.1 are used, as the fine structure splitting could not be resolved in their experiments. Using the

l	Rotational constant(B) in cm^{-1}		
	Cybulski et al. (2005)	**3D-avg PES**	**Cybulski PES**
1	0.3178	0.3166	0.3177
2	**0.3133**	**0.3108**	**0.3132**
3	0.3053	0.3029	0.3052

Table 9.4: Calculated Rotational Constants for different Pontential energy surfaces

equation, $E_l = E_0 + B\ l(l+1)$ and the bound state values of 3D-avg PES of table 9.1, we get the average rotational constant, $B = 0.311$ cm^{-1} which is slightly lower than the experimental value of 0.334 cm^{-1}. (B from Cybulski et al. (2005) paper is 0.313 cm^{-1}). We can clearly notice that the values are in good agreement.

If we use the equation, $E_l = E_0 + B\ l(l+1) - D\ l^2(l+1)^2$ and the bound state values of 3D-avg PES of table 9.1, we get rotational constant, $B = 0.3195$ cm^{-1} and $D = 0.0015$ cm^{-1} (B and D values calculated from Cybulski et al. (2005) paper are 0.3200 cm^{-1} and 0.0011 cm^{-1}, respectively).

Hence we can confirm that the constant values from the 3D-avg PES used in this thesis can be accurate enough to predict the rotational spectra of the NH-He complex. This also proves the correctness of our new method of calculating the fine-structure resolved bound states.

9.2 NH–Ar bound state calculations

Using the highly correlated 3D-avg PES, we have computed the bound-states of Ar-NH complex by the coupled-channel approach, as implemented in the BOUND program (Hutson, 1993). The bound state calculations were performed for the main ^{14}N and ^{40}Ar isotopes. The coupled equations were solved using the log-derivative propagator of Manolopoulos (LDMA) (Manolopoulos, 1988; Hutson, 1994a).
Similar to the case of NH-He complex, we first perform the bound state calculations neglecting the NH fine structures. The calculations were done with a propagator step size of 0.01 bohr, and the other propagation parameters were taken as the default BOUND values. The rotational basis includes the rotational states with $J_{max} \leq 10$. The bound energy levels of the Ar-NH complex computed with the 3D-avg PES are listed in Table 9.5.

J	l	Energy(in cm^{-1})
0	0	-73.1507
1	1	-72.9324
2	2	-72.4988
3	3	-71.8479

Table 9.5: NH-Ar bound energy levels (in cm^{-1}) obtained excluding the NH fine structure.

As mentioned in the previous section, the NH molecule exhibits a fine structure due to the presence of non-zero the electronic spin. The modified BOUND program which includes this fine structure of NH molecule as explained in the previous section is used. Table 9.6 presents the bound state energies for the first few values of the total angular momentum J.

9.2.1 Discussions

The bound energy levels indicate a weak coupling of the electron spin and rotation of the NH molecule. This is as expected, as the same is observed in the case of NH-He bound states. From the present calculations, dissociation energy (D_0) of the complex is 73.1503 cm^{-1} which is higher than the previously calculated value of Kendall et al. (1998) (D_0= 71.5 cm^{-1}). The difference (1.65 cm^{-1}) can be majorly attributed to the difference between the Ar-NH PESs used in the two calculations. Since the PES we

J	l	Energy(in cm^{-1})
1	0	-73.1519
0	1	-72.8964
1	1	-72.9507
2	1	-72.9305
1	2	-72.4804
2	2	-72.5169
3	2	-72.4947
2	3	-71.8333
3	3	-71.8658
4	3	-71.8426

Table 9.6: NH–Ar bound energy levels (in cm^{-1}) obtained **including** the NH fine structure. Energies are relative to the ground-state energy of NH. All the levels correspond to the approximate quantum numbers $N = 0$,F_1. J and l correspond to the total and orbital angular momentum of the complex, respectively.

used is highly correlated and also includes the vibration of the NH molecule, these values are more accurate. The differences can also to attributed to the method employed to calculate the dissociation energy.

Also, fitting the energies of Table 9.5 to the rigid rotor expression,$E_J = E_0 + BJ(J+1) - DJ^2(J+1)^2$ (J corresponds to the total angular momentum of the complex), we obtain the rotational constant $B = 0.1087$ cm^{-1} and $D = 0.000025$ cm^{-1}. Considering the accuracy of our new PES, we can posit that these values can be used for future reference and calculations.

PART IV

CONCLUSIONS

CHAPTER 10

Conclusions & Prospectives

In this thesis the theoretical study of 3 inelastic collisions of astrophysical interest were presented. The first two were the study of the collisions of open shell linear diatoms (NH & ND) with structureless atom (He), while the other was collisions between an open shell linear diatom (NH) and a closed shell linear diatomic molecule (H_2). A study of spectroscopy of the open shell linear diatom - structureless atom complex is also presented here. The conclusions reached in these studies are summarized here and the possible extensions of this work is also briefly mentioned.

We have presented a new highly accurate PES for the NH–He van der Waals complex. The 3D PES was obtained from highly correlated calculations at the RCCSD(T) level using a complete basis set extrapolation. The new PES is found to be in good agreement with the previously published one. We use the same NH-He interaction potential for ND-He by taking into account the displacement of the centre of mass of NH and ND in the analytical representation. Collisional excitation of NH and ND ($X^3\Sigma^-$) by He was studied at the close-coupling level using these highly correlated 3D-*avg* PESs for both fine structure and hyperfine structure resolved energy levels of NH and ND.

Calculations of the collisional excitation cross sections of the fine-structure level resolved NH by He were performed for energies up to 3500 cm^{-1}, which yield, after a thermal average, rate coefficients up to 350 K and for the fine-structure levels of ND by He for energies up to 2000 cm^{-1}, which after a thermal average, yielded rate coefficients up to 200 K. The calculated rate coefficients of NH-He were compared with available experimental measurements and previous theoretical results. A fairly global agreement was found between experimental and theoretical data. The significant differences

were surprising taking into account the accuracy of the present theoretical approach also given that this kind of theoretical modeling has been shown to well reproduce experiments for other systems. [for example,CN–He(Lique, Spielfiedel, Feautrier et al., 2010); OH-He (Kalugina et al., 2014,Kłos et al., 2007)]. Hence, the accuracy of the experimental data is legitimately challenged. This may also be supported by the fact that, in the experiments, some of the rate coefficients have not been directly measured but inferred through a master equation (Eq.(1) of Rinnenthal et al., 2002) which will propagate the errors.

The NH and ND rate coefficients were also compared in great detail and we found significant differences between the two sets of data. Fine structure resolved rate coefficients of both NH and ND present a strong propensity rules in favor of $\Delta j = \Delta N$ transitions, as expected from theory. The differences were clearly explained by the different rotational structure of the two molecules as well as the different expansion of their associated interaction potential with He. This comparison also shows that one has to be careful when using inelastic rate coefficients of the main isotopologues to interpret observation of deuterated isotopologues especially for a light hydride like NH.

We also present the hyperfine resolved state-to-state collisional rate coefficients of NH and ND by He. We have obtained hyperfine resolved rate coefficients for transitions involving the lowest levels of NH and ND for temperatures up to 150 K. The $\Delta j = \Delta F_1 = \Delta F$ propensity rule is observed for the hyperfine transitions of both isotopologues.

Using new 3D-avg PES of NH-He, we have also studied the spectroscopy of the NH–He complex including and excluding the fine structures of NH, and we have determined a new rotational constant ($B = 0.3195$ cm^{-1} and $D = 0.0015$ cm^{-1}) that agrees well with the available experimental data. Such an agreement confirms that the new 3D-avg PES is accurate enough. Hence, resonances that could be seen in experimental cross sections obtained with a cross molecular beam machine would possibly be accurately analyzed with this new interaction potential. As an additional task, the same bound state calculations were extended to NH-Ar complexes too.

We have also presented a new highly accurate PES for the NH–H_2 van der Waals complex for the first time. The 3D PES was obtained from highly correlated calculations at RCCSD(T) level of theory using F12a method with AVTZ basis set. Using this NH-H_2 4D PES, we performed the first scattering calculations for the transitions between the *pure* rotational levels of NH and H_2. It was noticed that the NH-pH$_2$ cross sections and NH-oH$_2$ are quite

different. For NH-pH$_2$, even-ΔN (especially ΔN=2) transitions had larger cross sections compared to other transitions, while the same propensity rule did not apply for for NH-oH$_2$. The comparisons demonstrated the need for dedicated calculations for NH-pH$_2$ and NH-oH$_2$ explicitly rather than using the same rate-coefficients for both or scaling one data to the other. For performing the fine structure resolved scattering calculations for NH-H$_2$, the 4D PES was averaged to a 2D NH-H$_2$ PES. Using this 2D PES, the closed coupled equations for the collision of open shell linear diatoms and structureless atom were solved. It was noticed that the propensity rules and pattern of cross section variation with respect to kinetic energy were similar to that of the NH-pH$_2$(j_2=*0*) and there were significant differences between the values of NH-He and NH-H$_2$ rate coefficients. Hence, It was concluded that He can neither be used as a model nor can be scaled even for H$_2$ in its ground rotational state and so, the rate coefficients for collisions with H$_2$ has to be calculated separately rather than using the data of He.

10.1 Prospective

"A universe of possibilities!!"

To start with, can use the new hyperfine rate coefficients of NH-He and ND-He to perform the non-LTE radiative transfer modeling calculations to revise the NH and ND abundances.

Another important prospect would to complete the inclusion of the fine structure of $^3\Sigma$ open shell molecules in the MOLSCAT codes for rigid rotor-rigid rotor collision system and using that, calculating the fine structure resolved state-to-state rate coefficients of NH-pH$_2$ and NH-oH$_2$ collisions using the new 4D NH-H$_2$ PES. If and when successful, we could use them for deriving the hyperfine rate coefficients of NH-H$_2$. As of now, we can also get the hyperfine rate coefficients from the S-matrix of fine-structure NH-H$_2$ which we calculated using the 2D averaged PES. Also, similar to what we did with NH-He PES, we can include the displacement of centre of mass, to get a PES for ND-H$_2$ and perform the scattering calculations.

It would be interesting to use the modified BOUND codes (that we presented and used in this thesis) for other similar systems. We can also modify the BOUND codes to include the fine structures of $^3\Sigma$ molecules to find the fine

structure resolved bound states for diatom-diatom complexes (keeping in mind NH-H_2). There is a lot to be done and can be done and will be done, I hope I Will contribute to atleast some of it!

Appendices

APPENDIX A

Convergence Parameters

For efficient computation with MOLSCAT we split total energies into smaller grids and for each segment we optimized the input parameters of MOLSCAT in order to converge cross sections among the levels of our interest. The main parameters that have been used are

STEPS which is the step size of the propagator,
RMIN is the starting point of the integration,
RMAX is the range of the integration,
JMAX defines the rotational basis set (**J1MAX** & **J2MAX** in case of 2 molecule collision) and
LMAX specifies the highest Legendre term to include in the expansion of the potential(**L1MAX** & **L2MAX** in case of 2 molecule collision).

Parameter	**Energy range (in cm^{-1})**				
	33-100	**101-500**	**501-1000**	**1001-2000**	**2001-3000**
RMAX	80	70	50	50	50
STEPS	70	50	20	20	10
LMAX	14	15	17	18	20
JMAX	10	9	15	18	20

Table A.1: Convergence Parameters used for NH-He calculations

Parameter	Energy range (in cm^{-1})				
	17-100	**101-500**	**501-1000**	**1001-2000**	**2001-3000**
RMAX	60	60	50	45	45
STEPS	40	30	20	15	10
LMAX	13	16	20	26	30
JMAX	11	15	18	22	26

Table A.2: Convergence Parameters used for ND-He calculations

Parameter	Energy range (in cm^{-1})		
	17-100	**101-500**	**501-1000**
RMAX	70	50	40
STEPS	50	30	25
L2MAX	10	10	10
J2MAX	9	12	15

Table A.3: Convergence Parameters used for pure rotational level resolved NH-*para*-H_2 (**J1MAX** = 0,2) calculations using 4D PES

Parameter	Energy range (in cm^{-1})		
	17-100	**101-500**	**501-1000**
RMAX	-	80	70
STEPS	-	30	20
L2MAX	-	10	10
J2MAX	-	12	18

Table A.4: Convergence Parameters used for pure rotational level resolved NH-*ortho*-H_2 (**J1MAX** = 1) calculations using 4D PES

Parameter	Energy range (in cm^{-1})		
	17-100	**101-500**	**501-1000**
RMAX	100	90	70
STEPS	30	25	20
LMAX	14	17	20
JMAX	10	13	18

Table A.5: Convergence Parameters used for fine structure resolved NH--H_2 calculations using averaged 2D PES

APPENDIX B

Published articles

A new *ab initio* potential energy surface for the NH–He complex

R. Ramachandran,[1] J. Kłos,[2] and F. Lique[1,a)]
[1]*LOMC-UMR 6294, CNRS-Université du Havre, 25 Rue Philippe Lebon, BP 1123, 76 063 Le Havre Cedex, France*
[2]*Department of Chemistry and Biochemistry, University of Maryland, College Park, Maryland 20742-2021, USA*

(Received 23 January 2018; accepted 10 February 2018; published online 27 February 2018)

We present a new three-dimensional potential energy surface (PES) for the NH($X^3\Sigma^-$)–He van der Waals system, which explicitly takes into account the NH vibrational motion. The NH–He PES was obtained using the open-shell single- and double-excitation coupled cluster approach with non-iterative perturbational treatment of triple excitations. The augmented correlation-consistent aug-cc-pVXZ (X = Q, 5, 6) basis sets were employed, and the energies obtained were then extrapolated to the complete basis set limit. Using this new PES, we have studied the spectroscopy of the NH–He complex and we have determined a new rotational constant that agrees well with the available experimental data. Collisional excitation of NH($X^3\Sigma^-$) by He was also studied at the close-coupling level. Calculations of the collisional excitation cross sections of the fine-structure levels of NH by He were performed for energies up to 3500 cm^{-1}, which yield, after thermal average, rate coefficients up to 350 K. The calculated rate coefficients are compared with available experimental measurements at room temperature, and a reasonably good agreement is found between experimental and theoretical data. *Published by AIP Publishing.* https://doi.org/10.1063/1.5023311

I. INTRODUCTION

The NH($^3\Sigma^-$) molecule is often used as a prototype for studies of ultracold molecules.[1] The rotational structure of the NH molecule makes it well suited for use in cryogenic techniques based on buffer gas cooling. The technique of buffer-gas cooling relies on collisions with cold buffer gas atoms to thermalize atoms or molecules to low temperature. Because of the magnetic moment of its $^3\Sigma^-$ ground electronic state, the NH molecule can also be used in a Zeeman decelerator optimized for applications in molecular beam experiments in order to study cold collisions and to probe the rotational excitation of the NH molecule by rare-gas atoms and diatomic molecules.[2]

In the NH($^3\Sigma^-$) electronic ground state, the rotational levels are split by spin-rotation coupling. In the intermediate coupling scheme, the rotational wave function of NH can be written as[3,4]

$$\begin{aligned} |F_1 jm\rangle &= \cos\alpha\,|N=j-1, Sjm\rangle + \sin\alpha\,|N=j+1, Sjm\rangle, \\ |F_2 jm\rangle &= |N=j, Sjm\rangle, \\ |F_3 jm\rangle &= -\sin\alpha\,|N=j-1, Sjm\rangle + \cos\alpha\,|N=j+1, Sjm\rangle, \end{aligned} \tag{1}$$

where $|N, Sjm\rangle$ denotes pure Hund's case (b) basis functions and the mixing angle α is obtained by diagonalisation of the molecular Hamiltonian. In this relation corresponding to Hund's case (b), the total molecular angular momentum j is defined by

$$\mathbf{j} = \mathbf{N} + \mathbf{S}, \tag{2}$$

where **N** and **S** are the nuclear rotational and the electronic spin angular momenta. In the pure case (b) limit, $\alpha \to 0$, the F_1 level corresponds to $N = j - 1$ and the F_3 level corresponds to $N = j + 1$. The levels in the spin multiplets are usually labeled by the nuclear rotational quantum number N [corresponding to the Hund's case (b) limit] and the spectroscopic index F_i, and this notation will be used hereafter.

Among the possible coolant and collisional partners in scattering experiments, He is certainly the most used. It is then crucial to study the interaction of NH with He atoms. Moreover, the study of these interactions is also useful from the astrophysical applications point of view since the NH molecule has been discovered in the interstellar medium in the early 1990s[5] and accurate rate coefficients for this molecule in collision with He are needed for accurate determination of the NH abundance in the interstellar medium from molecular lines.[6]

A decade ago, Cybulski *et al.*[7] computed a NH–He potential energy surface (PES) using a partially spin-restricted coupled cluster with single, double, and non-iterative triple excitations [RCCSD(T)][8,9] and augmented correlation-consistent triple zeta basis sets (aug-cc-pVTZ).[10] The NH intermolecular distance was fixed at the equilibrium distance of 1.95 bohr. This PES proved to be successful when applied in collision-induced Zeeman relaxation in the external magnetic field used to trap the NH($X^3\Sigma^-$) molecules in a buffer gas of ^{3}He.[11] The experimental energy transport cross sections and Zeeman relaxation of the magnetically trapped NH in He buffer gas of Campbell *et al.*[12] were also in good agreement with theoretical estimates of Krems *et al.*[11] using the Cybulski *et al.* PES.[7] More recently, rate coefficients[13] obtained from this PES were found to be in qualitative agreement with the experimental rate coefficients of Rinnenthal and Gericke.[14]

a)Electronic mail: francois.lique@univ-lehavre.fr

However, there is lack of NH–He PES that takes into account the NH vibrational motion. Indeed, recent studies[15–17] have shown the importance of using three-dimensional PESs for studying the collisional excitation of light molecular hydrides by rare-gas atoms, even if only the pure rotational excitation is considered. Such a PES can also be highly needed in order to interpret future experiments on the inelastic scattering of NH with He since it is common to prepare target molecules in an excited vibrational state. In addition, it is presently possible to compute the PES of van der Waals complexes using more accurate theoretical treatments than those used by Cybulski *et al.*,[7] and future analysis of scattering experiments as well as interstellar spectra would clearly benefit from highly accurate collisional data.

In this work, we compute a new *ab initio* PES for the ro-vibrational excitation of NH($^3\Sigma^-$) by He and we test the new PES versus spectroscopical and scattering experiments. This paper is organized as follows: Sec. II describes the *ab initio* calculations and the analytical fit of the PES obtained; in Sec. III, we present the bound states of the NH–He complex; and in Sec. IV, we present the calculations of NH–He new inelastic cross sections and rate coefficients and we compare them to the corresponding experimental data of Rinnenthal and Gericke.[14] Conclusions and outlook are also presented.

II. POTENTIAL ENERGY SURFACE

The two interacting species are considered in their ground electronic states NH($^3\Sigma^-$) and He(^1S). The ground electronic state of the NH($^3\Sigma^-$)–He van der Waals system is X^3A'' state. In this work, we used the Jacobi coordinate system. The center of coordinates is placed in the NH center of mass (c.m.), and the vector **R** connects the NH c.m. with the He atom. The rotation of NH molecule is defined by the θ angle, and the r coordinate describes the NH bond length.

Highly correlated *ab initio* calculations of the PES of the NH–He van der Waals complex were carried out at the partially spin-restricted coupled cluster with single, double, and perturbative triple excitations [RCCSD(T)][8,9] level of theory using MOLPRO 2010 package.[18] In order to determine the interaction potential, $V(R, \theta, r)$, the basis set superposition error (BSSE) was corrected at all geometries using the Boys and Bernardi counterpoise scheme:[19]

$$V(R,\theta,r) = E_{\mathrm{NH-He}}(R,\theta,r) - E_{\mathrm{NH}}(R,\theta,r) - E_{\mathrm{He}}(R,\theta,r), \quad (3)$$

where the energies of the NH and He monomers are computed in a full basis set of the complex.

To achieve a good description of the charge-overlap effects, the calculations were performed with rather large augmented correlation-consistent aug-cc-pVXZ (X = T, Q, 5) basis sets.[10] Then, the energies were extrapolated to the Complete Basis Set (CBS) limit using the following scheme:[20]

$$E_X = E_{\mathrm{CBS}} + Ae^{-(X-1)} + Be^{-(X-1)^2}, \quad (4)$$

where X is the cardinal number of the aug-cc-pVXZ basis set, E_X is the energy corresponding to the aug-cc-pVXZ basis set, E_{CBS} is the energy extrapolated to the CBS limit, and A and B are the parameters to adjust. The radial scattering coordinate R was assigned 42 values from 35.0 bohr to 3.0 bohr, and the θ grid ranged from 0° to 180° in steps of 10°. The calculations were performed for five NH bond lengths r = [1.6, 1.8, 1.95, 2.2, 2.4] bohr, which allows us to take into account the vibrational motion of NH molecule up to $v = 2$.

An analytic representation of the three-dimensional (3D) interaction potential was obtained following the method developed by Werner *et al.*:[21]

$$V_l(r,R,\theta) = \sum_{n=1}^{N_{max}} \sum_{l=1}^{L_{max}} d_{m,0}^{l+m-1}(\cos\theta) A_{ln}(R)(r-r_e)^{n-1}, \quad (5)$$

where the $d_{m,0}^{l+m-1}(\cos\theta)$ are the reduced Wigner rotation matrix elements, N_{max} equals the number of NH bond distances, L_{max} equals the number of angles θ for which the potential was calculated, $m = 0$, and r_e is the equilibrium distance of NH (r_e = 1.95 bohr). The analytic potential was found to reproduce the calculated energies quite well. Over the entire grid, the mean difference between the analytic fit and the *ab initio* computed interaction energies is less than 1%.

The NH–He PES, which takes into account the stretching of the NH molecule, can then be averaged over any vibrational state up to $v = 2$. The averaging is done using the following formula:

$$V_v(R,\theta) = \langle v(r)|V(R,\theta,r)|v(r)\rangle. \quad (6)$$

The NH vibrational wave functions $|v(r)\rangle$ were those computed in the work of Bouhafs and Lique[15] that were evaluated using a discrete variable representation (DVR) method[22] from *ab initio* calculations of the NH potential function using the internally contracted multireference configuration interaction (MRCI)[23] level and a large aug-cc-pV5Z atomic basis set.

Figure 1 depicts the contour plot of our 3D PES averaged over the ground vibrational state $v = 0$ as a function of R and θ. For this weakly bound system, the global minimum in the interaction energy was found to be −19.71 cm^{-1} (R = 6.30 bohr, θ = 64°).

It is interesting to compare our new *ab initio* PES with the NH–He PES previously published.[7] Cybulski *et al.*[7] determined the NH–He interaction at the RCCSD(T) levels using an aug-cc-pVTZ basis set augmented by mid-bond functions.

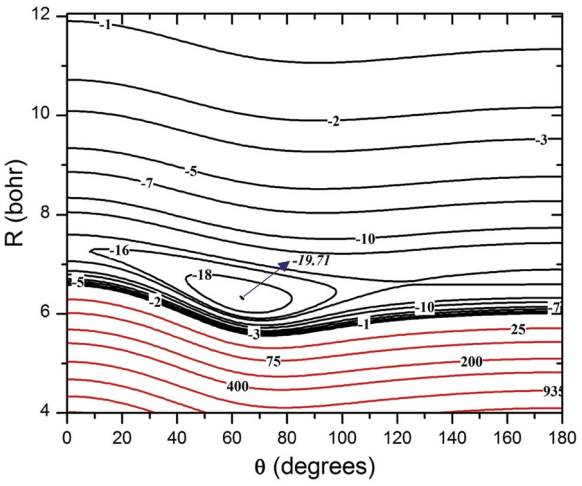

FIG. 1. Contour plot of the NH–He PES (cm^{-1}) as a function of Jacobi coordinates R and θ.

In their calculations, these authors fixed the NH intermolecular distance at a value of 1.95 bohr. The position (R = 6.33 bohr and θ = 62°) and well depth (19.86 cm^{-1}) of their PES is in good agreement with the position of our minimum (R = 6.35 bohr and θ = 64°) and well depth (19.83 cm^{-1}) for r = 1.95 bohr. The main features of their PES also agree well with those of the 3D PES averaged over the ground vibrational state v = 0.

III. NH–HE BOUND STATES

The NH–He van der Waals complex was characterized experimentally using Kerenskaya *et al.*'s[24] laser excitation of bands associated with the NH($A^3\Pi - X^3\Sigma^-$) transition. They found that the ground state electronic state of the complex supports a bound level with a rotational constant of $B = 0.334$ cm^{-1}. The experimental findings were in good agreement with theoretical predications of Kerenskaya *et al.*[24] based on the PES of Cybulski *et al.*[7] It is then interesting, as a first application, to determine the bound state energy levels from the present 3D PES averaged over the ground vibrational state v = 0 (hereafter 3D-ave PES).

We have computed the bound-state energies supported by the 3D-ave PES using the coupled-channel approach, as implemented in the BOUND program.[25] The bound state calculations were performed for the main ^{14}N and ^{4}He isotopes. The coupled equations were solved using the diabatic modified log-derivative method. We have first neglected the fine structure splitting of the NH molecule. The calculations were performed with a propagator step size of 0.01 bohr, and the other propagation parameters were taken as the default BOUND values. The rotational basis includes the rotational states with quantum number $N \leq 14$. The bound energy levels of the NH–He complex computed with the 3D-ave PES are listed in Table I. Energies are given relative to the ground state energy of NH. We also report the bound energy levels obtained in Cybulski *et al.*[7]

As one can see, we also found that NH–He complex supports a bound state and that the energy of this level is in very good agreement with that previously obtained. The dissociation energy of the complex is slightly smaller ($D_0 = 4.3237$ cm^{-1}) than the one calculated with the previous Cybulski *et al.*[7] PES ($D_0 = 4.4097$ cm^{-1}). The small difference (0.08 cm^{-1}) can be attributed to the small difference between the Cybulski *et al.*[7] and 3D-ave well depth of the NH–He PES.

As mentioned in the Introduction, the NH molecule exhibits a fine structure because of the coupling between the rotational momentum and the electronic spin. The BOUND program was then modified to include the fine structure of the NH molecule (e.g., Ref. 7). Briefly, we have introduced the exact energy levels of the fine structure levels and the corresponding matrix elements of the potential as described in Ref. 13. The NH molecular Hamiltonian includes the rotational Hamiltonian (as in the previous case) as well as the spin-rotation and spin-spin Hamiltonian. The basis set and the propagation parameters were the same than for the calculations without the NH fine structure. Table II presents the bound state energies for the first few values of the total angular momentum J. We also report the energy levels obtained with the PES of Cybulski *et al.*[7]

TABLE I. NH–He bound energy levels (in cm^{-1}) obtained excluding the NH fine structure. Energies are relative to the ground-state energy of NH. All the levels correspond to the approximate quantum numbers N = 0. J and l correspond to the total and orbital angular momentum of the complex, respectively.

J	l	Energy (this work)	Energy (Ref. 7)
0	0	−4.3237	−4.4097
1	1	−3.6904	−3.7741
2	2	−2.4587	−2.5298
3	3	−0.6887	−0.7461

TABLE II. NH–He bound energy levels (in cm^{-1}) obtained with the inclusion of the NH fine structure. Energies are relative to the ground-state energy of NH. All the levels correspond to the approximate quantum numbers $N = 0, F_1$. J and l correspond to the total and orbital angular momentum of the complex, respectively.

J	l	Energy (this work)	Energy (Ref. 7)
1	0	−4.3216	−4.4097
0	1	−3.6868	−3.7713
1	1	−3.6922	−3.7755
2	1	−3.6908	−3.7738
1	2	−2.4580	−2.5288
2	2	−2.4595	−2.5308
3	2	−2.4585	−2.5295
2	3	−0.6904	−0.7459
3	3	−0.6892	−0.7465
4	3	−0.6885	−0.7460

Again, the agreement with NH–He bound energy levels previously computed is very good. The predicted bound energy levels indicate that the coupling of the electron spin to the rotational motion of the complex is very weak. As a consequence, energy levels of NH–He are very similar to those obtained by neglecting the fine structure.

To compare the results with the experimental results of Ref. 24, we use the values in Table I, as the spin splitting could not be resolved in their experiments. Fitting the energies of Table I to the rigid rotor expression, $E_J = E_0 + BJ(J + 1) - DJ^2(J + 1)^2$ (J corresponds to the total angular momentum of the complex), we obtain the rotational constant $B = 0.3195$ cm^{-1} and $D = 0.0015$ cm^{-1} that agree very well with the experimental data (B = 0.334 cm^{-1}). Such an agreement confirms that the new 3D-ave PES is accurate enough for predicting the rotational spectra of the NH–He complex. Hence, resonances that could be seen in experimental cross sections obtained with a cross molecular beam machine would possibly be accurately analyzed with this new interaction potential. Our theoretical value is also in good agreement with the theoretical value of $B = 0.313$ cm^{-1} based on the PES of Cybulski *et al.*[7] computed by Kerenskaya *et al.*[24]

IV. COLLISIONAL DYNAMICS

As a second application, we have studied the collisional excitation of NH by He. The scattering calculations were performed for the main ^{14}N and ^{4}He isotopes. The detailed

description of the Close-Coupling (CC) calculations that consider the fine structure levels of the projectile is given in Ref. 4. The quantal coupled equations were solved in the intermediate coupling scheme using the MOLSCAT code[26] modified to take into account the fine structure of the energy levels. In the scattering calculations, we used the NH–He 3D-ave PES developed in this work.

We used a total energy grid with variable steps. For the energies below 1250 cm^{-1}, the step was equal to 1 cm^{-1}; then, between 1250 and 1500 cm^{-1}, it was increased to 5 cm^{-1}; and for the energy interval 1500–3500 cm^{-1}, it was increased to 10. Using this energy grid, the resonances (shape and Feshbach) that may appear in the cross sections at low energies were correctly represented.

In order to ensure convergence of the inelastic cross sections, it is necessary to include in the calculations several energetically inaccessible (closed) levels. At the largest energies considered in this work, the NH rotational basis was extended to $N = 12$ to ensure convergence of the rotational cross sections between levels with $N < 8$. One also needs to converge inelastic cross sections with respect to partial waves. The total angular momentum quantum number J needed for the convergence was set up to 81 for the inelastic cross sections.

Moreover, in MOLSCAT, it is necessary to adjust the propagator's parameters in order to ensure convergence of cross section calculations. For all the energies, the minimum and maximum integration distances were $R_{min} = 3.0$ bohr and $R_{max} = 50$ bohr, respectively. The STEPS parameter was adjusted for each value of energy in order to obtain a step length of the integrator sufficient to ensure convergence of the calculations. In our work, the value of the STEPS parameter decreases with increasing energy (from 50 to 7 for our energy range). The reduced mass of the NH–He system is $\mu = 3.1600$ amu.

Figure 2 presents the energy variation of the integral cross sections for transitions from the initial rotational level $N = 0$, F_1 of NH.

As one can see, resonances appear at low collisional energies. This is related to the presence of an attractive potential well of a depth of ~20 cm^{-1}, which allows for the He atom to be temporarily trapped there and hence quasi-bound states to be formed before the complex dissociates.[27,28] However, few resonances are seen in the excitation cross sections since the energy spacing between two rotational levels is generally large in comparison to the well depth of the NH–He PES.

The magnitude of the cross sections shown in Fig. 2 seems to be governed by the following propensity rules:

(i) The cross sections decrease with increasing ΔN, which is the usual trend for rotational excitation. In addition, even ΔN transitions are favored over odd ΔN transitions. This is a consequence of dominant even anisotropy of the PES over the odd anisotropy [i.e., the radial coefficients A_{ln} (R) of Eq. (5) with l even dominates those with l odd].

(ii) A propensity rule exists for fine-structure conserving transitions [$\Delta j = \Delta N$ in the case of pure Hund's case (b)].

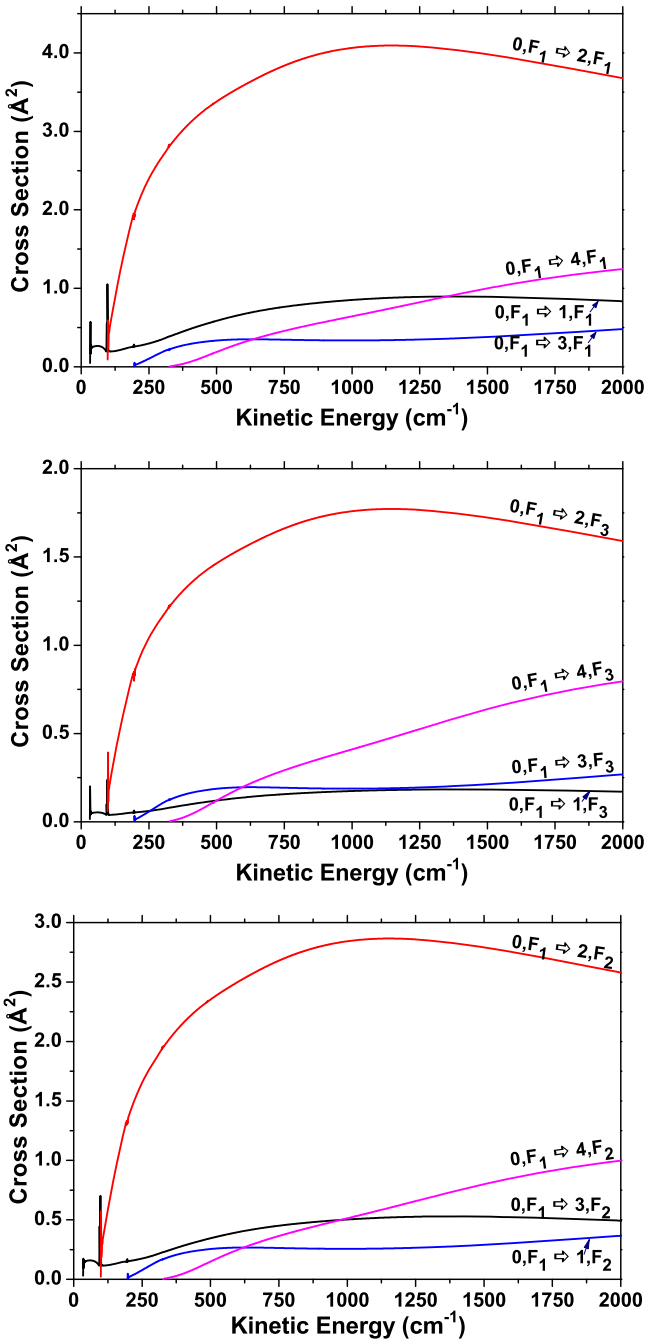

FIG. 2. Collisional excitation cross sections of NH by He from $N = 0, F_1$. The upper panel is for fine-structure conserving transitions, while the two others panels are for fine-structure changing transitions.

The same propensity rules were previously observed in NH–He[13] collisions. The latter propensity, predicted theoretically,[29] is general for molecules in the $^3\Sigma^-$ electronic state and was previously observed in $O_2(X^3\Sigma^-)$–He[30,31] or $SO(X^3\Sigma^-)$–He[4] collisions.

It is then interesting to compare the new results with that of Toboła *et al.*[13] Figure 3 presents the kinetic energy variation of the collisional cross sections for some selected transitions obtained from the new PES and from Toboła *et al.*[13] using the PES of Cybulski *et al.*[7]

As one can see, some deviations (as large as a factor of 2) exist between the two sets of data, especially for transitions

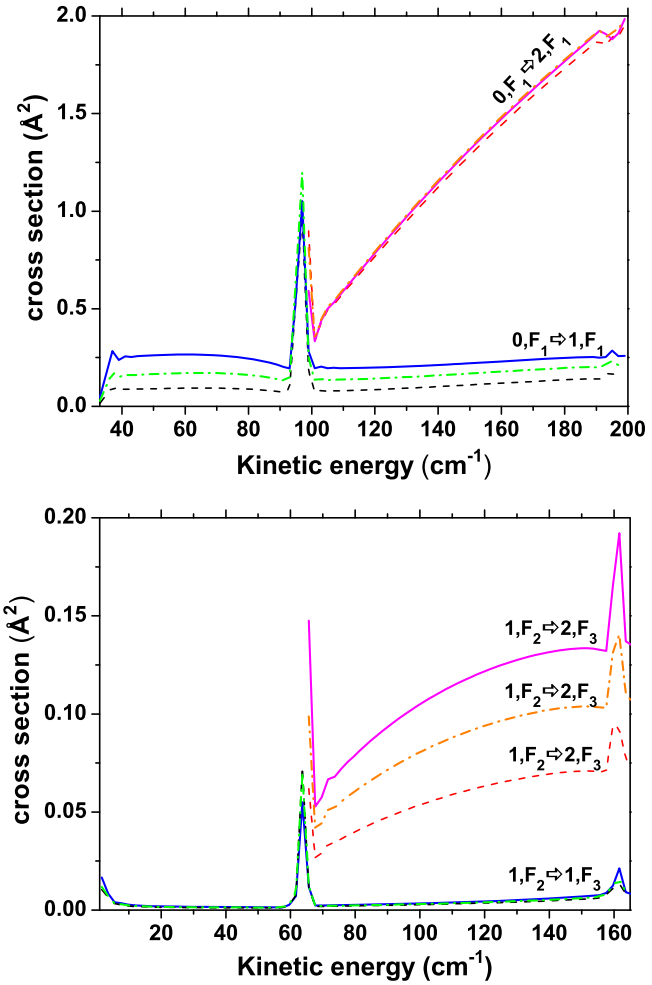

FIG. 3. Comparison between NH–He cross sections obtained from the 3D-ave PES (solid lines), the new 2D PES (dashed dotted lines), and the Cybulski *et al.*[7] PES (dashed lines). The upper panel is for fine-structure conserving transitions, while the lower panel is for fine-structure changing transitions.

with odd ΔN. These deviations are not only due to the use of different PESs but also due to the inclusion of the vibration of NH in the new PES. To analyze the effect of the vibration on the magnitude of the cross sections, we have also computed inelastic cross sections using the new PES but for a fixed internuclear distance (r = 1.95 bohr). The results are also shown in Fig. 3. As one can see, a significant part of the difference between the cross sections from the new PES and from the PES of Cybulski *et al.*[7] comes from the inclusion of the NH vibration, confirming again the importance of the intramolecular vibration even for computing pure rotational cross sections.

By averaging over a Maxwellian distribution of collision velocities, we have obtained thermal rate coefficients for excitation and de-excitation transitions between fine-structure levels of NH:

$$k_{N,F_i\to N,F_i'}(T) = \left(\frac{8k_BT}{\pi\mu}\right)^{\frac{1}{2}}\left(\frac{1}{k_BT}\right)^2 \times \int_0^\infty E_k\sigma_{N,F_i\to N,F_i'}(E_k)e^{\frac{-E_k}{k_BT}}dE_k, \quad (7)$$

where k_B is the Boltzmann constant.

We obtain rate coefficients for temperatures up to 350 K. A table of collisional rate coefficients is included in the supplementary material.

The thermal dependence of the state-to-state rate coefficients is illustrated in Fig. 4 for transitions out of the $N = 0, j = 1, F_1$ level.

The rate coefficients obviously display the same propensity rules as seen in the integral cross sections. In particular,

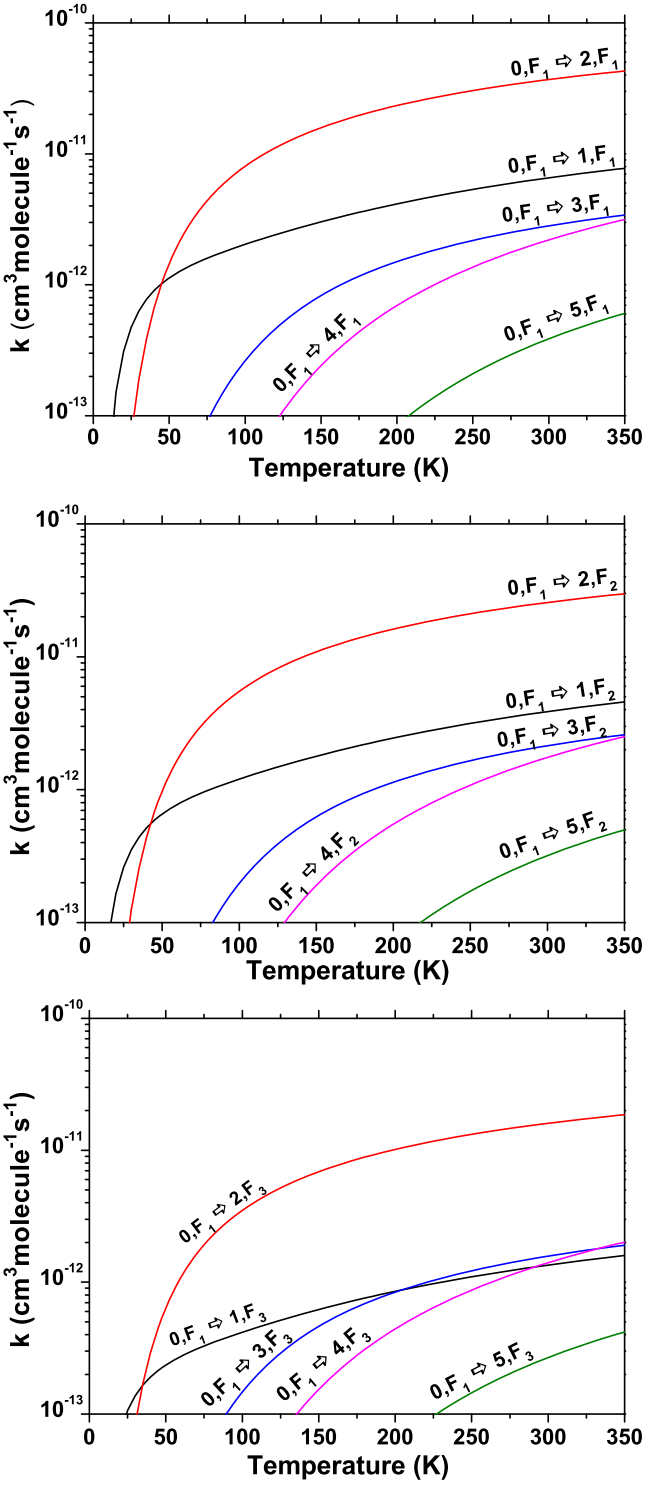

FIG. 4. Thermal dependence of the rate coefficients of NH by He from $N = 0$, F_1. The upper panel is for fine-structure conserving transitions, while the two other panels are for fine-structure changing transitions.

TABLE III. Total rate constant (summed over all final states) (in units of 10^{-11} cm^3 s^{-1}) out of the N, F_i states as a function of the initial nuclear rotation quantum number N at 300 K.

	F_1		F_2		F_3	
N	This work	Reference 14	This work	Reference 14	This work	Reference 14
0	10.26	8.3				
1	10.13	13.01	10.85	12.66	12.48	24.48
2	10.96	13.39	13.04	20.73	17.69	9.18
3	10.62	9.62	12.61	13.25	11.96	10.04
4	9.67	8.44	11.38	12.87	10.45	16.28
5	8.52	6.13	9.89	11.07	9.02	9.48
6	7.31	3.44	8.45	7	7.63	6.98
7	5.99	3.11	6.91	6.01	6.21	6.26

the rate coefficients for fine-structure conserving transitions are generally larger than those for fine-structure changing transitions.

The calculated rate coefficients at 300 K can be compared with the experimental results measured by Rinnenthal and Gericke.[14] In Table III, we compare the theoretical and experimental sum over all rate constants out of the N, F_i states as a function of the initial nuclear rotation quantum number N.

One can see a good agreement between the theoretical and experimental results. The total theoretical and experimental rate coefficients decrease with increasing N, as can be seen very clearly for the average total rate constants. Such behavior can be explained by the energy gap with the closest levels that increase with increasing N.

In Fig. 5, we compare all the calculated and experimental[14] state-to-state rate coefficients.

As one can see, the overall agreement between theoretical and experimental data is reasonably good despite some significant deviations. Most of the experimental collisional data are reproduced within a factor of 2–3. The mean deviation between the experimental and theoretical rate coefficients is a factor of 5 with very few exceptions. These large deviations are for the rate coefficients with the smaller magnitude that are probably more difficult to measure experimentally. Indeed, the error bar

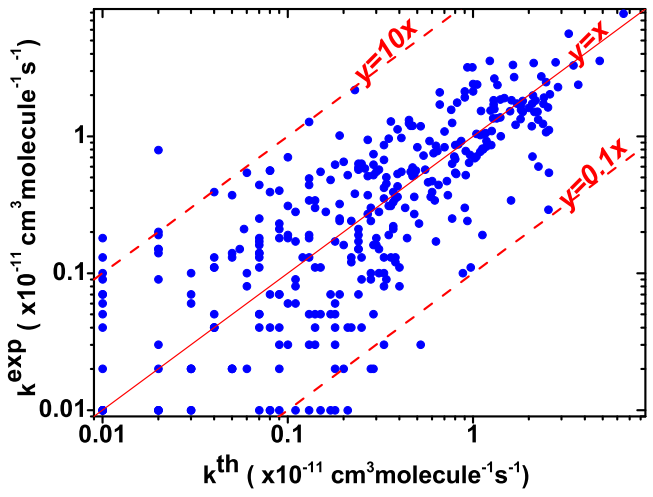

FIG. 5. Experimental and theoretical state-to-state NH–He rate coefficients.

mentioned by Rinnenthal and Gericke[14] is $0.08 \cdot 10^{-11}$ cm^3 s^{-1} and largely exceeds the value of these low magnitude rate coefficients.

The significant differences are surprising taking into account the accuracy of the present theoretical approach. This kind of theoretical modeling has been shown to well reproduce experiments for other systems, for example, CN–He[32] or OH–He.[16,33] Hence, the accuracy of the experimental data can be legitimately challenged. Indeed, the experimental results do not show the usual fine-structure conserving propensity rules, and the experimental rate coefficients do not fulfill the detailed balance as already noticed in the work of Toboła *et al.*[13] Such unusual behavior may be explained by the fact that some of the rate coefficients have not been directly measured but inferred through a master equation [Eq. (1) of Ref. 14] which will propagate the errors.

V. CONCLUSION

We have presented a new highly accurate PES for the NH–He van der Waals complex. The 3D PES was obtained from highly correlated calculations at the RCCSD(T) level using a complete basis set extrapolation. The new PES is found to be in good agreement with the previously published one.

Using this new PES, we have studied the spectroscopy of the NH–He complex and we have determined a new rotational constant that agrees well with the available experimental data. Collisional excitation of NH($X^3\Sigma^-$) by He was also studied at the close-coupling level. Calculations of the collisional excitation cross sections of the fine-structure levels of NH by He were performed for energies up to 3500 cm^{-1}, which yield, after a thermal average, rate coefficients up to 350 K. The calculated rate coefficients are compared with available experimental measurements at room temperature, and a fairly good agreement is found between experimental and theoretical data, confirming the accuracy of the PES developed in this work.

It is interesting to note that the use of vibrational averaging of the PES induces a small difference in the bound state calculations as attested by the good agreement with previous bound state studies, whereas the effect is much more important on the scattering calculation. This is probably due to the fact that bound state calculations are sensitive to the well depth and to the isotropic potential that are only slightly influenced by the

vibrational averaging contrary to the inelastic scattering that is determined by the anisotropy of the PES that is significantly modified by the vibrational averaging.

The new PES is shown to be accurate enough for further use in the calculation of state-to-state rate coefficients for astrophysical applications and for studying dynamics of the NH–He collisional system using the Zeeman decelerator.

SUPPLEMENTARY MATERIAL

See supplementary material for the analytic forms of the NH–He potential energy surface and the NH–He collisional rate coefficients.

ACKNOWLEDGMENTS

This work was supported by the Programme National Physique et Chimie du Milieu Interstellaire (PCMI) of CNRS/INSU with INC/INP co-funded by CEA and CNES. F.L. acknowledges the Agence Nationale de la Recherche (ANR-HYDRIDES), Contract No. ANR-12-BS05-0011-01, and the financial support from the Institut Universitaire de France. J.K. acknowledges financial support from the U.S. National Science Foundation, Grant No. CHE-1565872, to M. H. Alexander.

[1]D. Egorov, W. C. Campbell, B. Friedrich, S. E. Maxwell, E. Tsikata, L. D. van Buuren, and J. M. Doyle, Eur. Phys. J. D **31**, 307 (2004).
[2]T. Cremers, S. Chefdeville, N. Janssen, E. Sweers, S. Koot, P. Claus, and S. Y. T. van de Meerakker, Phys. Rev. A **95**, 043415 (2017).
[3]W. Gordy and R. L. Cook, *Microwave Molecular Spectra* (Wileys and Sons, 1984).
[4]F. Lique, A. Spielfiedel, M. L. Dubernet, and N. Feautrier, J. Chem. Phys. **123**, 134316 (2005).
[5]D. M. Meyer and K. C. Roth, Astrophys. J. **376**, L49 (1991).
[6]E. Roueff and F. Lique, Chem. Rev. **113**, 8906 (2013).
[7]H. Cybulski, R. V. Krems, H. R. Sadeghpour, A. Dalgarno, J. Kłos, G. C. Groenenboom, A. van der Avoird, D. Zgid, and G. Chałasiński, J. Chem. Phys. **122**, 094307 (2005).
[8]P. J. Knowles, C. Hampel, and H.-J. Werner, J. Chem. Phys. **99**, 5219 (1993).
[9]P. J. Knowles, C. Hampel, and H.-J. Werner, J. Chem. Phys. **112**, 3106 (2000).
[10]T. H. Dunning, J. Chem. Phys. **90**, 1007 (1989).
[11]R. V. Krems, H. R. Sadeghpour, A. Dalgarno, J. K. D. Zgid, and G. Chałasiński, Phys. Rev. A **68**, 051401 (2003).
[12]W. C. Campbell, E. Tsikata, H. Lu, L. D. van Buuren, and J. M. Doyle, Phys. Rev. Lett. **98**, 213001 (2007).
[13]R. Toboła, F. Dumouchel, J. Kłos, and F. Lique, J. Chem. Phys. **134**, 024305 (2011).
[14]J. L. Rinnenthal and K.-H. Gericke, J. Chem. Phys. **116**, 9776 (2002).
[15]N. Bouhafs and F. Lique, J. Chem. Phys. **143**, 184311 (2015).
[16]Y. Kalugina, F. Lique, and S. Marinakis, Phys. Chem. Chem. Phys. **16**, 13500 (2014).
[17]F. Lique, J. Chem. Phys. **142**, 241102 (2015).
[18]H.-J. Werner, P. J. Knowles, G. Knizia, F. R. Manby, M. Schütz, P. Celani, T. Korona, R. Lindh, A. Mitrushenkov, G. Rauhut, K. R. Shamasundar, T. B. Adler, R. D. Amos, A. Bernhardsson, A. Berning, D. L. Cooper, M. J. O. Deegan, A. J. Dobbyn, F. Eckert, E. Goll, C. Hampel, A. Hesselmann, G. Hetzer, T. Hrenar, G. Jansen, C. Köppl, Y. Liu, A. W. Lloyd, R. A. Mata, A. J. May, S. J. McNicholas, W. Meyer, M. E. Mura, A. Nicklass, D. P. O'Neill, P. Palmieri, K. Pflüger, R. Pitzer, M. Reiher, T. Shiozaki, H. Stoll, A. J. Stone, R. Tarroni, T. Thorsteinsson, M. Wang, and A. Wolf, MOLPRO, version 2010.1, a package of *ab initio* programs, 2010, see http://www.molpro.net.
[19]S. F. Boys and F. Bernardi, Mol. Phys. **19**, 553 (1970).
[20]K. A. Peterson, D. E. Woon, and T. H. Dunning, Jr., J. Chem. Phys. **100**, 7410 (1994).
[21]H.-J. Werner, B. Follmeg, M. H. Alexander, and D. Lemoine, J. Chem. Phys. **91**, 5425 (1989).
[22]D. T. Colbert and W. H. Miller, J. Chem. Phys. **96**, 1982 (1992).
[23]H.-J. Werner and P. J. Knowles, J. Chem. Phys. **89**, 5803 (1988).
[24]G. Kerenskaya, U. Schnupf, M. C. Heaven, and A. van der Avoird, J. Chem. Phys. **121**, 7549 (2004).
[25]J. M. Hutson, BOUND computer code, version 5, distributed by Collaborative Computational Project No. 6 of the Science and Engineering Research Council (UK), 1993.
[26]J. M. Hutson and S. Green, MOLSCAT computer code, version 14, distributed by Collaborative Computational Project No. 6 of the Engineering and Physical Sciences Research Council (UK), 1994.
[27]L. N. Smith, D. J. Malik, and D. Secrest, J. Chem. Phys. **71**, 4502 (1979).
[28]K. M. Christoffel and J. M. Bowman, J. Chem. Phys. **78**, 3952 (1983).
[29]M. H. Alexander and P. J. Dagdigian, J. Chem. Phys. **79**, 302 (1983).
[30]T. Orlikowski, Mol. Phys. **56**, 35 (1985).
[31]F. Lique, J. Chem. Phys. **132**, 044311 (2010).
[32]F. Lique, A. Spielfiedel, N. Feautrier, I. F. Schneider, J. Kłos, and M. H. Alexander, J. Chem. Phys. **132**, 024303 (2010).
[33]J. Kłos, F. Lique, and M. H. Alexander, Chem. Phys. Lett. **445**, 12 (2007).

The Journal of Chemical Physics ARTICLE scitation.org/journal/jcp

Collisional excitation of NH($^3\Sigma^-$) by Ar: A new *ab initio* 3D potential energy surface and scattering calculations

Cite as: J. Chem. Phys. 150, 214302 (2019); doi: 10.1063/1.5097651
Submitted: 27 March 2019 • Accepted: 10 May 2019 •
Published Online: 4 June 2019

D. Prudenzano,[1,a] F. Lique,[2] R. Ramachandran,[2] L. Bizzocchi,[1] and P. Caselli[1]

AFFILIATIONS

[1] Center for Astrochemical Studies, Max-Planck-Institut für Extraterrestrische Physik, Gießenbachstraße 1, 85748 Garching, Germany
[2] LOMC—UMR 6294, CNRS-Université du Havre, 25 Rue Philippe Lebon, BP 1123, 76063 Le Havre, France

[a] **Email:** prudenzano@mpe.mpg.de

ABSTRACT

Collisional excitation of light hydrides is important to fully understand the complex chemical and physical processes of atmospheric and astrophysical environments. Here, we focus on the NH($X^3\Sigma^-$)-Ar van der Waals system. First, we have calculated a new three-dimensional Potential Energy Surface (PES), which explicitly includes the NH bond vibration. We have carried out the *ab initio* calculations of the PES employing the open-shell single- and double-excitation couple cluster method with noniterative perturbational treatment of the triple excitations. To achieve a better accuracy, we have first obtained the energies using the augmented correlation-consistent aug-cc-pVXZ (X = T, Q, 5) basis sets and then we have extrapolated the final values to the complete basis set limit. We have also studied the collisional excitation of NH($X^3\Sigma^-$)-Ar at the close-coupling level, employing our new PES. We calculated collisional excitation cross sections of the fine-structure levels of NH by Ar for energies up to 3000 cm^{-1}. After thermal average of the cross sections, we have then obtained the rate coefficients for temperatures up to 350 K. The propensity rules between the fine-structure levels are in good agreement with those of similar collisional systems, even though they are not as strong and pronounced as for lighter systems, such as NH–He. The final theoretical values are also compared with the few available experimental data.

I. INTRODUCTION

The study of inelastic collisions plays a relevant role in the understanding of important processes in different fields, such as atmospheric and astrophysical chemistry and physics. In particular, open-shell molecules are crucial, being highly reactive compounds, and intermediate in a large number of chemical reactions. A relevant chemical species is the NH radical. This compound serves as a prototype for other collisional studies involving open-shell molecules. Being diatomic, it is also preferred for both experimental and theoretical scattering studies, owing to its large rotational energy level spacings. In addition, the magnetic moment of its $^3\Sigma^-$ electronic ground state makes NH suitable for studies of ultracold molecules[1,2] because it can be easily thermalized at low temperatures through collision with cold buffer gas atoms. In the past, NH has been the subject of many theoretical and experimental collisional studies in different electronic states and with a variety of perturbers, such as the rare gases He[3–10] and Ne.[11–13]

In our work, we focus on the calculation of a new *ab initio* 3D-averaged Potential Energy Surface (PES) and collisional excitation of the NH($^3\Sigma^-$)-Ar system. To our knowledge, there are no theoretical scattering studies for the fine-structure excitation of NH($^3\Sigma^-$) by Ar, while there is only one experimental work performed by Dagdigian,[14] employing a crossed beam apparatus. However, this experiment provides only relative collisional cross sections up to the rotational level $N = 4$ and no rate coefficients are available.

The most recent PES is given by Kendall *et al.*[15] They employed a combination of supermolecular and intermolecular unrestricted

Møller-Plesset perturbation theory (UMPPT)[16,17] and a selection of monomer-centered basis sets augmented with bond functions. However, the NH bond length was kept frozen at 1.96 bohrs. Recent studies[10,13,18,19] have proven that the use of a 3D PES which takes into account molecular vibration leads to more accurate results when employed in collisional excitation studies of light hydrides by rare gases. Moreover, inclusion of the bond vibrational motion makes it possible to comprise excited vibrational states. Hence, we have computed a new *ab initio* PES for the NH($^3\Sigma^-$)–Ar van der Waals complex including the NH bond vibration.

Then, we present the first fully quantum close-coupling (CC) calculations of rotational inelastic cross sections for the NH($^3\Sigma^-$)–Ar collisional system. In addition, we have taken into account the spin-coupling splitting of the rotational levels and we have included the temperature dependence of the fine-structure resolved rate coefficients in the final results.

The paper is organized as follows: Sec. II covers the calculation of the new NH–Ar PES and information about the bound states of the NH–Ar complex; in Sec. III, we present the scattering calculations, including the inelastic cross sections and rate coefficients. In Sec. IV, we compare the resulting cross sections with the available experimental data in Ref. 14. Conclusions are given in Sec. V.

II. POTENTIAL ENERGY SURFACE

The two interacting species are considered in their ground electronic states NH($^3\Sigma^-$) and Ar(^1S). The NH($^3\Sigma^-$)–Ar van der Waals system has the $^3A''$ ground electronic state. In this work, we used the Jacobi coordinate system (see Fig. 1). The center of coordinates is placed in the NH center of mass (c.m.), and the vector **R** connects the NH c.m. with the Ar atom. The rotation of the NH molecule is defined by the θ angle, and the r coordinate describes the NH bond length.

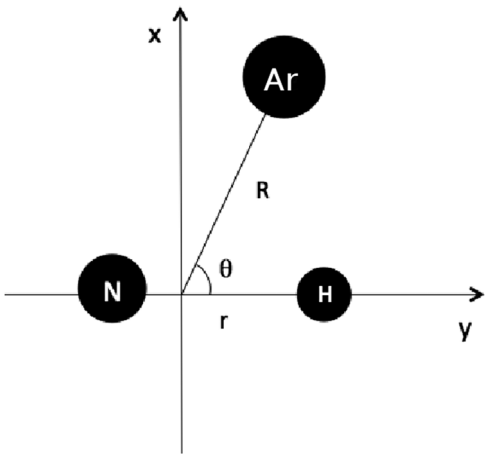

FIG. 1. Definition of the Jacobi coordinate system. The origin of the coordinate system corresponds to the NH center of mass. R is the distance between the origin and the Ar atom, θ is the angle at which the Ar approaches the NH molecule, and r is the NH bond length.

We performed the calculations for five NH bond lengths r = [1.6, 1.8, 1.95, 2.15, 2.5] bohrs which allows us to take into account vibrational motion of the NH molecule up to v = 2. We have carried out *ab initio* calculations of the PES of the NH–Ar van der Waals complex with the partially spin-Restricted Coupled Cluster with Single, Double, and perturbative Triple excitation method [RCCSD(T)],[20,21] using the MOLPRO 2015 package.[22] In order to determine the interaction potential, $V(R, \theta, r)$, the basis set superposition error (BSSE) was corrected at all geometries using the Boys and Bernardi counterpoise scheme,[23]

$$V(R,\theta,r) = E_{\text{NH-Ar}}(R,\theta,r) - E_{\text{NH}}(R,\theta,r) - E_{\text{Ar}}(R,\theta,r), \quad (1)$$

where the energies of the NH and Ar monomers are computed using the full basis set of the complex.

To achieve a good description of the charge-overlap effects, we have performed the calculations in a rather large augmented correlation-consistent basis set aug-cc-pVXZ (X = T, Q, 5).[24] Then, we have extrapolated the energies to the Complete Basis Set (CBS) limit using the following scheme:[25]

$$E_X = E_{CBS} + Ae^{-(X-1)} + Be^{-(X-1)^2}, \quad (2)$$

where X is the cardinal number of the aug-cc-pVXZ basis set, E_X is the energy corresponding to the aug-cc-pVXZ basis set, E_{CBS} is the energy extrapolated to the CBS limit, and A and B are the parameters to adjust. We have carried out the calculations for θ angle values from 0° to 180° in steps of 10°. R-distances were varied from 3.0 to 40.0 bohrs, yielding 52 points for each angular orientation. Overall, ~5000 single point energies were calculated for the NH–Ar complex.

A. Analytical representation of the potential energy surface

The analytical expression employed for the interaction potential $V(R, \theta, r)$ has the following form:[26]

$$V(R,\theta,r) = \sum_{n=1}^{N}\sum_{l=1}^{L} B_{l,n}(R)(r-r_e)^{n-1} d_{m0}^{l+m-1}(\cos(\theta)), \quad (3)$$

where

$$B_{l,n}(R) = e^{-a_{l,n}(R-R_{l,n}^{(0)})}\left(\sum_{i=0}^{2} b_{l,n}^{(i)} R^i\right) - \frac{1}{2}\left(1+\tanh\frac{R-R_{l,n}^{(1)}}{R_{l,n}^{ref}}\right)\sum_{j=6,8,10}\frac{c_{l,n}^{(j)}}{R^j}. \quad (4)$$

The basis functions $d_{m0}^{l+m-1}(\cos(\theta))$ are Wigner rotation functions, N is the total number of r-distances, and L is the total number of angles. The analytic potential was found to reproduce the calculated energies quite well: the mean difference between the analytic fit and the *ab initio* computed interaction energies is less than 2% over the entire grid.

Previous studies[18] have shown that averaging of the PES over the corresponding vibrational level v leads to a better agreement with experimental results than using a purely two-dimensional PES. The newly constructed PES, which takes into account the stretching

of the NH molecule, can be averaged over any vibrational state, up to $v = 2$. The averaging is done using the following formula:

$$V_v(R,\theta) = \langle v(r)|V(R,\theta,r)|v(r)\rangle. \quad (5)$$

The NH vibrational wave functions $|v(r)\rangle$ were those computed by Bouhafs *et al.*,[13] which were evaluated using a discrete variable representation (DVR) method[27] from *ab initio* calculations of the NH potential function using the internally contracted multireference configuration interaction (MRCI)[28] level and a large aug-cc-pV5Z atomic basis set.

Figure 2 depicts the contour plot of our 3D PES averaged over the ground vibrational state $v = 0$ as a function of R and θ (hereafter referred to as 3D-ave PES). For this weakly bound system, the global minimum in the interaction energy was found to be -104.138 cm^{-1} ($R = 6.7$ bohrs, $\theta = 69^\circ$).

Our study is in good agreement with the NH–Ar PES previously published.[15] Kendall *et al.*[15] carried out calculations for the NH–Ar interaction with the supermolecular unrestricted Møller-Plesset (UMP) perturbation theory and a combination of different basis sets. The NH intermolecular distance was fixed at 1.95 bohrs. According to the authors, the best results have been obtained with the aug-cc-pVTZ(ext-b) basis set, augmented with bond functions, and the global minimum is found at $R = 6.75$ bohrs and $\theta = 67^\circ$, with a well depth of -100.3 cm^{-1} and an uncertainty within the 5%. These values are very close to our results for $r = 1.95$ bohrs ($R = 6.7$, $\theta = 67^\circ$, 103.787 cm^{-1}). Furthermore, the results of our 3D-ave PES also agree well with those listed above, confirming the high accuracy of our study. The slightly increased deepness of our well-depth is mostly due to the use of CBS extrapolation, since the energy follows a monotonic trend toward negative values, by approaching the infinite basis set limit. Figure 3 depicts the variation of the angle at which occurs the minimum of the interaction potential, for different NH bond distances. While the equilibrium angle changes substantially over increasing r, the R distance is always close to $R = 6.7$.

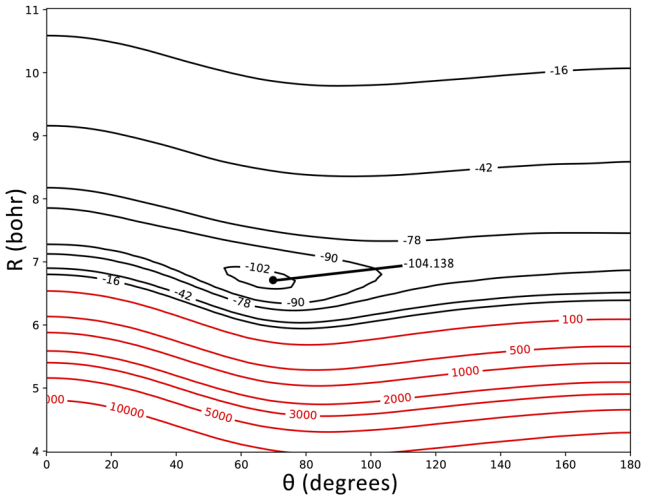

FIG. 2. Contour plot (in cm^{-1}) of the NH–Ar PES averaged over the ground vibrational state $v = 0$ as a function of Jacobi coordinates R and θ.

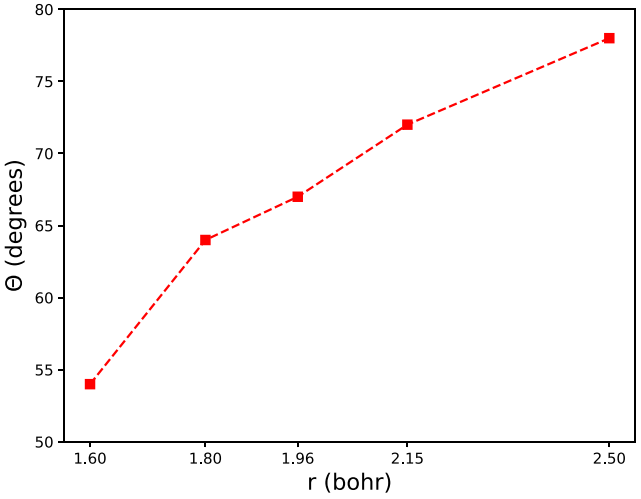

FIG. 3. Equilibrium angles at different NH bond lengths. The R coordinate at the minimum energy does not change with r and has always a value of ~6.7 bohrs.

B. NH–Ar bound states and dissociation energy

Using the highly correlated 3D-ave PES described in Sec. II A, we have computed the bound states of the NH–Ar complex using a coupled-channel approach, as implemented in the BOUND program.[29] The bound state calculations were performed for the main ^{14}N and ^{40}Ar isotopes.

As a first step, we performed bound state calculations neglecting the NH fine structure (i.e., NH was considered as a closed shell molecule). The calculations were performed with a propagator step size of 0.01 bohr, and the other propagation parameters were taken as the default BOUND values. The rotational basis includes the rotational states with $N_{max} \leq 10$. The bound energy levels of the NH–Ar complex computed with the 3D-ave PES are listed in Table I. From the present calculations, dissociation energy (D_0) of the complex is 73.15 cm^{-1} which is slightly larger than the previously calculated value of Kendall *et al.*[15] ($D_0 = 71.5$ cm^{-1}). The difference (1.65 cm^{-1}) can be mainly attributed to the difference between the two NH–Ar PESs used in the calculations. Indeed, the well depth of

TABLE I. NH–Ar bound energy levels (in cm^{-1}) obtained excluding the NH fine structure. Energies are relative to the ground-state energy of NH. All the levels correspond to the approximate quantum numbers $N = 0$. J and l correspond to the total and orbital angular momentum of the complex, respectively.

J	l	Energy (cm^{-1})
0	0	−73.1507
1	1	−72.9324
2	2	−72.4988
3	3	−71.8479

TABLE II. NH–Ar bound energy levels (in cm^{-1}) obtained with the inclusion of the NH fine structure. Energies are relative to the ground-state energy of NH. All the levels correspond to the approximate quantum numbers $N = 0$, F_1. J and l correspond to the total and orbital angular momentum of the complex, respectively.

J	l	Energy (cm^{-1})
1	0	−73.1519
0	1	−72.8964
1	1	−72.9507
2	1	−72.9305
1	2	−72.4804
2	2	−72.5169
3	2	−72.4947
2	3	−71.8333
3	3	−71.8658
4	3	−71.8426

the 3D-ave PES considering the vibration motion is slightly deeper (by few cm^{-1}) than the rigid rotor one of Kendall *et al.*,[15] and this difference leads to a larger estimated value of the dissociation energy.

In order to derive the rotational constant of the NH–Ar complex, we have fitted the energies of Table I to the rigid rotor expression $E_J = E_0 + BJ(J+1) - DJ^2(J+1)^2$, where J corresponds to the total angular momentum of the complex. We have obtained for the rotational and quartic centrifugal distortion constants, $B = 0.1087$ cm^{-1} and $D = 0.000\,025$ cm^{-1}. Such estimates allow generating the energetic structure of the complex and are useful for the interpretation of future experimental spectra. As a comparison, our rotational constant is in good agreement with the value obtained by Jansen *et al.*,[30] i.e., B = 0.1007.

As previously mentioned, the NH molecule exhibits a fine structure because of the coupling between the rotational angular momentum and the electronic spin. The BOUND program was modified to include this fine structure of the NH molecule.[10] Table II presents the bound state energies for the first total angular momentum J. The predicted bound energy levels indicate that the coupling of the electron spin to the rotational motion of the complex is very weak. As a consequence, energy levels of NH–Ar are very similar to those obtained by neglecting the fine structure, as already found for the NH–He complex.[10] The dissociation energy is thus not significantly impacted by the fine structure.

III. SCATTERING CALCULATIONS

Rotational transitions in the NH($^3\Sigma^-$) electronic ground state show fine-structure splitting, due to spin-rotation coupling. The rotational wave function of NH for $j \geq 1$ in the intermediate coupling scheme can be written as[31,32]

$$\begin{aligned} |F_1 jm\rangle &= \cos\alpha |N = j-1, Sjm\rangle + \sin\alpha |N = j+1, Sjm\rangle, \\ |F_2 jm\rangle &= |N = j, Sjm\rangle, \\ |F_3 jm\rangle &= -\sin\alpha |N = j-1, Sjm\rangle + \cos\alpha |N = j+1, Sjm\rangle, \end{aligned} \quad (6)$$

where $|N, Sjm\rangle$ denotes pure Hund's case (b) basis functions and the mixing angle α is obtained by diagonalization of the molecular Hamiltonian. In this relation corresponding to the Hund's case (b), the total molecular angular momentum j is defined by

$$\mathbf{j} = \mathbf{N} + \mathbf{S}, \quad (7)$$

where $\mathbf{N}$ and $\mathbf{S}$ are the nuclear rotational and the electronic spin angular momenta. In the pure case (b) limit, $\alpha \to 0$, the F_1 level corresponds to $N = j - 1$ and the F_3 level to $N = j + 1$. The levels in the spin multiplets are usually labeled by the nuclear rotational quantum number N and the spectroscopic index F_i. This notation will be used hereafter.

Using the new 3D-ave PES, we have studied the collisional excitation of NH by Ar. The scattering calculations were performed for the main ^{14}N and ^{40}Ar isotopes. The detailed description of the Close-Coupling (CC) calculations that consider the fine structure levels of the colliders is given in Ref. 32. The quantal coupled equations have been solved in the intermediate coupling scheme using the MOLSCAT code[33] modified to take into account the fine structure of the rotational energy levels.

We used a total energy grid with variable steps. For the energies below 500 cm^{-1}, the step was equal to 1 cm^{-1}, and then, between 500 and 1000 cm^{-1}, it was increased to 2 cm^{-1} and to 20 for the interval 1000–3000 cm^{-1}. Using this energy grid, the resonances (shape and Feshbach) that usually appear in the cross sections at low energies were correctly represented.

In order to ensure the convergence of the inelastic cross sections, it is necessary to include in the calculations several energetically inaccessible (closed) levels. At the largest energies considered in this work, the NH rotational basis was extended to $N = 12$ to ensure the convergence of the rotational cross sections between levels with $N < 8$. One also needs to converge inelastic cross sections with respect to partial waves. The total angular momentum quantum number J needed for the convergence was set up to 238 for the inelastic cross sections.

Moreover, in MOLSCAT, it is necessary to adjust the propagator's parameters in order to ensure the convergence of cross section calculations. For all the energies, the minimum and maximum integration distances were $R_{min} = 3.0$ bohrs and $R_{max} = 50$ bohrs, respectively. The `STEPS` parameter was adjusted for each value of energy in order to obtain a step length of the integrator sufficient to achieve the convergence. In our work, the value of the `STEPS` parameter decreases with increasing energy, going from 50 to 7 and, therefore, constraining the R spacing below 0.1–0.2 bohr at all energies. The reduced mass of the NH–Ar system is $\mu = 10.912$ u, and the NH($^3\Sigma^-$) rotational and centrifugal distortion constants have been taken from Ref. 34.

Figure 4 presents the energy variation of the integral cross sections for transitions from the initial rotational level $N = 0$, F_1 of NH. The resonances shown at low collisional energies are related to the presence of a ~104 cm^{-1} deep attractive potential well. As a consequence, the Ar atom can be temporarily trapped there forming quasibond states before dissociation of the complex.[35,36] However, excitation cross sections are less affected and therefore show few resonances. Indeed, the energy spacing between rotational levels is generally larger than the well depth of the PES.

The magnitude of the cross sections shown in Fig. 4 seems to present the following propensity rules:

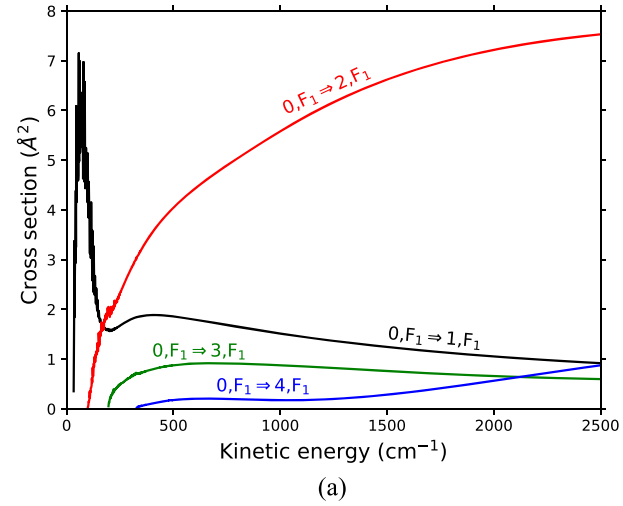

(a)

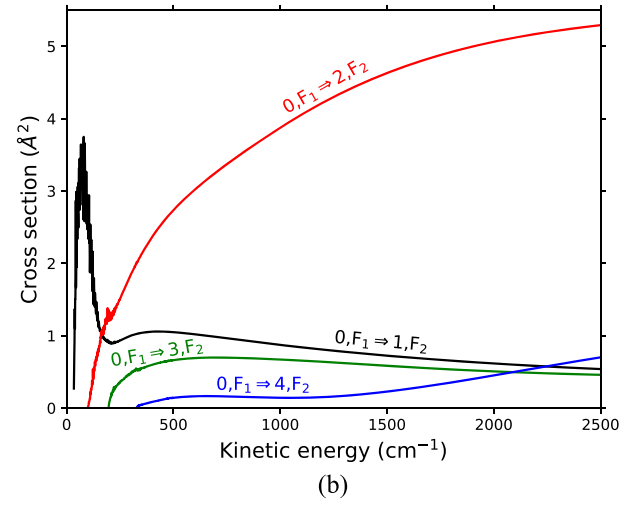

(b)

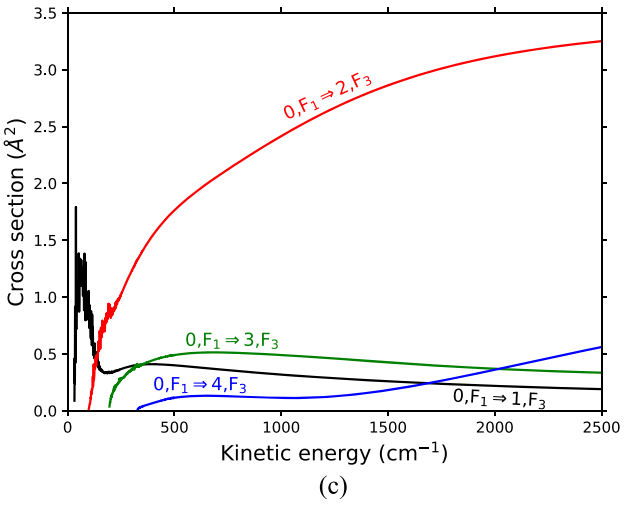

(c)

FIG. 4. Collisional excitation cross sections of NH by Ar from $N = 0$, F_1. (a) is for fine-structure conserving transitions, while (b) and (c) are for fine-structure changing transitions.

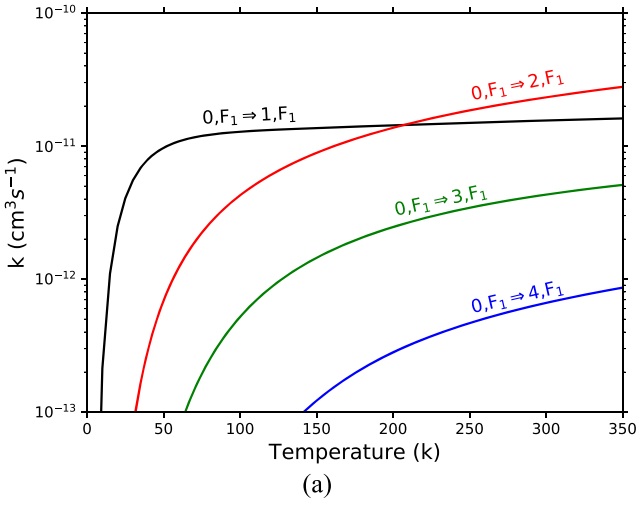

(a)

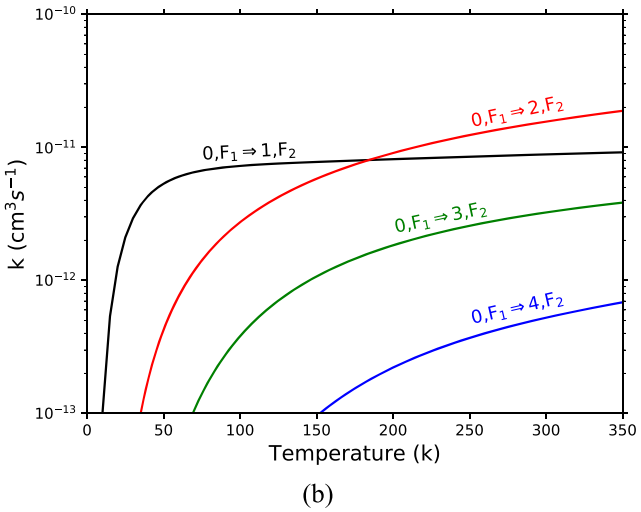

(b)

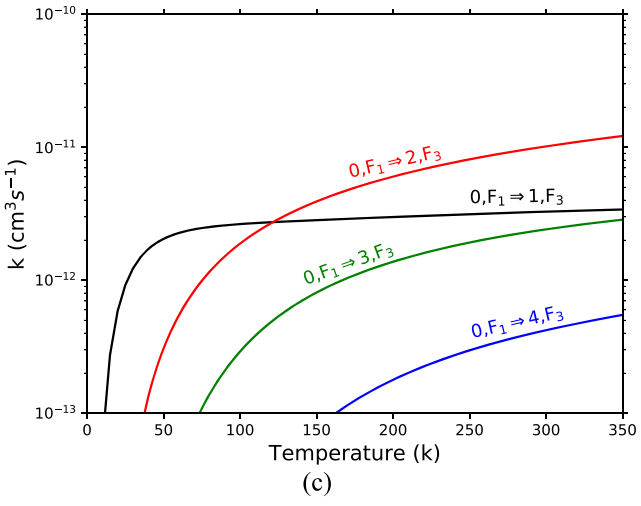

(c)

FIG. 5. Thermal dependence of the rate coefficients of NH by Ar from $N = 0$, F_1. (a) is for fine-structure conserving transitions, while (b) and (c) are for fine-structure changing transitions.

(1) Overall decreasing of the cross sections with increasing ΔN, according to the usual trend for rotational excitation. In addition, even ΔN transitions are favored over odd ΔN transitions as a consequence of near-homonuclearity of the PES.
(2) Fine-structure conserving transitions are favored, i.e., $\Delta j = \Delta N$ in the case of pure Hund's case (b).

The same propensity rules are shown in similar systems, such as NH-He and NH-Ne collisions.[8,10,13] In particular, the latter applies in general to molecules in the $^3\Sigma^-$ electronic state. Both propensity rules have been predicted theoretically[37] and also observed for the O_2-He[38,39] or SO($X^3\Sigma^-$)–He[32] collisions.

The thermal rate coefficients, $k_{F_ij\to F'_{i'}j'}(T)$, for excitation and de-excitation transitions between fine-structure levels of NH can be calculated by averaging CC excitation cross sections, $\sigma_{F_ij\to F'_ij}$, over a Maxwellian distribution of collision velocities, as follows:

$$k_{F_ij\to F'_{i'}j'}(T) = \left(\frac{8k_BT}{\pi\mu}\right)^{\frac{1}{2}}\left(\frac{1}{k_BT}\right)^2\int_0^\infty E_k\sigma_{F_ij\to F'_{i'}j'}(E_k)e^{\frac{-E_k}{k_BT}}dE_k, \quad (8)$$

where k_B is the Boltzmann constant, μ is the reduced mass of the system, and E_k is the translational energy.

The thermal dependence of these state-to-state rate coefficients for temperatures up to 350 K is shown in Fig. 5 for transitions out of the $N = 0, j = 1, F_1$ level.

The rate coefficients display the same propensity rules as seen for the integral cross sections. In particular, the rate coefficients for F-conserving transitions are generally larger than those for F-changing transitions.

IV. COMPARISON WITH EXPERIMENTS

Our new calculated cross sections can be compared with the previous experimental results, obtained for a collisional energy of 410 cm^{-1} and for rotational levels up to $N = 4, F_1$ (Ref. 14). Table III shows experimental and theoretical values normalized with respect to the $N = 0, F_1 \to N' = 1, F_1$ cross section. The F-conserving propensity rule is overall fulfilled in both the experimental and calculated values. In addition, the F-conserving cross sections follow the simple scaling relation observed by Dagdigian,[14] as shown in Fig. 6.

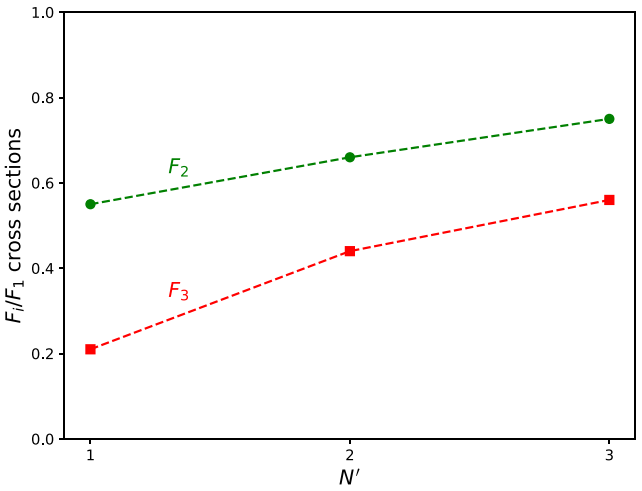

FIG. 6. Scaling relation for different F-levels over increasing final N'. The values correspond to the $N = 0, F_1 \to N' = X, F_2$ and $N = 0, F_1 \to N' = X, F_3$ cross sections normalized with respect to the $N = 0, F_1 \to N' = X, F_1$ one, with X = 1, 2, and 3.

The main discrepancy is the trend of the cross sections over increasing ΔN and over even/odd ΔN, as discussed for the first propensity rule in Sec. III. Furthermore, according to the results of Ref. 14, the largest cross sections are those with $N' = 1$, whereas this is not the case in our study. In fact, larger values are related to the transitions involving $N' = 2$, as also shown in Fig. 4.

It is likely that these discrepancies are due to a particular feature of the experiment. In fact, as declared by the author, the NH beam was not entirely pure, with 68% of the population in the rotational ground state $N = 0, F_1$, and approximately 16% and 9% in the $N = 1, F_1$ and $N = 1, F_2$ levels, respectively. By taking into account this NH beam population composition, the propensity rules observed in the experiment can be reproduced making a convolution of the various cross sections involved. This is shown in Table IV, which gathers values computed using 68% contribution from the inelastic cross section for transitions out of the $N = 0, F_1$, 16% from cross

TABLE III. Comparison between experimental and our theoretical cross sections at a collisional energy of 410 cm^{-1} and for transitions out of the $N = 0, F_1$ rotational level. All the values are normalized with respect to the cross section for the $N = 0, F_1 \to N' = 1, F_1$ transition. Experimental error in parentheses is in unit of the last quoted digit.

	F_1		F_2		F_3	
N'	Expt.[a]	Theory[b]	Expt.[a]	Theory[b]	Expt.[a]	Theory[b]
1	1.0	1.0	0.662(40)	0.560	0.255(54)	0.217
2	0.407(54)	1.906	0.284(46)	1.275	0.154(20)	0.833
3	0.068(15)	0.427	0.059(10)	0.321	0.047(08)	0.239
4	0.023(05)	0.061	...	...	...	...

[a]Reference 14.
[b]Our work.

TABLE IV. Comparison between experimental and convolved theoretical cross sections at a collisional energy of 410 cm^{-1} and for transitions out of the $N = 0, F_1$ rotational level. All the values are normalized with respect to the cross section of the $N = 0, F_1 \to N' = 1, F_1$ transition. Experimental error in parentheses is in unit of the last quoted digit. The convolution of the theoretical values is described in Sec. IV.

	F_1		F_2		F_3	
N'	Expt.[a]	Theory[b]	Expt.[a]	Theory[b]	Expt.[a]	Theory[b]
1	1.0	1.0	0.662(40)	0.842	0.255(54)	0.365
2	0.407(54)	0.954	0.284(46)	0.654	0.154(20)	0.411
3	0.068(15)	0.224	0.059(10)	0.172	0.047(08)	0.123
4	0.023(05)	0.037	...	...	...	...

[a]Reference 14.
[b]Our work. See text for details.

sections involving the $N = 1$, F_1, and 9% from those involving the $N = 1$, F_2.

It should be pointed out that there is a 7% population with unknown distribution and thus the theoretical results obtained through convolution are still different in magnitude from the experimental ones.

V. CONCLUSION

We have computed a new highly accurate 3D PES for the NH–Ar collisional system by taking into account the stretching of the NH bond. We carried out these *ab initio* calculations at the RCCSD(T) level and a complete basis set extrapolation. The results are in good agreement with the most recent PES available.[15]

Employing our new 3D-ave PES, we have calculated the dissociation energy of the NH–Ar van der Waals complex and the corresponding rotational and centrifugal distortion constants. We have also performed scattering calculations at the close-coupling level, obtaining collisional cross sections for energies up to 3000 cm^{-1}. We have then determined rate coefficients for temperatures up to 350 K. The resulting values follow the same propensity rules seen in other similar systems,[10,13] i.e., overall decreasing with increasing ΔN, even ΔN favored over odd ΔN and larger values for F-conserving transitions.

Our theoretical results have been compared to a previous experimental study.[14] The discrepancy concerning the ΔN propensity rules can be explained with the impurity of the NH population of the experimental molecular beam, since we have been able to reproduce the results of the experiment through convolution of various cross sections, as discussed in Sec. IV.

We hope that our results will encourage new experimental studies concerning collisional excitation of $NH(^3\Sigma^-)$ by Ar. In particular, it would be interesting to fill the gap of missing data regarding Ar as a collisional partner, with respect to systems involving He or Ne, more widely studied. Furthermore, a complete overview of these systems could also encourage studies with ortho- and para-H_2, highly important for astrophysical environments.

SUPPLEMENTARY MATERIAL

The supplementary material provides the analytic form of the NH–Ar potential energy surface and the NH–Ar collisional rate coefficients.

ACKNOWLEDGMENTS

F.L. acknowledges the Institut Universitaire de France. We would also thank P. Dagdigian for the interesting discussion about the comparison between our theoretical and his experimental results.

REFERENCES

[1] B. Friedrich and J. M. Doyle, ChemPhysChem **10**, 604 (2009).
[2] D. Egorov, W. Campbell, B. Friedrich, S. Maxwell, E. Tsikata, L. Van Buuren, and J. Doyle, Eur. Phys. J. D **31**, 307 (2004).
[3] M. H. Alexander, P. J. Dagdigian, and D. Lemoine, J. Chem. Phys. **95**, 5036 (1991).
[4] J. L. Rinnenthal and K.-H. Gericke, J. Chem. Phys. **116**, 9776 (2002).
[5] R. Krems, H. Sadeghpour, A. Dalgarno, D. Zgid, J. Kłos, and G. Chałasiński, Phys. Rev. A **68**, 051401 (2003).
[6] H. Cybulski, R. Krems, H. Sadeghpour, A. Dalgarno, J. Kłos, G. Groenenboom, A. van der Avoird, D. Zgid, and G. Chałasiński, J. Chem. Phys. **122**, 094307 (2005).
[7] T. Stoecklin, Phys. Rev. A **80**, 012710 (2009).
[8] R. Toboła, F. Dumouchel, J. Kłos, and F. Lique, J. Chem. Phys. **134**, 024305 (2011).
[9] F. Dumouchel, J. Kłos, R. Toboła, A. Bacmann, S. Maret, P. Hily-Blant, A. Faure, and F. Lique, J. Chem. Phys. **137**, 114306 (2012).
[10] R. Ramachandran, J. Kłos, and F. Lique, J. Chem. Phys. **148**, 084311 (2018).
[11] J. L. Rinnenthal and K.-H. Gericke, J. Chem. Phys. **113**, 6210 (2000).
[12] G. Kerenskaya, U. Schnupf, M. C. Heaven, A. van der Avoird, and G. C. Groenenboom, Phys. Chem. Chem. Phys. **7**, 846 (2005).
[13] N. Bouhafs and F. Lique, J. Chem. Phys. **143**, 184311 (2015).
[14] P. J. Dagdigian, J. Chem. Phys. **90**, 6110 (1989).
[15] R. A. Kendall, G. Chałasiński, J. Kłos, R. Bukowski, M. W. Severson, M. Szczęśniak, and S. M. Cybulski, J. Chem. Phys. **108**, 3235 (1998).
[16] S. M. Cybulski, R. Burcl, G. Chal/asiński, and M. Szczęśniak, J. Chem. Phys. **103**, 10116 (1995).
[17] S. Cybulski, J. Chem. Phys. **91**, 7048 (1989).
[18] Y. Kalugina, F. Lique, and S. Marinakis, Phys. Chem. Chem. Phys. **16**, 13500 (2014).
[19] F. Lique, "Communication: Rotational excitation of HCL by H: Rigid rotor vs reactive approaches," J. Chem. Phys. **142**, 241102 (2015).
[20] C. Hampel, K. A. Peterson, and H.-J. Werner, Chem. Phys. Lett. **190**, 1 (1992).
[21] J. D. Watts, J. Gauss, and R. J. Bartlett, J. Chem. Phys. **98**, 8718 (1993).
[22] H.-J. Werner, P. J. Knowles, G. Knizia, F. R. Manby, M. Schütz, P. Celani, T. Korona, R. Lindh, A. Mitrushenkov, G. Rauhut, K. R. Shamasundar, T. B. Adler, R. D. Amos, A. Bernhardsson, A. Berning, D. L. Cooper, M. J. O. Deegan, A. J. Dobbyn, F. Eckert, E. Goll, C. Hampel, A. Hesselmann, G. Hetzer, T. Hrenar, G. Jansen, C. Köppl, Y. Liu, A. W. Lloyd, R. A. Mata, A. J. May, S. J. McNicholas, W. Meyer, M. E. Mura, A. Nicklass, D. P. O'Neill, P. Palmieri, K. Pflüger, R. Pitzer, M. Reiher, T. Shiozaki, H. Stoll, A. J. Stone, R. Tarroni, T. Thorsteinsson, M. Wang, and A. Wolf, MOLPRO, version 2010.1, a package of *ab initio* programs, 2010, see http://www.molpro.net.
[23] S. F. Boys and F. d. Bernardi, Mol. Phys. **19**, 553 (1970).
[24] T. H. Dunning, Jr, J. Chem. Phys. **90**, 1007 (1989).
[25] K. A. Peterson, D. E. Woon, and T. H. Dunning, Jr, J. Chem. Phys. **100**, 7410 (1994).
[26] H.-J. Werner, B. Follmeg, and M. H. Alexander, J. Chem. Phys. **89**, 3139 (1988).
[27] D. T. Colbert and W. H. Miller, J. Chem. Phys. **96**, 1982 (1992).
[28] H.-J. Werner and P. J. Knowles, J. Chem. Phys. **89**, 5803 (1988).
[29] J. M. Hutson, BOUND computer code, version 5 (1993), distributed by Collaborative Computational Project No. 6 of the Science and Engineering Research Council (UK), 1993.
[30] G. Jansen, B. A. Hess, and P. E. Wormer, Chem. Phys. Lett. **214**, 103 (1993).
[31] W. Gordy and R. L. Cook, *Microwave Molecular Spectra* (Wiley, 1984).
[32] F. Lique, A. Spielfiedel, M.-L. Dubernet, and N. Feautrier, J. Chem. Phys. **123**, 134316 (2005).
[33] J. M. Hutson and S. Green, MOLSCAT computer code, version 14 (1994), distributed by Collaborative Computational Project No. 6 of the Engineering and Physical Sciences Research Council (UK), 1994.
[34] F. Lewen, S. Brünken, G. Winnewisser, M. Šimečková, and Š. Urban, J. Mol. Spectrosc. **226**, 113 (2004).
[35] L. N. Smith, D. J. Malik, and D. Secrest, J. Chem. Phys. **71**, 4502 (1979).
[36] K. M. Christoffel and J. M. Bowman, J. Chem. Phys. **78**, 3952 (1983).
[37] M. H. Alexander and P. J. Dagdigian, J. Chem. Phys. **79**, 302 (1983).
[38] T. Orlikowski, Mol. Phys. **56**, 35 (1985).
[39] F. Lique, J. Chem. Phys. **132**, 044311 (2010).

APPENDIX C

Rate-coefficients

All the rate coefficient datas of are available here.

For all the rate coefficients of specific systems, you can click on the specific links:

NH-He Fine Structure
NH-He Hyperfine Structure
ND-He Fine structure
NH-pH$_2$ pure rotational level
NH-oH$_2$ pure rotational level
NH-H$_2$ Fine structure

The values will be updated in the LAMBA and BASECOL databases as they are published.

REFERENCES

Bibliography

Adler, T. B., Knizia, G. and Werner, H.-J. (2007). 'A simple and efficient CCSD(T)-F12 approximation'. In: *The Journal of Chemical Physics* vol. 127, no. 22, p. 221106. eprint: https://doi.org/10.1063/1.2817618.

Alexander, M. H. (1982). 'Rotationally inelastic collisions between a diatomic molecule in a2Π electronic state and a structureless target'. In: *The Journal of Chemical Physics* vol. 76, no. 12, pp. 5974–5988. eprint: https://doi.org/10.1063/1.442951.

Alexander, M. H. and Dagdigian, P. J. (1983). 'Propensity rules in rotationally inelastic collisions of diatomic molecules in 3Σ electronic states'. In: *The Journal of Chemical Physics* vol. 79, no. 1, pp. 302–310. eprint: https://doi.org/10.1063/1.445578.

— (1985). 'Collision-induced transitions between molecular hyperfine levels: Quantum formalism, propensity rules, and experimental study of CaBr($X^2\Sigma^+$)+Ar'. In: *The Journal of Chemical Physics* vol. 83, no. 5, pp. 2191–2200. eprint: https://doi.org/10.1063/1.449311.

Alexander, M. H., Dagdigian, P. J. and Lemoine, D. (1991). 'Quantum scattering studies of inelastic collisions of NH($A^3\Pi$) with helium: Fine-structure and Λ-doublet propensities'. In: *The Journal of Chemical*

Physics vol. 95, no. 7, pp. 5036–5046. eprint: https://doi.org/10.1063/1.461792.

Allamandola, L. J., Tielens, A. G. G. M. and Barker, J. R. (Dec. 1989). 'Interstellar Polycyclic Aromatic Hydrocarbons: The Infrared Emission Bands, the Excitation/Emission Mechanism, and the Astrophysical Implications'. In: *The Astrophysical Journal Supplement* vol. 71, p. 733.

Arthurs, A. M. and Dalgarno, A. (July 1960). 'The Theory of Scattering by a Rigid Rotator'. In: *Proceedings of the Royal Society of London Series A* vol. 256, no. 1287, pp. 540–551.

Arthurs, A. M., Dalgarno, A. and Bates, D. R. (1960). 'The theory of scattering by a rigid rotator'. In: *Proceedings of the Royal Society of London. Series A. Mathematical and Physical Sciences* vol. 256, no. 1287, pp. 540–551. eprint: https://royalsocietypublishing.org/doi/pdf/10.1098/rspa.1960.0125.

Atkins, P. and Friedman, R. (2011). *Molecular Quantum Mechanics*. OUP Oxford.

Bacmann, A., Caux, E. et al. (Oct. 2010). 'First detection of ND in the solar-mass protostar IRAS16293-2422'. In: *Astronomy & Astrophysics* vol. 521, L42, p. L42. arXiv: 1007.4691 [astro-ph.GA].

Bacmann, A., Daniel, F., Caselli, P., Ceccarelli, C., Lis, D., Vastel, C., Dumouchel, F., Lique, F. and Caux, E. (Mar. 2016). 'Stratified NH and ND emission in the prestellar core 16293E in L1689N'. In: *Astronomy & Astrophysics* vol. 587, A26, A26. arXiv: 1512.02629 [astro-ph.GA].

Bernstein, R. (2013). *Atom - Molecule Collision Theory: A Guide for the Experimentalist*. International Studies in Economic Modelling. Springer US.

Böhm-Vitense, E. (1992). *Introduction to Stellar Astrophysics:* Introduction to Stellar Astrophysics. Cambridge University Press.

Born, M. and Oppenheimer, R. (1927). 'Zur Quantentheorie der Molekeln'. In: *Annalen der Physik* vol. 389, pp. 457–484.

Bouhafs, N. (Oct. 2017). 'Excitation des hydrures d'azote par l'hydrogéne atomique et moléculaire'. PhD thesis.

Bouhafs, N., Lique, F., Faure, A., Bacmann, A., Li, J. and Guo, H. (2017). 'Rotational excitation of the interstellar NH_2 radical by H_2'. In: *The Journal of Chemical Physics* vol. 146, no. 6, p. 064309. eprint: https://doi.org/10.1063/1.4975324.

Bouhafs, N. and Lique, F. (2015). 'Collisional excitation of NH($X\ ^3\Sigma^-$) by Ne: Potential energy surface, scattering calculations, and comparison with experiments'. In: *The Journal of Chemical Physics* vol. 143, no. 18, p. 184311. eprint: https://doi.org/10.1063/1.4935513.

Boys, S. and Bernardi, F. (1970). 'The calculation of small molecular interactions by the differences of separate total energies. Some procedures with reduced errors'. In: *Molecular Physics* vol. 19, no. 4, pp. 553–566. eprint: https://doi.org/10.1080/00268977000101561.

Carruthers, G. R. (Aug. 1970). 'Rocket Observation of Interstellar Molecular Hydrogen'. In: *The Astrophysical Journal Letters* vol. 161, p. L81.

Cernicharo, J., Goicoechea, J. R. and Caux, E. (2000). 'Far-infrared detection of C3 in Sagittarius B2 and IRC+ 10216'. In: *The Astrophysical Journal Letters* vol. 534, no. 2, p. L199.

Chandler, D. W. (Mar. 2010). 'Cold and ultracold molecules: Spotlight on orbiting resonances'. In: *The Journal of Chemical Physics* vol. 132, no. 11, pp. 110901–110901.

Chefdeville, S., Kalugina, Y., Meerakker, S., Naulin, C., Lique, F. and Costes, M. (Sept. 2013). 'Observation of Partial Wave Resonances in Low-Energy O_2-H_2 Inelastic Collisions'. In: *Science (New York, N.Y.)* Vol. 341, pp. 1094–6.

Chefdeville, S., Stoecklin, T., Bergeat, A., Hickson, K. M., Naulin, C. and Costes, M. (July 2012). 'Appearance of Low Energy Resonances in CO-Para-H_2 Inelastic Collisions'. In: *Phys. Rev. Lett.* Vol. 109 (2), p. 023201.

Cheung, A. C., Rank, D. M., Townes, C. H., Thornton, D. D. and Welch, W. J. (Dec. 1968). 'Detection of NH_3 Molecules in the Interstellar Medium by Their Microwave Emission'. In: *Physical Review Letters* vol. 21, no. 25, pp. 1701–1705.

Child, M. (1996). *Molecular Collision Theory*. Dover Books on Chemistry Series. Dover Publications.

Christoffel, K. M. and Bowman, J. M. (1983). 'Complex coordinate calculations of Feshbach resonance energies and widths for a collinear triatomic system'. In: *The Journal of Chemical Physics* vol. 78, no. 6, pp. 3952–3958. eprint: https://doi.org/10.1063/1.445119.

Copernicus, N. (1543). *De Revolutionibus orbium coelestium*. Roskam's Boeken Verkoop Kantoor.

Cordiner, M. A. et al. (Apr. 2019). 'Confirming Interstellar C60 + Using the Hubble Space Telescope'. In: *The Astrophysical Journal* vol. 875, no. 2, p. L28.

Corey, G. C. and McCourt, F. R. (1983). 'Inelastic differential and integral cross sections for $^{2S+1}\Sigma$. linear molecule-1S atom scattering: the use of Hund's case b representation'. In: *The Journal of Physical Chemistry* vol. 87, no. 15, pp. 2723–2730. eprint: https://doi.org/10.1021/j100238a009.

Corey, G. C. and Alexander, M. H. (1988). 'Inelastic collisions of OH($X^2\Pi$) with para-H_2: Λ-doublet and hyperfine-structure transitions'. In: *The Journal of Chemical Physics* vol. 88, no. 11, pp. 6931–6937. eprint: https://doi.org/10.1063/1.454390.

Crawford, I. and Williams, D. (1997). 'Detection of interstellar NH towards ζ Ophiuchi by means of ultra-high-resolution spectroscopy'. In: *Monthly Notices of the Royal Astronomical Society* vol. 291, no. 3, pp. L53–L56.

Curtiss, C. F. (1968a). 'Molecular Collisions. VI. Diagrammatic Methods'. In: *The Journal of Chemical Physics* vol. 48, no. 4, pp. 1725–1731. eprint: https://doi.org/10.1063/1.1668900.

— (1968b). 'Molecular Collisions. VIII'. In: *The Journal of Chemical Physics* vol. 49, no. 4, pp. 1952–1957. eprint: https://doi.org/10.1063/1.1670333.

Curtiss, C. F. and Bernstein, R. B. (1969). 'Molecular Collisions. IX. Restricted Distorted-Wave Approximation for Rotational Excitation and Scattering of Diatomic Molecules'. In: *The Journal of Chemical Physics* vol. 50, no. 3, pp. 1168–1176. eprint: https://doi.org/10.1063/1.1671174.

Cybulski, H., Krems, R. V., Sadeghpour, H. R., Dalgarno, A., Kłos, J., Groenenboom, G. C., Avoird, A. van der, Zgid, D. and Chałasiński, G. (2005). 'Interaction of NH($X\ ^3\Sigma^-$) with He: Potential energy surface, bound states, and collisional Zeeman relaxation'. In: *The Journal of Chemical Physics* vol. 122, no. 9, p. 094307. eprint: https://doi.org/10.1063/1.1857473.

Dagdigian, P. J. (1989). 'Scaling relations in the rotational excitation of NH($X^3\Sigma^-$) N=0 by argon'. In: *The Journal of Chemical Physics* vol. 90, no. 11, pp. 6110–6115. eprint: https://doi.org/10.1063/1.456376.

Dagdigian, P. J. and Kłos, J. (2018). 'The effect of nonadiabaticity on the C+ + HF reaction'. In: *The Journal of Chemical Physics* vol. 149, no. 20, p. 204309. eprint: https://doi.org/10.1063/1.5056312.

Daniel, F., Dubernet, M.-L. and Meuwly, M. (2004). 'Selective hyperfine excitation of N2H+ by He: Potential energy surface, cross sections, and propensity rules'. In: *The Journal of Chemical Physics* vol. 121, no. 10, pp. 4540–4549. eprint: https://doi.org/10.1063/1.1774978.

Dixon, R. N., Field, D. and Porter, G. (1979). 'Rotationally inelastic collisions of orbitally degenerate molecules; maser action in OH and CH'. In: *Proceedings of the Royal Society of London. A. Mathematical and Physical Sciences* vol. 368, no. 1732, pp. 99–123. eprint: https://royalsocietypublishing.org/doi/pdf/10.1098/rspa.1979.0118.

Douglas, A. E. and Herzberg, G. (Sept. 1941). 'Note on CH^+ in Interstellar Space and in the Laboratory.' In: *The Astrophysical Journal* vol. 94, p. 381.

Dubernet, M.-L., Daniel, F., Grosjean, A., Faure, A., Valiron, P., Wernli, M., Wiesenfeld, L., Rist, C., Noga, J. and Tennyson, J. (2006). 'Influence of a new potential energy surface on the rotational (de)excitation of H_2O by H_2 at low temperature'. In: *A&A* vol. 460, no. 1, pp. 323–329.

Dulieu, O. and Osterwalder, A. (2017). *Cold Chemistry: Molecular Scattering and Reactivity Near Absolute Zero*. Theoretical and Computational Chemistry Series. Royal Society of Chemistry.

Dumouchel, F., Kłos, J., Toboła, R., Bacmann, A., Maret, S., Hily-Blant, P., Faure, A. and Lique, F. (2012). 'Fine and hyperfine excitation of NH and ND by He: On the importance of calculating rate coefficients of isotopologues'. In: *The Journal of Chemical Physics* vol. 137, no. 11, p. 114306. eprint: https://doi.org/10.1063/1.4753423.

Dunning, T. H. (1989). 'Gaussian basis sets for use in correlated molecular calculations. I. The atoms boron through neon and hydrogen'. In: *The Journal of Chemical Physics* vol. 90, no. 2, pp. 1007–1023. eprint: https://doi.org/10.1063/1.456153.

Dupeyrat, G., Marquette, J. B. and Rowe, B. R. (1985). 'Design and testing of axisymmetric nozzles for ion-molecule reaction studies between 20 K and 160 K'. In: *The Physics of Fluids* vol. 28, no. 5, pp. 1273–1279. eprint: https://aip.scitation.org/doi/pdf/10.1063/1.865010.

Eddington, A. S. (July 1926). 'Bakerian Lecture. Diffuse Matter in Interstellar Space'. In: *Proceedings of the Royal Society of London Series A* vol. 111, no. 759, pp. 424–456.

Edmonds, A. R. (1957). *Angular Momentum in Quantum Mechanics*.

Eppink, A. T. J. B. and Parker, D. H. (1997). 'Velocity map imaging of ions and electrons using electrostatic lenses: Application in photoelectron and photofragment ion imaging of molecular oxygen'. In: *Review of Scientific Instruments* vol. 68, no. 9, pp. 3477–3484. eprint: https://doi.org/10.1063/1.1148310.

Faure, A. and Lique, F. (Sept. 2012). 'The impact of collisional rate coefficients on molecular hyperfine selective excitation'. In: *Monthly Notices of the Royal Astronomical Society* vol. 425, no. 1, pp. 740–748. eprint: http://oup.prod.sis.lan/mnras/article-pdf/425/1/740/3234819/425-1-740.pdf.

Fléchard, X. et al. (July 2015). 'Primary processes: from atoms to diatomic molecules and clusters'. In: *Journal of Physics: Conference Series* vol. 629, p. 012001.

Freeman, J., Paresce, F., Bowyer, S., Lampton, M., Stern, R. and Margon, B. (July 1977). 'The local interstellar helium density.' In: *The Astrophysical Journal Letters* vol. 215, pp. L83–L86.

Gautier T. N., I., Fink, U., Treffers, R. R. and Larson, H. P. (July 1976). 'Detection of molecular hydrogen quadrupole emission in the Orion nebula.' In: *The Astrophysical Journal Letters* vol. 207, pp. L129–L133.

Gilijamse, J. J., Hoekstra, S., Meerakker, S. Y. T. van de, Groenenboom, G. C. and Meijer, G. (2006). 'Near-Threshold Inelastic Collisions Using Molecular Beams with a Tunable Velocity'. In: *Science* vol. 313, no. 5793, pp. 1617–1620. eprint: https://science.sciencemag.org/content/313/5793/1617.full.pdf.

Goicoechea, J. R., Rodríguez-Fernández, N. J. and Cernicharo, J. (2004). 'The Far-Infrared Spectrum of the Sagittarius B2 Region: Extended Molecular Absorption, Photodissociation, and Photoionization'. In: *The Astrophysical Journal* vol. 600, no. 1, p. 214.

Goldflam, R. and Kouri, D. J. (1979). 'On angular momentum decoupling approximations and factorization in diatom–diatom scattering'. In: *The Journal of Chemical Physics* vol. 70, no. 11, pp. 5076–5091. eprint: https://doi.org/10.1063/1.437350.

Gordon, R. G. (July 1969). 'New Method for Construction Wavefunctions for Bound States and Scattering'. In: *The Journal of Chemical Physics* vol. 51, pp. 14–25.

Green, S. (1975). 'Rotational excitation in H2–H2 collisions: Close-coupling calculations'. In: *The Journal of Chemical Physics* vol. 62, no. 6, pp. 2271–2277. eprint: https://doi.org/10.1063/1.430752.

— (1976). 'Rotational excitation of symmetric top molecules by collisions with atoms: Close coupling, coupled states, and effective potential

calculations for NH_3–He'. In: *The Journal of Chemical Physics* vol. 64, no. 8, pp. 3463–3473. eprint: https://aip.scitation.org/doi/pdf/10.1063/1.432640.

— (1979). 'Rotational excitation of symmetric top molecules by collisions with atoms. II. Infinite order sudden approximation'. In: *The Journal of Chemical Physics* vol. 70, no. 2, pp. 816–829. eprint: https://aip.scitation.org/doi/pdf/10.1063/1.437515.

Griffiths, D. (2017). *Introduction to Quantum Mechanics*. Cambridge University Press.

Hartmann, J. (May 1904). 'Investigations on the spectrum and orbit of delta Orionis.' In: *The Astrophysical Journal* vol. 19, pp. 268–286.

Hawking, S. and Mlodinow, L. (2010). *The Grand Design*. Random House Publishing Group.

Heger, M. L. (Jan. 1922). 'Further study of the sodium lines in class B stars'. In: *Lick Observatory Bulletin* vol. 10, no. 337, pp. 141–145.

Herbst, E. and Klemperer, W. (Oct. 1973). 'The Formation and Depletion of Molecules in Dense Interstellar Clouds'. In: *The Astrophysical Journal* vol. 185, pp. 505–534.

Herschel, W. and Dreyer, J. (1912). *The Scientific Papers of Sir William Herschel, Including Early Papers Hitherto Unpublished*. The Royal society.

Herzberg, G. (June 1988). 'Historical Remarks on the Discovery of Interstellar Molecules'. In: *Journal of the Royal Astronomical Society of Canada* vol. 82, p. 115.

Hily-Blant, P., Walmsley, M., Pineau Des Forêts, G. and Flower, D. (Apr. 2010). 'Nitrogen chemistry and depletion in starless cores'. In: *Astronomy & Astrophysics* vol. 513, A41, A41. arXiv: 1001.3930 [astro-ph.SR].

Hily-Blant, P., Maret, S., Bacmann, A., Bottinelli, S., Parise, B., Caux, E., Faure, A., Bergin, E., Blake, G., Castets, A. et al. (2010). 'Nitrogen hydrides in the cold envelope of IRAS 16293-2422'. In: *Astronomy & Astrophysics* vol. 521, p. L52.

Hiraoka, K., Yamashita, A., Yachi, Y., Aruga, K., Sato, T. and Muto, H. (Apr. 1995). 'Ammonia Formation from the Reactions of H Atoms with N Atoms Trapped in a Solid N_2 Matrix at 10-30 K'. In: *The Astrophysical Journal* vol. 443, p. 363.

Huggins, W. and Miller, W. A. (1864). 'On the Spectra of Some of the Nebulae. By William Huggins, F.R.A.S. A Supplement to the Paper "On the Spectra of Some of the Fixed Stars William Huggins F.R.A.S., and W. A. Miller, M.D., LL.D., Treas. and V.P.P.S."' In: *Philosophical Transactions of the Royal Society of London* vol. 154, pp. 437–444.

Hutson (1993). *BOUND computer code, version 5, distributed by Collaborative Computational Project No. 6 of the Science and Engineering Research Council (UK).* URL: http://www.ccp6.ac.uk/downloads/bound.htm.

— (Nov. 1994a). 'Coupled channel methods for solving the bound-state Schrödinger equation'. In: *Computer Physics Communications* vol. 84, pp. 1–18.

— (1994b). *MOLSCAT computer code, version 14, distributed by Collaborative Computational Project No. 6 of the Science and Engineering Research Council (UK).*

Jankunas, J., Bertsche, B. and Osterwalder, A. (May 2014). 'Study of the Ne($^3P_2$) + CH_3F Electron Transfer Reaction below 1 Kelvin'. In: *The journal of physical chemistry. A* vol. 118.

Jankunas, J., Jachymski, K., Hapka, M. and Osterwalder, A. (Apr. 2015). 'Observation of orbiting resonances in He(3_1^S) + NH_3 Penning ionization'. In: *The Journal of chemical physics* vol. 142, p. 164305.

— (Apr. 2016). 'Importance of rotationally inelastic processes in low-energy Penning ionization of CHF_3'. In: *The Journal of Chemical Physics* vol. 144.

Jansky, K. G. (Oct. 1933). 'Electrical Disturbances Apparently of Extraterrestrial Origin'. In: *Proceedings of the Institute of Radio Engineers* vol. 21, no. 10, pp. 1387–1398.

Johnson, B. R. (Nov. 1978). 'The renormalized Numerov method applied to calculating bound states of the coupled-channel Schroedinger equation'. In: *The Journal of Chemical Physics* vol. 69, pp. 4678–4688.

Kalugina, Y., Lique, F. and Marinakis, S. (2014). 'New ab initio potential energy surfaces for the ro-vibrational excitation of OH($X^2\Pi$) by He'. In: *Phys. Chem. Chem. Phys.* Vol. 16 (26), pp. 13500–13507.

Kendall, R. A., Chałasiński, G., Kłos, J., Bukowski, R., Severson, M. W., Szczęśniak, M. M. and Cybulski, S. M. (1998). 'Ab initio study of the van der Waals interaction of NH($X^3\Sigma^-$) with Ar(^1S)'. In: *The Journal of Chemical Physics* vol. 108, no. 8, pp. 3235–3242. eprint: https://doi.org/10.1063/1.475737.

Kerenskaya, G., Schnupf, U., Heaven, M. C. and Avoird, A. van der (2004). 'Bound state spectroscopy of NH–He'. In: *The Journal of Chemical Physics* vol. 121, no. 16, pp. 7549–7552. eprint: https://aip.scitation.org/doi/pdf/10.1063/1.1808416.

Kirste, M., Wang, X., Schewe, H. C., Meijer, G., Liu, K., Avoird, A. van der, Janssen, L. M. C., Gubbels, K. B., Groenenboom, G. C. and Meerakker, S. Y. T. van de (2012). 'Quantum-State Resolved Bimolecular Collisions

of Velocity-Controlled OH with NO Radicals'. In: *Science* vol. 338, no. 6110, pp. 1060–1063. eprint: https://science.sciencemag.org/content/338/6110/1060.full.pdf.

Klein, A. et al. (Oct. 2017). 'Directly probing anisotropy in atom–molecule collisions through quantum scattering resonances'. In: *Nature Physics* vol. 13, pp. 35–38.

Kłos, J., Lique, F. and Alexander, M. (2007). 'Temperature dependence of rotational excitation rate coefficients of OH($X^2\Pi$) in collision with He'. In: *Chemical Physics Letters* vol. 445, no. 1, pp. 12–16.

Knizia, G., Adler, T. B. and Werner, H.-J. (2009). 'Simplified CCSD(T)-F12 methods: Theory and benchmarks'. In: *The Journal of Chemical Physics* vol. 130, no. 5, p. 054104. eprint: https://doi.org/10.1063/1.3054300.

Kouri, D. J., Heil, T. G. and Shimoni, Y. (1976). 'On the Lippmann–Schwinger equation for atom–diatom collisions: A rotating frame treatment'. In: *The Journal of Chemical Physics* vol. 65, no. 1, pp. 226–235. eprint: https://doi.org/10.1063/1.432802.

Krems, R. V., Sadeghpour, H. R., Dalgarno, A., Zgid, D., Kłos, J. and Chałasiński, G. (Nov. 2003). 'Low-temperature collisions of NH($X\ ^3\Sigma^-$) molecules with He atoms in a magnetic field: An ab initio study'. In: *Phys. Rev. A* vol. 68, no. 5, p. 051401.

Lanza, M., Kalugina, Y., Wiesenfeld, L. and Lique, F. (2014). 'Near-resonant rotational energy transfer in HCl–H_2 inelastic collisions'. In: *The Journal of Chemical Physics* vol. 140, no. 6, p. 064316. eprint: https://doi.org/10.1063/1.4864359.

Lavert, E., Shagam, Y., Henson, A., Gersten, S., Klos, J., Zuchowski, P., Narevicius, J. and Narevicius, E. (Apr. 2014). 'Observation of the isotope effect in sub-kelvin reactions'. In: *Nature chemistry* vol. 6, pp. 332–5.

Le Gal, R., Hily-Blant, P., Faure, A., Pineau des Forêts, G., Rist, C. and Maret, S. (Feb. 2014). 'Interstellar chemistry of nitrogen hydrides in dark clouds'. In: *Astronomy & Astrophysics* vol. 562, A83, A83. arXiv: 1311.5313 [astro-ph.SR].

Lewars, E. (2010). *Computational Chemistry: Introduction to the Theory and Applications of Molecular and Quantum Mechanics*. Springer Netherlands.

Lique, F. (2015). 'Communication: Rotational excitation of HCl by H: Rigid rotor vs. reactive approaches'. In: *The Journal of Chemical Physics* vol. 142, no. 24, p. 241102. eprint: https://doi.org/10.1063/1.4922987.

Lique, F., Spielfiedel, A., Dubernet, M.-L. and Feautrier, N. (2005). 'Rotational excitation of sulfur monoxide by collisions with helium at low temperature'. In: *The Journal of Chemical Physics* vol. 123, no. 13, p. 134316. eprint: https://doi.org/10.1063/1.2004994.

Lique, F. (2010). 'Temperature dependence of the fine-structure resolved rate coefficients for collisions of O2($X^3\Sigma^-$) with He'. In: *The Journal of Chemical Physics* vol. 132, no. 4, p. 044311. eprint: https://doi.org/10.1063/1.3299283.

Lique, F., Spielfiedel, A., Feautrier, N., Schneider, I. F., Kłos, J. and Alexander, M. H. (2010). 'Rotational excitation of CN($X\ ^2\Sigma^+$) by He: Theory and comparison with experiments'. In: *The Journal of Chemical Physics* vol. 132, no. 2, p. 024303. eprint: https://doi.org/10.1063/1.3285811.

Lockyer, J. N. (1891). 'On the chief line in the spectrum of the nebulae;' in: *Proceedings of the Royal Society of London* vol. 48, no. 292-295, pp. 167–198. eprint: https://royalsocietypublishing.org/doi/pdf/10.1098/rspl.1890.0024.

Loreau, J., Faure, A. and Lique, F. (2018). 'Scattering of CO with H_2O: Statistical and classical alternatives to close-coupling calculations'. In: *The Journal of Chemical Physics* vol. 148, no. 24, p. 244308. eprint: https://doi.org/10.1063/1.5036819.

Loreau, J., Lique, F. and Faure, A. (Jan. 2018). 'An Efficient Statistical Method to Compute Molecular Collisional Rate Coefficients'. In: *The Astrophysical Journal* vol. 853, no. 1, p. L5.

Manolopoulos, D. E. (1988). 'Close-coupled equations: the log-derivative approach to inelastic scattering, bound-state and photofragmentation problems'. PhD thesis. Cambridge University, Cambridge.

McGuire, P. (1973). 'Elastic and inelastic angular distributions in the jz-conserving coupled states approximation for molecular collisions'. In: *Chemical Physics Letters* vol. 23, no. 4, pp. 575–578.

McGuire, P. and Kouri, D. J. (1974). 'Quantum mechanical close coupling approach to molecular collisions. jz -conserving coupled states approximation'. In: *The Journal of Chemical Physics* vol. 60, no. 6, pp. 2488–2499. eprint: https://doi.org/10.1063/1.1681388.

McKellar, A. (June 1940). 'Evidence for the Molecular Origin of Some Hitherto Unidentified Interstellar Lines'. In: *Publications of the Astronomical Society of the Pacific* vol. 52, no. 307, p. 187.

Merrill, P. W. (Aug. 1934). 'Unidentified Interstellar Lines'. In: *Publications of the Astronomical Society of the Pacific* vol. 46, no. 272, pp. 206–207.

Mertens, L., Labiad, H., Denis-Alpizar, O., Fournier, M., Carty, D., Picard, S., Stoecklin, T. and Sims, I. (May 2017). 'Rotational energy transfer in collisions between CO and Ar at temperatures from 293 to 30 K'. In: *Chemical Physics Letters*.

Meyer, D. M. and Roth, K. C. (Aug. 1991). 'Discovery of Interstellar NH'. In: *The Astrophysical Journal letters* vol. 376, p. L49.

Naulin, C. and Costes, M. (2014). 'Experimental search for scattering resonances in near cold molecular collisions'. In: *International Reviews in Physical Chemistry* vol. 33, no. 4, pp. 427–446. eprint: https://doi.org/10.1080/0144235X.2014.957565.

Ndengué, S., Dawes, R., Gatti, F. and Meyer, H.-D. (2017). 'Atom-triatom rigid rotor inelastic scattering with the MultiConfiguration Time Dependent Hartree approach'. In: *Chemical Physics Letters* vol. 668, pp. 42–46.

Ndengué, S., Scribano, Y., Gatti, F. and Dawes, R. (2019). 'State-to-state inelastic rotational cross sections in five-atom systems with the multiconfiguration time dependent Hartree method'. In: *The Journal of Chemical Physics* vol. 151, no. 13, p. 134301. eprint: https://doi.org/10.1063/1.5119381.

Orlikowski, T. (1985). 'Theoretical studies of rotationally inelastic collisions of molecules in 3σ electronic states: $O_2(X\ ^3\sigma_g^-)$ + He'. In: *Molecular Physics* vol. 56, no. 1, pp. 35–46. eprint: https://doi.org/10.1080/00268978500102141.

Pack, R. T. (1974). 'Space-fixed vs body-fixed axes in atom-diatomic molecule scattering. Sudden approximations'. In: *The Journal of Chemical Physics* vol. 60, no. 2, pp. 633–639. eprint: https://doi.org/10.1063/1.1681085.

Paresce, F., Bowyer, S. and Kumar, S. (July 1973). 'Evidence for an Interstellar or Interplanetary Source of Diffuse he i 584 Å Radiation'. In: *The Astrophysical Journal Letters* vol. 183, p. L87.

Parker, G. A. and Pack, R. T. (1977). 'Identification of the partial wave parameter and simplification of the differential cross section in the jzCCS

approximation in molecular scattering'. In: *The Journal of Chemical Physics* vol. 66, no. 7, pp. 2850–2853. eprint: https://doi.org/10.1063/1.434342.

Pauling, L. and Wilson, E. (1935). *Introduction to Quantum Mechanics: with applications to chemistry*.

Payne, C. H. (Jan. 1925). 'Stellar Atmospheres; a Contribution to the Observational Study of High Temperature in the Reversing Layers of Stars.' PhD thesis. RADCLIFFE COLLEGE.

Persson, C. M., Black, J. H., Cernicharo, J., Goicoechea, J., Hassel, G., Herbst, E., Gerin, M., De Luca, M., Bell, T., Coutens, A. et al. (2010). 'Nitrogen hydrides in interstellar gas-Herschel/HIFI observations towards G10. 6-0.4 (W31C)'. In: *Astronomy & Astrophysics* vol. 521, p. L45.

Persson, C. et al. (Aug. 2012). 'Nitrogen hydrides in interstellar gas II. Analysis of Herschel/HIFI observations towards W49N and G10.6-0.4 (W31C)'. In: *Astronomy and Astrophysics* vol. 543.

Ptolemaeus, C. (1515). *Almagestum*. Petrus Liechtenstein.

Raghavachari, K., Trucks, G. W., Pople, J. A. and Head-Gordon, M. (May 1989). 'A fifth-order perturbation comparison of electron correlation theories'. In: *Chemical Physics Letters* vol. 157, pp. 479–483.

Rinnenthal, J. L. and Gericke, K.-H. (2000). 'State-to-state studies of ground state NH($X^3\Sigma$-,v=0,J,N)+Ne'. In: *The Journal of Chemical Physics* vol. 113, no. 15, pp. 6210–6226. eprint: https://doi.org/10.1063/1.1309523.

— (2002). 'State-to-state energy transfer of NH($X\ ^3\Sigma^-$,v=0,J,N) in collisions with He and N_2'. In: *The Journal of Chemical Physics* vol. 116, no. 22, pp. 9776–9791. eprint: https://doi.org/10.1063/1.1473662.

Rose, M. E. (1957). *Elementary Theory of Angular Momentum*.

Roueff, E., Lis, D. C., van der Tak, F. F. S., Gerin, M. and Goldsmith, P. F. (Aug. 2005). 'Interstellar deuterated ammonia: from NH_3 to ND_3'. In: *Astronomy & Astrophysics* vol. 438, no. 2, pp. 585–598. arXiv: astro-ph/0504445 [astro-ph].

Roueff, E., Loison, J. C. and Hickson, K. M. (Apr. 2015). 'Isotopic fractionation of carbon, deuterium, and nitrogen: a full chemical study'. In: *Astronomy & Astrophysics* vol. 576, A99, A99. arXiv: 1501.01141 [astro-ph.GA].

Roueff, E. and Lique, F. (Oct. 2013). 'Molecular Excitation in the Interstellar Medium: Recent Advances in Collisional, Radiative, and Chemical Processes'. In: *Chemical reviews* vol. 113.

Russell, . . (May 1935). 'The Analysis of Spectra and its Applications in Astronomy.' In: *Monthly Notices of the Royal Astronomical Society* vol. 95, no. 8, pp. 610–636. eprint: http://oup.prod.sis.lan/mnras/article-pdf/95/8/610/3897874/mnras95-0610.pdf.

S.M.Blinder (1998). *On the Quantum theory of Molecules*. URL: http://www.chm.bris.ac.uk/pt/manby/papers/bornop.pdf.

Sandford, S. A. and Allamandola, L. J. (June 1993). 'H_2 in Interstellar and Extragalactic Ices: Infrared Characteristics, Ultraviolet Production, and Implications'. In: *The Astrophysical Journal Letters* vol. 409, p. L65.

Sarma, K. and Shukla, K. S. (1896). *Aryabhatiya of Aryabhata*.

Sawyer, B. C., Stuhl, B. K., Yeo, M., Tscherbul, T. V., Hummon, M. T., Xia, Y., Kłos, J., Patterson, D., Doyle, J. M. and Ye, J. (Jan. 2011). 'Cold heteromolecular dipolar collisions'. In: *Physical Chemistry Chemical Physics (Incorporating Faraday Transactions)* vol. 13, no. 42, p. 19059. arXiv: 1008.5127 [physics.chem-ph].

Scott, G. B. I., Freeman, C. G. and McEwan, M. J. (Oct. 1997). 'The interstellar synthesis of ammonia'. In: *Monthly Notices of the Royal Astronomical Society* vol. 290, no. 4, pp. 636–638.

Semenov, A. and Babikov, D. (Apr. 2013a). 'Equivalence of the Ehrenfest theorem and the fluid-rotor model for mixed quantum/classical theory of collisional energy transfer'. In: *The Journal of chemical physics* vol. 138, p. 164110.

— (Nov. 2013b). 'Mixed quantum/classical theory of rotationally and vibrationally inelastic scattering in space-fixed and body-fixed reference frames'. In: *The Journal of chemical physics* vol. 139, p. 174108.

Semenov, A. and Babikov, D. (2015). 'Mixed Quantum/Classical Approach for Description of Molecular Collisions in Astrophysical Environments'. In: *The Journal of Physical Chemistry Letters* vol. 6, no. 10. PMID: 26263260, pp. 1854–1858. eprint: https://doi.org/10.1021/acs.jpclett.5b00496.

Shankar, R. (1994). *Principles of Quantum Mechanics*. second edition. Springer.

Sims, I. R., Queffelec, J., Defrance, A., Rebrion-Rowe, C., Travers, D., Bocherel, P., Rowe, B. R. and Smith, I. W. M. (1994). 'Ultralow temperature kinetics of neutral–neutral reactions. The technique and results for the reactions CN+O_2 down to 13 K and CN+NH_3 down to 25 K'. In: *The Journal of Chemical Physics* vol. 100, no. 6, pp. 4229–4241. eprint: https://doi.org/10.1063/1.467227.

Siro Brigiano, F., Jeanvoine, Y., Largo, A. and Spezia, R. (Nov. 2017). 'The formation of urea in space I. Ion-molecule, neutral-neutral, and radical gas-phase reactions'. In: *Astronomy & Astrophysics* vol. 610.

Smith, L. N., Malik, D. J. and Secrest, D. (1979). 'Rotational compound state resonances for an argon and methane scattering system'. In: *The*

Journal of Chemical Physics vol. 71, no. 11, pp. 4502–4514. eprint: https://doi.org/10.1063/1.438203.

Spitzer L., J., Cochran, W. D. and Hirshfeld, A. (Oct. 1974). 'Column densities of interstellar molecular hydrogen.' In: *The Astrophysical Journal Supplement Series* vol. 28, pp. 373–389.

Stoecklin, T. (July 2009). 'Combining electric and magnetic static fields for the tuning of the lifetime of zero energy Feshbach resonances: Application to $^3He + NH(^3\Sigma)$ collisions'. In: *Phys. Rev. A* vol. 80 (1), p. 012710.

Swings, P. (Jan. 1937). 'A note on molecular absorption in interstellar space'. In: *Monthly Notices of the Royal Astronomical Society* vol. 97, p. 212.

Swings, P. and Rosenfeld, L. (Nov. 1937). 'Considerations Regarding Interstellar Molecules'. In: *The Astrophysical Journal* vol. 86, pp. 483–486.

Tak, F., Black, J., Schöier, F., Jansen, D. and Dishoeck, E. (May 2007). 'A computer program for fast non-LTE analysis of interstellar line spectra'. In: *http://dx.doi.org/10.1051/0004-6361:20066820* vol. 468.

Taylor, J. (1972). *Scattering theory: the quantum theory on nonrelativistic collisions*. Wiley.

Taylor, T. (2010). *The Treatises of Aristotle on the Heavens, on Generation and Corruption and on Meteors: Part Seven of the Works of Aristotle*. Kessinger Publishing.

Tielens, A. G. G. M. (July 2013). 'The molecular universe'. In: *Rev. Mod. Phys.* Vol. 85 (3), pp. 1021–1081.

— (2005). *The Physics and Chemistry of the Interstellar Medium*. Cambridge University Press.

Toboła, R., Dumouchel, F., Kłos, J. and Lique, F. (2011). 'Calculations of fine-structure resolved collisional rate coefficients for the NH($X^3\Sigma^-$)-He

system'. In: *The Journal of Chemical Physics* vol. 134, no. 2, p. 024305. eprint: https://doi.org/10.1063/1.3524311.

Toennies, J. P., Welz, W. and Wolf, G. (July 1979). 'Molecular beam scattering studies of orbiting resonances and the determination of van der Waals potentials for H-Ne, Ar, Kr, and Xe and for H_2-Ar, Kr, and Xe'. In: *The Journal of Chemical Physics* vol. 71, no. 2, pp. 614–642.

Treffers, R. R., Fink, U., Larson, H. P. and Gautier T. N., I. (Nov. 1976). 'The spectrum of the planetary nebula NGC 7027 from 0.9 to 2.7 microns.' In: *The Astrophysical Journal Letters* vol. 209, p. 793.

Trumpler, R. J. (Jan. 1930). 'Preliminary results on the distances, dimensions and space distribution of open star clusters'. In: *Lick Observatory Bulletin* vol. 420, pp. 154–188.

Vogels, S. N., Onvlee, J., Chefdeville, S., van der Avoird, A., Groenenboom, G. C. and van de Meerakker, S. Y. T. (Nov. 2015). 'Imaging resonances in low-energy NO-He inelastic collisions'. In: *Science* vol. 350, no. 6262, pp. 787–790. arXiv: 1510.00299 [physics.atm-clus].

Weinreb, S., BARRETT, A., MEEKS, M. and HENRY, J. (Nov. 1963). 'Radio Observations of OH in the Interstellar Medium'. In: *Nature* vol. 200, pp. 829–831.

Werner, H.-J., Knowles, P. J., Knizia, G., Manby, F. R., Schütz, M. et al. (2010). *MOLPRO, version2010.1, a package of ab initio programs,2010.* see.

Weselak, T., Galazutdinov, G., Beletsky, Y. and Krełowski, J. (2009). 'Interstellar NH molecule in translucent sightlines'. In: *Monthly Notices of the Royal Astronomical Society* vol. 400, no. 1, pp. 392–397.

Willitsch, S., Bell, M. T., Gingell, A. D., Procter, S. R. and Softley, T. P. (Jan. 2008). 'Cold Reactive Collisions between Laser-Cooled Ions and

Velocity-Selected Neutral Molecules'. In: *Phys. Rev. Lett.* Vol. 100 (4), p. 043203.

Wollin, G. and Ericson, D. B. (Oct. 1971). 'Amino-acid Synthesis from Gases detected in Interstellar Space'. In: *nature* vol. 233, no. 5322, pp. 615–616.